Catalytic Esterification of Acetic Acid with Methanol by Constant Heat Supply and Batch Reactive Distillation Modelling by Rate Based Approach

Submitted in partial fulfillment of the requirements for the award of the degree of

DOCTOR OF PHILOSOPHY

IN

CHEMICAL ENGINEERING

By

PATAN AMEER KHAN

(Roll No.715057)

Under the supervision of

Dr. S. SRINATH

&

Dr. T. SUNIL KUMAR

DEPARTMENT OF CHEMICAL ENGINEERING

NATIONAL INSTITUTE OF TECHNOLOGY

WARANGAL - 506004, INDIA.

MARCH 2020

NATIONAL INSTITUTE OF TECHNOLOGY- WARANGAL
Warangal – 506004, Telangana, INDIA.

CERTIFICATE

This is to certify that the thesis entitled "**Catalytic Esterification of Acetic Acid with Methanol by Constant Heat Supply and Batch Reactive Distillation Modelling by Rate Based Approach"** being submitted by **Mr. PATAN AMEER KHAN (Roll No.715057)** for the award of the degree of Doctor of Philosophy (Ph.D) in Chemical Engineering to the National Institute of Technology, Warangal, India is a record of the bonafide research work carried out by her under my supervision. The thesis has fulfilled the requirements according to the regulations of this Institute and in my opinion has reached the standards for submission. The results embodied in the thesis have not been submitted to any other University or Institute for the award of any degree or diploma.

Date:

(**Dr. S. Srinath, NIT Warangal**)
Supervisor

(**Dr. T. Sunil Kumar, IIT Tirupati**)
Co-Supervisor

Department of Chemical Engineering
National Institute of Technology
Warangal 506004, Telangana State
INDIA

DECLARATION

This is to certify that the work presented in the thesis entitled "**Catalytic Esterification of Acetic Acid with Methanol by Constant Heat Supply and Batch Reactive Distillation Modelling by Rate Based Approach"** is a bonafide work done by me under the supervision of Dr. S. Srinath & Dr. T. Sunil Kumar and was not submitted elsewhere for award of any degree.

I declare that this written submission represents my ideas in my own words and where others' ideas or words have been included, I have adequately cited and referenced the original source. I also declare that I have adhered to all principles of academic honesty and integrity and have not misrepresented or fabricated or falsified any idea/data/fact/source in my submission. I understand that any violation of the above will be a cause for disciplinary action by the Institute and can also evoke penal action from the sources which have thus not been properly cited or from whom proper permission has not been taken when needed.

PATAN AMEER KHAN

(Roll No.715057)

Acknowledgements

A state of reverence for me to express my indebtedness to my respected supervisors ***Dr. S. Srinath*** Department of Chemical Engineering, National Institute of Technology, Warangal, India and ***Dr. T. Sunil Kumar*** Department of Chemical Engineering, Indian Institute of Technology, Tirupati, India for giving me an opportunity to carry out doctoral work under their supervision. They are to me personally an inspiring personalities and uncut diamonds who actually carved the phrases "Knowledge is treasure but practice is key to it" and "True knowledge is to know one's own ignorance" in my life. They both are best guides I happened to come across. I have learned much more things by interactions and discussions with them. Their experience in teaching and research provided grater insights that helped in professional growth of my career. Their outstanding guidance and support in technical as well as in my career prospects has been extremely helpful.

I am grateful to ***Prof. N.V. Ramana Rao***, Director, NIT Warangal for providing me institute fellowship for completing the Ph.D. I am thankful to ***Prof. Shirish H Sonawane***, Head of the Department, Chemical Engineering for providing necessary facilities in the department and for his valuable suggestions. I am also thankful to earlier HODs, ***Prof. A. Sarat Babu*** and ***Prof. K. Anand Kishore***.

I would like to express my sincere gratitude to DSC members ***Prof. Y. Pydi Setty*** **and** ***Dr. G. Uday Bhaskar Babu*** for their helpful comments and suggestions on my work. I am thankful to ***Dr. D. Kashinath*** Department of Chemistry for his valuable suggestions. My sincere thanks to ***Dr. N. Venkatathri*** and ***Mr. S. Suresh*** Department of Chemistry for providing the support in analyses of the experimental samples.

I would like to express heart-felt thanks to the faculty of the Chemical Engineering Department, National Institute of Technology, Warangal for their suggestions and sparing time for all the discussions.

I wish to express my profound thanks to ***Prem***, ***Raju*** and other staff members of the Department and Institute who have directly or indirectly helped me during the course of the work.

I wish to express sincere thanks to my beloved friends and lab mates ***Dr. Shaik Liyakhath Ahmed (Connoisseur of Food)*** and ***Dr. Dorca R J Chandrika*** for their constant encouragement and help acquired during my research period at NITW. My sincere thanks to my fellow scholars ***Mr. Semal Sekhar, Mr. Sheik Abdul Gaffar*** and ***Mr. Sheik Abdulla*** for their help and support in conducting experiments and having technical discussions that helped me in approaching newer insights of research.

My deepest thanks to my elder brother ***Mr. Patan Sharif Khan***. Without his monotonic increase in support and encouragement at every phase of my life things wouldn't be much easier for me to pursue both in professional and personal aspects.

I would like to express my profound gratitude to my family members: my parents ***Mr. Patan Chan Basha*** (Mr. Cook) and ***Mrs. Rehana Parveen***, my sister ***Mrs. Patan Farhana***, my sister-in-law ***Mrs. Najma Khanam*** and other members of my family for their support and continuous encouragement throughout my years of study and through process of researching and writing this thesis.

Finally, I would like to express my special thanks to my better half ***Mrs. Shaik Sheema Hafsa*** (Mo Chuisle). Her presence of mind, understanding capabilities and encouragement meant a lot to me in maintaining balance between family life and professional career.

Patan Ameer Khan

Abstract

There has been considerable research in the recent past on batch reactive distillation (BRD). One such example is the esterification of acetic acid with methanol in the presence of solid catalysts such as Indion 180/190, Amberlyst and other similar cationic resins. In such as heterogeneous reaction the products are methyl acetate and water. The process of separation of product that is methyl acetate by distillation is also carried out along with reaction in the reboiler. Such simultaneous reaction and distillation in one unit operation is termed as BRD. In the present work, the heterogeneous reaction is modeled and simulated at catalyst particle scale as well as at reactor scale. One non-isothermal kinetic study itself was shown to yield all the four parameters of this reversible reaction. Experimentally novel heat input to the reboiler in the form of constant heat supply instead of isothermal condition was explored for a reboiler-rectification column combination. Modeling and simulation of packed distillation column was carried out using rate based approach to predict the composition in vapor along the column and finally in the distillate. It was found that smaller heat input gives highest purity of methyl acetate in distillate but start-up time being high. Simulation results also matched experimental results regarding the trend in distillate purity versus heat supply rate to reboiler.

Table of contents

Acknowledgements---------- i
Abstract ---------- iii
Table of contents ---------- iv
List of Figures---------- vi
List of Tables---------- x
Nomenclature ----------xii

CHAPTER 1 ---------- 1
Introduction ---------- 2
CHAPTER 2 ---------- 5
Literature Survey ---------- 6
2.1 Pore diffusion models for solid catalysed reactions ---------- 6
2.2 Kinetics of esterification reaction ----------11
2.3 Reactive Distillation-Experiments and Modelling----------12
2.4 Evaporation Rate Based Simulation of Distillation----------14
2.5 Gaps Identified in Literature ----------15
CHAPTER 3 ----------18
Objectives of the Study ----------19
CHAPTER 4 ----------20
Experimental Studies----------21
4.1 Materials and Methods----------21
4.2 Kinetics from non-isothermal reaction----------24
4.3 Distillation of non-reacting binary mixture----------26
4.3.1 Determination of evaporation rate constants ----------27
4.3.2 Batch distillation under total reflux----------31
4.4 Batch reactive distillation - Esterification of Acetic Acid ----------35
CHAPTER 5 ----------58
Mathematical Modelling and Simulation ----------59
5.1 Pore diffusion model – Improvised for heterogeneous esterification----------59
5.1.1 Determination of Rate Constants ----------61
5.1.1.1 Homogeneous rate constant ----------61

5.1.1.2 Heterogeneous rate constant----------63
5.2 Determination of kinetic constants from non-isothermal data----------66
5.3 Dynamic Model for reaction kinetics based on constant heat supply ----------66
5.4 Rate based model for distillation of binary non-reacting mixture ----------67
5.5 Application of rate based model for batch reactive distillation (BRD)----------71
CHAPTER 6 ----------75
Results and Discussion----------76
6.1 Particle scale simulation of pore diffusion model and validation ----------76
6.1.1 Validation of model ----------77
6.1.1.1 Effect of temperature----------78
6.1.1.2 Effect of particle diameter ----------80
6.1.1.3 Effect of catalyst loading ----------82
6.2 Predicted rate constants for pseudo homogeneous model from non-isothermal data---83
6.3 Prediction of distillate composition in non-reacting system----------85
6.4 Prediction of distillate composition in esterification reaction carried out in BRD apparatus----------89
CHAPTER 7 ----------98
Conclusions ----------99
Scope for future work---------- 100
References---------- 101
Appendix ---------- 106
Appendix 1 ---------- 107
Appendix 2 ---------- 111
Algorithm – 1---------- 111
Algorithm - 2---------- 112
Algorithm - 3---------- 113
Publications in Present Work ---------- 114

List of Figures

Figure No.	Description	Page No.
Fig. 2.1	(a) Catalyst particles mixed in reactant product solution	9
	(b) Catalyst particle surrounded by liquid	9
Fig. 4.1	(a) Schematic experimental apparatus for study of kinetics	22
	(b) Schematic representation of the experimental apparatus used in this study for BRD	22
Fig. 4.2	Experimental temperature and concentration dynamics in reactor for 32 W.	25
Fig. 4.3	Experimental temperature and concentration dynamics in reactor for 50 W.	26
Fig. 4.4	Schematic of a heated beaker used to evaluate the evaporation rate of a liquid	27
Fig. 4.5	Evaporation mass transfer coefficients of benzene (A) at various temperatures	29
Fig. 4.6	Evaporation mass transfer coefficients of toluene (B) at various temperatures.	30
Fig. 4.7	Experimental temperature dynamics for three different heat inputs to the reboiler for mixture of benzene-toluene with a mole fraction of 0.5.	32
Fig. 4.8	Experimental time to reach the bubble point for three heat inputs to the reboiler.	33
Fig. 4.9	Time for onset of distillation for three heat inputs to the reboiler.	33
Fig. 4.10	Calibration chart of Refractive Index vs mole fraction of benzene in benzene-toluene mixture at temperature of 30 ^{0}C	34
Fig. 4.11	Experimental distillate composition of benzene for three heat inputs to the reboiler at total reflux	35
Fig. 4.12	GC peaks obtained for reboiler mixture at steady state (100 W and 50 ^{0}C wall temperature). The four peaks in sequence are for methanol, methyl acetate, water and acetic acid	38
Fig. 4.13	GC peaks obtained for distillate at steady state (100 W and 50 ^{0}C wall temperature). The peaks in sequence are of methanol and methyl acetate	38

Fig. 4.14	Experimental temperature dynamics of reboiler	
	(a) Insulated wall condition	54
	(b) Wall at room temperature	54
	(c) Wall at 40 ^{0}C.	55
	(d) wall at 50 ^{0}C	55
	(e) wall at 60 ^{0}C	56
Fig. 5.1	Geometry in COMSOL Multiphysics simulation for the catalyst particle surrounded by a cube of reactant liquid mixture. Units of length is in meters	59
Fig. 5.2	Experimental conversion of acetic acid without catalyst at different temperatures	62
Fig. 5.3	Error plot for evaluating optimum kf2 at a temperature of 343.15 K using comsol solution for reaction-diffusion equation	63
Fig. 5.4	Arrhenius plot for reaction rate constant inside the catalyst pores	
	(a) For Model 1 and Model 3	65
	(b) For Model 2	65
Fig. 5.5	Shell of thickness dz for material and component balance	68
Fig. 6.1	Spatial concentration distribution inside the catalyst particle and around it in the solution at an instant of time 180 s during dynamic simulation	76
Fig. 6.2	Concentration profiles along an arc length from one face of cell to opposite face passing through the catalyst at different times	77
Fig. 6.3	Kinetics of acetic acid conversion for temperature of 353.15 K at constant catalyst loading of 0.025 g/cc and particle diameter of 725 µm as calculated from experimental data and predicted by the simulation	78
Fig. 6.4	Kinetics of acetic acid conversion for temperature of 343.15 K at constant catalyst loading of 0.025 g/cc and particle diameter of 725 µm as calculated from experimental data and predicted by the simulation.	79
Fig. 6.5	Kinetics of acetic acid conversion for temperature of 333.15 K at constant catalyst loading of 0.025 g/cc and particle diameter of 725 µm as calculated from experimental data and predicted by the simulation.	79
Fig. 6.6	Kinetics of acetic acid conversion for different temperatures at constant catalyst loading of 0.025 g/cc and particle diameter of 725 µm as predicted by the simulation using Model 3.	80

Fig. 6.7	Kinetics of acetic acid conversion for various particle sizes at constant loading of 0.025 g/cc as predicted by the simulation using k_{f1} evaluated with MATLAB and k_{f2} evaluated with COMSOL Multiphysics.	81
Fig. 6.8	Kinetics of acetic acid conversion for various catalyst loading with particle diameter of 725 μm as predicted by the simulation using k_{f1} evaluated with MATLAB and k_{f2} evaluated with COMSOL Multiphysics.	82
Fig. 6.9	Reboiler temperature dynamics for different heat inputs	
	(a) 32 W	83
	(b) 50 W	84
Fig. 6.10	Experimental and predicted concentration dynamics of acetic acid for two different heat inputs	
	(a) 32 W	84
	(b) 50 W	85
Fig. 6.11	Temperature variation along the height of the column at steady state	86
Fig. 6.12	Benzene mole fraction in liquid along the height of the column	86
Fig. 6.13	Benzene mole fraction in vapor along the height of the column	87
Fig. 6.14	Local relative volatility as obtained from steady state simulation composition and from temperature.	88
Fig. 6.15	Schematic representation of temperature dynamics and corresponding phenomena occurring in the reboiler.	89
Fig. 6.16	(a) Vapour-air interface for low heat input rate	90
	(b) Vapour-air interface for high heat input rate	90
Fig. 6.17	Dynamics of mole fraction of methyl acetate (solid line) in the reboiler obtained from kinetics	
	(a) Insulated 50 W and compared with isothermal conditions	91
	(b) Insulated 100 W and compared with isothermal conditions	91
	(c) Insulated 150W and compared with isothermal conditions	92
Fig. 6.18	Comparative dynamics of mole fraction of methyl acetate in the reboiler obtained from kinetics for insulated conditions with three different heat inputs	92

Fig. 6.19	Mole fraction of components in vapor of packed column	
	(a) Q = 32 Watt and ac = 90 m^2/m^3	94
	(b) Q = 50 Watt and ac = 60 m^2/m^3	94
	(c) Q = 100 Watt and ac = 90 m^2/m^3	95
	(d) Q = 150 Watt and ac = 120 m^2/m^3	95
Fig. 6.20	Effect of heat input (Q) on distillate composition of Methyl acetate (y_c) with a_c = 100 m^2/m^3	96
Fig. 6.21	Effect of heat input (Q) on distillate composition of Methyl acetate (y_c) with a_c as variable.	97

List of Tables

Table No.	Description	Page No.
Table 2.1	Description of model for evaluation of rate constants	10
Table 4.1	Physical properties of INDION 180 and Indion 190 catalysts.	21
Table 4.2	Experimental data pertaining to the evaporation of benzene-toluene mixture	28
Table 4.3	Experimental data at steady state.	31
Table 4.4	Refractive index of a benzene-toluene mixture	34
Table 4.5	Experimental observations for 50 W and Insulated column	39
Table 4.6	Experimental observations for 100 W and Insulated column	40
Table 4.7	Experimental observations for 150 W and Insulated column	41
Table 4.8	Experimental observations for 50 W and column at room temperature	42
Table 4.9	Experimental observations for 100 W and column at room temperature	43
Table 4.10	Experimental observations for 150 W and column at room temperature	44
Table 4.11	Experimental observations for 50 W and column at 40 ^{0}C	45
Table 4.12	Experimental observations for 100 W and column at 40 ^{0}C	46
Table 4.13	Experimental observations for 150 W and column at 40 ^{0}C	47
Table 4.14	Experimental observations for 50 W and column at 50 ^{0}C	48
Table 4.15	Experimental observations for 100 W and column at 50 ^{0}C	49
Table 4.16	Experimental observations for 150 W and column at 50 ^{0}C	50
Table 4.17	Experimental observations for 50 W and column at 60 ^{0}C	51
Table 4.18	Experimental observations for 100 W and column at 60 ^{0}C	52
Table 4.19	Experimental observations for 150 W and column at 60 ^{0}C	53
Table 4.20	Experimental data on onset of distillate	56
Table 4.21	Distillate compositions in weight percent	57
Table 5.1	Rate constant values for all the three models at different temperatures	64
Table 5.2	k_0 and E values for k_{f1} and k_{f2} for all three models	66
Table 6.1	Kinetic constants for pseudo homogenous model for two different heat inputs	83

Table 6.2	Simulation results as compared to experimental data	87
Table 6.3	Simulated Mole fraction of methyl acetate in reactor at onset of distillation	93
Table 6.4	Experimental and simulated mole fractions in distillate of BRD for different heat inputs	93

Nomenclature

A	Acetic Acid - Section 2.1, Section 5.5; Benzene – Section – 4.3, Section 5.4, Section 6.3
B	Methanol – Section 2.1, Section 5.5; Toluene – Section – 4.3, Section 5.4
C	Methyl Acetate – Section 2.1, Section 5.5, Section 6.4
D	Water – Section 2.1, Section 5.5
$A_{c,b}$	Cross sectional area of the liquid surface in beaker (m^2)
a_c	specific surface area available inside the column in the form of raschig rings (m^2/m^3)
A_c	Cross sectional area of the column (m^2)
E_b	Activation Energy for backward reaction rate constant (J/mol)
E_f	Activation Energy for forward reaction rate constant (J/mol)
k_{b_o}	Pre-exponential factor for backward reaction rate constant (l/mol min)
k_{f_o}	Pre-exponential factor for forward reaction rate constant (l/mol min)
k_{f1_o}	Pre-exponential factor for forward reaction rate constant in bulk (l/mol min)
k_{f2_o}	Pre-exponential factor for forward reaction rate constant inside catalyst (l/mol min)
p_A^{sat}	saturated vapor pressure of component ‘A’ at a location inside the column (atm)
p_B^{sat}	Saturated vapor pressure of component ‘B’ at a location inside the column (atm)
p_C^{sat}	Saturated vapor pressure of component ‘C’ at a location inside the column (atm)
p_D^{sat}	Saturated vapor pressure of component ‘D’ at a location inside the column (atm)
p_t	Total pressure or atmospheric pressure (atm)
x_A	Mole fraction of component ‘A’ in liquid phase
x_{AR}	mole fraction of component ‘A’ in reboiler
x_B	Mole fraction of component ‘B’ in liquid phase
x_{BR}	Mole fraction of component ‘B’ in reboiler
x_C	Mole fraction of component ‘C’ in liquid phase
x_{CR}	mole fraction of component ‘C’ in reboiler
x_D	Mole fraction of component ‘D’ in liquid phase
x_{DR}	mole fraction of component ‘D’ in reboiler
$y_{A,D}$	Mole fraction of component ‘A’ in distillate
y_A	Mole fraction of component ‘A’ in vapor phase
y_B	Mole fraction of component ‘B’ in vapor phase

$y_{C,D}$	Mole fraction of component 'C' in distillate
y_C	Mole fraction of component 'C' in vapor phase
y_D	Mole fraction of component 'D' in vapor phase
ρ_P	Density of catalyst particle (g/cc)
Δm	Mass of evaporated liquid component (g)
Δt	Time of evaporation (s)
C_A	Concentration of Acetic Acid (mol/l)
C_{A0}	Initial concentration of acetic acid (mol/l)
C_B	Concentration of Methanol (mol/l)
C_C	Concentration of Methyl Acetate (mol/l)
C_D	Concentration of Water (mol/l)
D_{A1}	Diffusivity of acetic acid in the bulk (m^2/s)
D_{A2}	Diffusivity of acetic acid inside the catalyst particle (m^2/s)
E_{f1}	Activation Energy for forward reaction rate constant in bulk (J/mol)
E_{f2}	Activation Energy for forward reaction rate constant inside catalyst (J/mol)
K_A	mass transfer coefficient of component 'A' ($mol/m^2.atm.s$)
k_b	Backward reaction rate constant (l/mol.min)
K_B	Mass transfer coefficient of component 'B' ($gmol/m^2.atm.s$)
k_{b1}	Backward reaction rate constant in bulk (l/mol min)
k_{b2}	Backward reaction rate constant inside catalyst particle (l/mol min)
K_C	Mass transfer coefficient of component 'C' ($gmol/m^2.atm.s$)
K_D	Mass transfer coefficient of component 'D' ($gmol/m^2.atm.s$)
K_e	Equilibrium reaction rate constant
k_f	Forward reaction rate constant (l/mol.min)
k_{f1}	Forward reaction rate constant in bulk (l/mol.min)
k_{f2}	Forward reaction rate constant inside catalyst particle (l/mol.min)
L	Molar flow rate of liquid from column to the reboiler (mol/sec)
L_A	Molar flow rate of component 'A' in liquid from column to the reboiler (mol/sec)
L_B	Molar flow rate of component 'B' in liquid from column to the reboiler (mol/sec)
L_C	Molar flow rate of component 'C' in liquid from column to the reboiler (mol/sec)
L_D	Molar flow rate of component 'D' in liquid from column to the reboiler (gmol/sec)
Q	Heat input to the reboiler (W)
R	Universal gas constant (J/mol.K)

R_P	Radius of the catalyst particle (µm)
T	Temperature (K)
V	Molar flow rate of vapor from column to the reboiler (mol/sec)
V_A	Molar flow rate of component 'A' in vapor from column to the reboiler (mol/sec)
V_B	Molar flow rate of component 'B' in vapor from column to the reboiler (mol/sec)
V_C	Molar flow rate of component 'C' in vapor from column to the reboiler (mol/sec)
V_D	Molar flow rate of component 'D' in vapor from column to the reboiler (mol/sec)
X_A	Conversion of acetic acid (A)
BRD	Batch Reactive Distillation
CRD	Continuous Reactive Distillation
MW	Molecular Weight of liquid component (g/mol)

Greek Symbols

β_{expt}	Beta experimental (ml/g.s)
β_{sim}	Beta Simulation (ml/g.s)
ε	Porosity
λ_A	Latent heat of vaporization of component 'A' (J/mol)
λ_B	Latent heat of vaporization of component 'B' (J/mol)
λ_C	Latent heat of vaporization of component 'C' (J/mol)
λ_D	Latent heat of vaporization of component 'D' (J/mol)

CHAPTER 1
INTRODUCTION

Introduction

The manufacture of any synthetic organic chemical requires reaction followed by separation. The reactions are conducted in reactors conventionally and separation is carried out in distillation columns for miscible system. The first part of the above process can be enhanced by adding catalyst which were in the form of liquids initially and later got replaced by solid resin catalyst. This invention has directly reduced one separation process because simple filtration can be used to separate the solid catalyst. Further distillation unit operation can also be combined with the reactor where the reactor acts as a reboiler and the column above it becomes the rectification section. If the desired product has the least boiling point then it can be obtained as distillate. If the desired has highest boiling point then it can be obtained in the bottom. In the past patents were also granted for such technologies (Agreda and Partin, 1984). It is significant in the view of process intensification and energy minimization. In this work the esterification reaction between acetic acid and methanol producing methyl acetate and water in the presence of solid cationic resin catalyst such as INDION 190 is studied. To predict the kinetics of this solid catalyzed esterification, a dynamic simulation of reaction and transport at particle scale using COMSOL Multiphysics was carried out. The reaction kinetic data utilized for parameter evaluation and validation is from the esterification reaction with similar solid catalyst such as Indion 180. When the reactant mixture is mixed with solid catalyst particles it becomes a uniform particulate-liquid suspension at sufficiently high mixing speed in a batch reactor [Patan et al., 2018]. Keeping this as assumption for the determination of kinetics, each solid catalyst particle is surrounded by reactant mixture which is of equal volume for all the catalyst particles. A dynamic simulation is carried out using COMSOL Multiphysics which has solver for diffusion-reaction equation for both in liquid phase and inside particle. The intrinsic reaction rate constants for bulk liquid phase and inside the particle are assumed different and obtained by solving the full diffusion-reaction equation and using optimization method with more accurate boundary condition at particle-liquid interface. Three different models are proposed for evaluating the rate constants from micro simulation and the experimental kinetic data.

For pseudo homogeneous assumptions, a novel method of obtaining reaction kinetic constants of the same reversible reaction is proposed. It consists of measuring both concentration and temperature dynamics in a batch reactor supplied with a constant heat input rate. By just one experiment it is shown possible that the four kinetic constants such as frequency factor and

activation energies for both forward and backward reactions by the use of multi parameter optimization technique.

When a distillation column is attached above the reactor it becomes batch reactive distillation (BRD). Modeling and simulation of a distillation column is very important in many chemical industries where ever it requires reaction, separation or purification of a liquid mixture into its pure components in one unit. Particularly in the context of improving efficiency, process scale up, intensification and control it requires a validated model. In this work, a batch distillation equipment which consists of a reboiler, a packed column and a top condenser is used to distil a non-reacting mixture of benzene and toluene with various heat inputs to the reboiler. Such a study gives a validated model suitable for implementing for multi-component mixtures. The distillation process in the column is modelled by evaporation rate based approach or non-equilibrium approach. This particular feature is different from the stage wise equilibrium model. The model is for a packed bed distillation column with a continuous variation of liquid and gas phase composition along the height of the column. It is a 1-D model and solved by Finite Difference Method. The distillate compositions at total reflux obtained from experiments and the simulations are compared for validating of model.

Experimental results related to various wall heating conditions for a batch reactive distillation (BRD) were conducted. A solid catalyzed esterification reaction as mentioned earlier is chosen as the system for study. An experimental apparatus with reboiler and a rectification column along with top total condenser were used. As a novelty the rectification section is provided with a jacket through which hot water can be circulated. The intention was to check if higher wall temperature would lead to less onset time for distillate formation and steady state in distillate composition. The start-up dynamics of temperature in the reboiler, the onset of distillation and the purity of product were recorded. The reboiler is supplied constant heat input rate at three different values. An objective pertaining to high throughput of the desired product methyl acetate is defined to select the most suitable operating option among all the above mentioned operating conditions. Modelling and simulation of BRD using the earlier pseudo homogeneous reaction kinetics and evaporation rate based model for packed column was carried out and trends are validated with experimental data. New insights are obtained in regard to scale up of lab scale BRD apparatus which can be applied for scale-up. Hence sufficient contribution is made to the field of a heterogeneous batch reactive distillation through this thesis.

The thesis is organized as several chapters. In chapter 2 the literature survey and a few gaps identified are presented. In chapter 3 the objectives of the study are proposed. In chapter 4 the experimental work is presented. In chapter 5 the modeling and simulations methodologies implemented in this work are described. In chapter 6 the results are presented along with discussion on mechanism wherever applicable. In chapter 7 the concluding remarks are presented.

CHAPTER 2
LITERATURE SURVEY

Literature Survey

2.1 Pore diffusion models for solid catalysed reactions

In solid catalyzed heterogeneous reaction there is a simultaneous reaction and diffusion occurring in the catalyst particles. Such a system is generally difficult to simulate or obtain analytical expression for overall kinetics of reaction conversion.

Simulation of reaction-convection-diffusion equation inside porous catalysts was carried out and found to be useful to obtain internal mass transfer coefficients [Joshi et al., 2009]. It was applied in the context of gas phase reactions in porous catalysts like monolith of catalytic converters in automobiles.

The concept of microscopic reaction rates was explained with combination of mass transfer limitation in minute pores of catalyst. Multiscale modelling where the details of smaller scale are transmitted to larger scale features was explored. Simultaneous mass transfer and reaction were also simulated for porous media such as catalytic monoliths [Valdes-Parada et al., 2011].

Transport of charged drug molecules by electric field through porous membrane was attempted to model the transdermal and transmucosal delivery. This drug delivery model was carried out successfully using COMSOL Multiphysics involving simultaneous diffusion, convection and electrophoretic mobility [Moscicka-Studzinska and Ciach, 2012].

Irreversible gas-solid reactions were studied to understand the assumption of spatial uniformity in deriving the overall kinetic model. For reactor modelling purpose both non porous and porous catalysts were explored. A 1-D reactor model with a thin zone allocated for reaction was simulated using COMSOL Multiphysics. Difficulty in obtaining rate constants for heterogeneous catalysis is also recently reported [Pietrzyk et al., 2015].

Catalyst efficiency in micro-reactors was evaluated by using CFD simulation. The effect of internal heat input on increasing the conversion efficiency of certain industrial reactants like methane steam reforming was studied in micro scale CFD simulations [Butcher and Wilhite, 2016].

The mathematical modeling approach of single layered monolithic catalysts was extended to two layered concept. The effect of pore geometry on reaction kinetics in catalytic converter is also modeled and simulated using reaction diffusion and convection equation. The mathematical models were justified to take less computational time [Mozaffari et al., 2016].

Esterification of acetic acid with methanol in liquid phase using porous solid catalyst particle is one such example of reaction inside pores [Mekala et al., 2013]. It was one of the first papers to model esterification reaction using pore diffusion model. In this previous work there is an assumption of quasi steady state in simulating the dynamics of concentration profile inside the catalyst particle. The liquid side was assumed to be well stirred and hence a uniform concentration was attributed to all the species. This forms a Dirichlet boundary condition instead of flux continuity which is addressed in the present work. The general reaction is

$$CH_3COOH(A) + CH_3OH(B) \leftrightarrow CH_3COOCH_3(C) + H_2O(D) \quad (2.1)$$

A hydrodynamic flow pattern is developed in the dispersion of the catalyst particles and liquid reactants at sufficiently high RPM of the magnetic stirrer. At such high rates of mixing it is reasonable to assume a zero relative velocity between the catalyst particles and liquid reactants. For high mixing rates the external mass transfer resistance is negligible and there is no much effect in conversion of acetic acid beyond certain RPM as observed experimentally in batch reactors.

Similarly liquid phase reaction of propanol with isobutene in the presence of Amberlyst 35 catalyst was studied. Pressures up to 2 bar were also explored to examine its effect on reaction conversion. The Langmuir – Hinshelwood – Hougen – Watson (LHHW) and Eley – Rideal (ER) mechanisms were applied in obtaining the reaction rate equations [Titus et al., 2007].

Liquid phase esterification of propionic acid with propanol over an ionic exchange resin catalyst Dowex 50WX8 – 400 was studied to obtain the kinetics. A high stirrer speed of 900 RPM was used to exclude external mass transfer coefficient surrounding the catalyst particles. In addition to using ER type model activity coefficients were also used based UNIFAC models. Surface reaction was concluded as the rate controlling step [Ali et al., 2007].

In another study tertiary amyl methyl ether (TAME) was synthesized by reacting methyl butane with methanol using a cation exchange resin D005II. In this study also the mechanism of LH and ER were adopted along with Wilson method for determining the activity coefficients [Mao et al., 2008].

For this liquid state reaction there will be two rate constants one for the forward reaction and another for reverse reaction or it is equivalent to specify forward reaction rate constant k_f and equilibrium constant K_e. The reaction rate expression assuming it as elementary reaction is

$$-r_A = k_f \left(C_A C_B - \frac{C_C C_D}{K_e} \right) \tag{2.2}$$

This is applicable for homogeneous reactions but for heterogeneous reactions due to diffusional limitation inside the catalyst particles. It is well established that K_e equals 4.95 for Indion 180, an anionic resin catalyst [JagadeeshBabu et al., 2011].

Another research work on esterification of acetic acid with methanol over Amberlyst 36 as the porous solid catalyst has determined the K_e value as similar. The kinetic parameters determined were similar both for LHHW and ER models. It was found that equilibrium conversion for this reversible reaction was independent of temperature which implies that the reaction is neither exothermic nor endothermic [Tsai et al., 2011].

The cationic resin catalyst particles mentioned in the above studies are spherical in shape and with a diameter in the range of 400 – 1000 µm. The catalyst particles are porous in nature and hence the reactant liquids ingress into the catalyst particles, react and produce products which have to diffuse outward. Due to high catalytic activity inside the pores, the value of k_f will be higher inside the catalyst particle than in the surrounding bulk liquid.

When certain number of catalyst particles are added to the reactant mixture as shown in Fig. 1 (a), during stirring the particles are uniformly distributed in the liquid and hence each of the particle is surrounded by certain amount of liquid as shown in Fig. 1 (b).

Therefore to obtain the kinetics of heterogeneous catalytic reaction, the phenomena of reaction and diffusion occurring in this single cell consisting of one spherical catalyst particle

surrounded by the liquid is sufficient for simulation purpose. For this purpose it requires the expression for k_{f1} in the liquid phase and k_{f2} in the solid phase. If there is a data of conversion Vs time (X_A Vs t) for a reaction then it was shown for pore diffusion model that the initial rate of conversion dX_A/dt at time 0 is a linear function of catalyst loading w_c (gm of catalyst/cc of liquid) as below [Mekala et al., 2013].

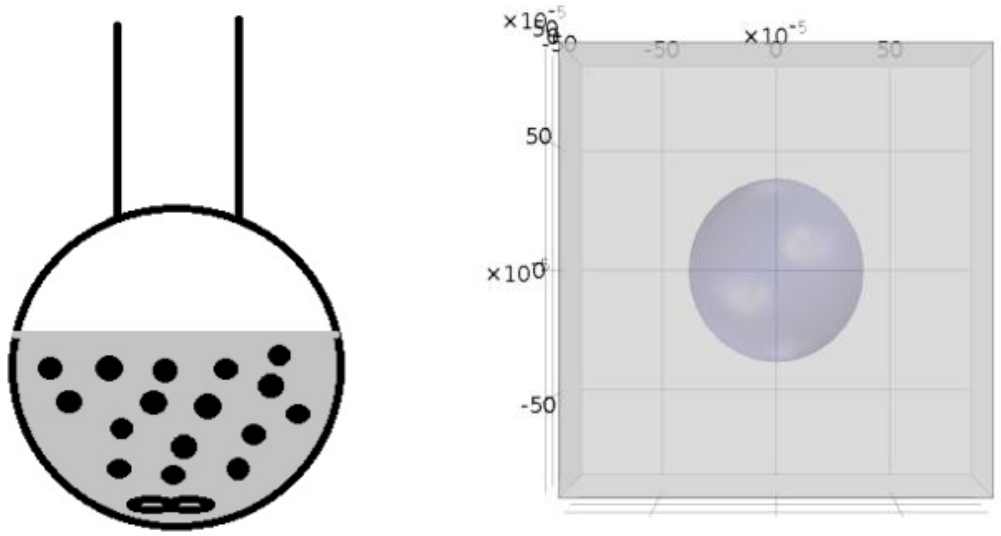

(a) **(b)**

Fig. 2.1 (a) Catalyst particles mixed in reactant product solution. (b) Catalyst particle surrounded by liquid.

$$\frac{dX_A}{dt} = \beta_{expt} w_c + C_{A0} k_{f1} \tag{2.3}$$

Here C_{A0} is the initial concentration of A. Hence from a plot of dX_A/dt vs w_c will provide the value of k_{f1} from the intercept. Here k_{f1} is the rate constant on the liquid side. The slope β_{expt} is related to the rate constant inside the particle k_{f2} by the following relationship [Mekala et al., 2013].

$$\beta_{sim} = \left(\frac{3D_{A2}}{R_p^2 \rho_p}\right)\left(\frac{\partial C_A}{\partial r}\right)_{r=R_p} \tag{2.4}$$

Where $D_{A2} * \left(\frac{\partial C_A}{\partial r}\right)$ represents the inward flux of A into the catalyst particle at its surface. The concentration profile $C_A(r)$ in Eq. (2.5) is the solution to the following reaction-diffusion equation inside the catalyst particle.

$$\frac{\partial C_A}{\partial t} = D_{A2}\frac{1}{r^2}\frac{\partial}{\partial r}\left(r^2\frac{\partial C_A}{\partial r}\right) - \varepsilon\left[k_{f2}C_A C_B - k_{b2}C_C C_D\right] \quad (2.5)$$

It depends on the choice of k_{f2} value which in turn provides such that β_{expt} is matched. Given the possibilities of evaluating k_{f1} and k_{f2} at any temperature, the following three methods are delineated.

Table 2.1 Description of model for evaluation of rate constants

Type of Model	k_{f1}	k_{f2}
Model 1 **Particle Scale:** Flux Continuity **Macro Scale:** Initial rate based on first two data of conversion	From homogeneous kinetics without catalyst	Adjust or optimize k_{f2} in Eq. (2.5) such that β_{sim} from Eq. (2.4) averaged over first 15 minutes matches with β_{expt} from Eq. (2.3). And with flux continuity at the surface of the catalyst particle implying that there exists concentration profile of A on both liquid and particle side.(experimental data is available for every 15 minutes)
Model 2 **Particle Scale:** Dirichlet Condition **Macro Scale:** Initial rate based on curve fitting of conversion	From intercept of Eq. (2.3)	Adjust or optimize k_{f2} in Eq. (2.5) such that β_{sim} from Eq. (2.4) evaluated at t=0 mathces with β_{expt} from Eq. (2.3). And with a assumption that the liquid side concentration of A is uniform (Dirichlet condition) is used as in Mekala et al. 2013

Model 3 **Particle Scale:** Flux Continuity **Macro Scale:** Initial rate based on curve fitting of conversion	From intercept of Eq. (2.3)	Adjust or optimize k_{f2} in Eq. (2.5) such that β_{sim} from Eq. (2.4) averaged over first 15 minutes matches with β_{expt} from Eq. (2.3). And with flux continuity at the surface of the catalyst particle implying that there exists concentration profile of A on both liquid and particle side.

2.2 Kinetics of esterification reaction

Reaction kinetic constants obtained from lab-scale experiments help in designing of large-scale chemical reactors either in batch or in a flow mode. Generally, the reaction in a lab scale is conducted in a batch reactor. The data of concentration of a key reactant verses time is used to fit either first-order model or a second-order model and so on. For example, the first-order rate law can be $-dC_A/dt = kC_A$. Here k is the rate constant which is further expressed as $k = k_0 * \exp(-E/RT)$, where k_0 is the pre-exponential factor and E is the activation energy in the Arrhenius form governing the reaction mechanism, R is the constant 8.314 J/gmol K, and T is the temperature of the reaction medium in K. To obtain k_0 and E, first, the reaction is conducted at least three different temperatures and the data is used [Fogler, 1999; Levenspiel, 1972]. In that process, k can be determined either by differential approach or integral approach. Similarly, this methodology is applied for such irreversible second-order reactions as well as to reversible catalysed reactions.

One example is that of esterification of acetic acid (A) with methanol (B) in the presence of a cationic resin catalyst leading to formation of methyl acetate (C) and water (D). [Banchero and Gozzelino, 2018; Tesser et al., 2005]. It was found in literature that the pseudo-homogenous rate law is expressed as Eq. (2.6) [JagadeeshBabu et al., 2011]:

$$-\frac{dC_A}{dt} = k_f C_A C_B - k_b C_C C_D \qquad (2.6)$$

The assumption involved in Eq. (2.6) is that the reaction rate proceed according to elementary stoichiometry. Further k_f and k_b depend on temperature and catalyst concentration. This is the concept of pseudo homogenous model.

If we incorporate the Arrhenius form of k_f and k_b in Eq. (2.6), then it becomes the following for 1:1 mole ratio of the reactants:

$$\frac{-dC_A}{dt} = k_{f_0} e^{\frac{-E_f}{RT}} C_A^2 - k_{b_0} e^{\frac{-E_b}{RT}} (C_{A_0} - C_A)^2 \quad (2.7)$$

2.3 Reactive Distillation-Experiments and Modelling

Reaction followed by separation is the conventional approach to produce mainly synthetic organic compounds [Luyben et al., 2004]. It widely involves a batch reactor and a series of distillation columns. Reactions are of two types namely irreversible and reversible. For an irreversible reaction the conversion of reactants can reach up to 100% if waited for infinite time in principle. Whereas reversible reactions reach a constant conversion in spite of long reaction time. Reversible reactions such as esterification reaction can be experimentally investigated to obtain the kinetics and determine the required time to reach 90% conversion or above as a practical limit [Mekala et al., 2013].

Batch Reactive Distillation (BRD) was studied for the system of acetic acid esterification with butanol to produce butyl acetate and water. Interestingly butyl acetate appears in distillate at higher mole fractions compared to other components although butyl acetate has the highest boiling point among the other components. This may be because the aqueous phase comes in the distillate. Batch reactor combined with a rectification column or distillation column conventionally termed as BRD has many advantages. The reaction in the reboiler is modeled using activity coefficients in place of concentrations as in Eq. (2.6). This system had the complication of aqueous and organic phases which were immiscible. The startup dynamics seems not captured detailed. The reaction is assumed to takes place in the reboiler only. The column is modeled as a number of theoretical stages at steady state [Venimadhavan et al., 1999].

In another study esterification of lactic acid with butanol was carried out to produce an ester butyl lactate and water. Here also organic and aqueous phases were found. The kinetic model was a simplified pseudo homogeneous expression where k_f and k_b of Eq. (2.6) were assumed to vary linearly with catalyst loading. Owing to this simplification the four kinetic parameters of Eq. (2.6) were estimated by ASPEN custom modeler. The reaction was assumed to occur in the liquid phase surrounding the catalyst. The experiment was carried out using continuous reactive distillation (CRD). A model for the distillation in the column was proposed to predict the distillate composition [Kumar and Mahajani, 2007].

A general heterogeneous reaction along with distillation similar to BRD was modeled using some assumptions such as reaction taking place in liquid phase of reboiler, negligible liquid hold up in the column. Selectivity of an intermediate product for the case of two step serial reaction was investigated by modeling. A non-dimensional parameter named Damköhler number representing the ratio of process time to reaction time was proposed and used as a characteristic number to determine selectivity. It was shown that the selectivity increases with decrease in Damköhler number. It lead to an optimum reflux ratio to yield highest possible concentration of intermediate product [Qi and Malone, 2010].

McCabe-Thiele method was proposed as a simpler approach to model rectification in BRD. The concept of reactive difference points was introduced to account for reaction in the liquid phase of column in combination with equilibrium stages. Both batch and continuous operations were modeled [Huerta-Garrido et al., 2004].

As a process intensification approach the applicable domain in the space of reflux ratio and number of stages was arrived at for conducting reactive distillation to recover the desirable product based on their individual boiling points and mixture properties [Muthia et al., 2018].

The principle of BRD is that if the product mixture in the reboiler is evaporated or distilled then lighter components will more present in the distillate and thereby provide a synergistic effect of reactor and distillation column in one unit process. Unlike reactive distillation by liquid catalyst [Agreda and Partin, 1984] this advantage of BRD is further enhanced if a solid catalyst is used for the reaction.

Esterification of acetic acid with methanol in the presence of solid cationic resin is a good example for study of BRD [Popken et al., 2000]. Catalyst loaded columns were also used for continuous reactive distillation [Gorak and Hoffmann, 2001; Taylor and Krishna, 2000]. It was reported that for above esterification reaction the mole fraction of methyl acetate the product in the batch reactor was 0.3 approximately. Hence to recover this methyl acetate the product mixture has to be distilled into four components namely methyl acetate, water, methanol and acetic acid. It happens that methyl acetate the product has the least boiling point among the four components. Hence if a rectification column is provided above the reboiler then the product the methyl acetate can be collected as distillate at the top of the column.

The kinetics of acetic acid esterification with methanol is available in literature for homogenous catalyst [Ronnback et al., 1997] and for solid catalyst [Patan et al., 2018]. It indicates that this esterification reaction is only mildly exothermic and the rate constants are available for the range of 40 ^{0}C- 70 ^{0}C.

2.4 Evaporation Rate Based Simulation of Distillation

Modeling of a distillation process with all its complexity is a challenging area of science and engineering [Taylor et al., 2003]. Yet because of the wide application of distillation in separating and purifying of organic liquids in particular there is a need for a reliable model. Also with the contemporary application of process control for achieving high degree of separation in distillation apparatus it requires a model amenable for real time computation which helps in suitable selection of controller type and their parameters settings [Mutalib and Smith, 1998]. Keeping in view the above design considerations and development of control strategies, the equilibrium models are often considered as deficient [Ramesh et al., 2007]. Alternately rate based model requires a distributed parameter model approach [Ivo and Eugeny, 2007]. In principle rate based model can be implemented if the values of evaporation rate constants and the activity coefficients are available for a component liquid in a mixture at both sub and super-heated condition relative to its boiling points. If the rate based model is successful for steady state prediction of a packed column performance then it can be extended to variants such as reactive distillation and divided column processes for efficient design of such equipment [Taylor and Krishna, 2000; Jianjun et al., 2002].

Although steady state simulations can predict the distillate composition accurately, it still remains perplexing about the start of a packed bed distillation column. This is because as the reboiler contents are heated the generated vapor moves upward due to buoyancy in the voids of the packed column. As the vapor is passing upwards a portion of it condenses and trickles down along the packing. It is difficult to establish whether the packing surface area can be taken as equal to the actual interfacial area between vapor and liquid. So, there is some finite start up time required for establishment of hydro dynamically developed vapor and liquid flows in the packed column. In addition to this thermal steady state also takes some more time for composition in the distillate to reach a steady state value in the case of a batch with total reflux or a continuously fed column. In principle a rate based model also has to incorporate material and energy balance along with interfacial evaporation models [Higler et al., 1999; Dhole and Linnhoff, 1993; Silva et al., 2003]. A multi component distillation in a batch column was modelled assuming mass transfer resistance on both liquid and vapor phase with Maxwell – Stefan equations [Kreul et al., 1999]. The rate based model was applied to a tray column with assumption of completely mixed liquid phase and plug flow for vapor phase. The error in prediction was found more for higher heat input rates [Alopaeus and Aittamaa, 2000]. It was found that the dynamic rate based model needs simplification in order to carry out the computation. Mass transfer coefficients were suggested to be taken as constants for reasonable accuracy in prediction [Peng et al., 2003]. The rate based model was applied to a tray column for a ternary system. It was further used in economic analysis for finding optimum reflux ratio [Mortaheb and Kasuge, 2004]. The rate based model was applied for a ternary system in a dividing wall distillation column for a reactive system with pseudo homogeneous kinetics [Mueller and Kenig, 2007].

2.5 Gaps Identified in Literature

In literature there is an assumption of quasi steady state in simulating the dynamics of concentration profile inside the catalyst particle [Mekala et al., 2013]. The liquid side was assumed to be well stirred and hence a uniform concentration was attributed to all the species. This forms a Dirichlet boundary condition instead of flux continuity which is addressed in the present work.

There are certain issues or gaps of obtaining rate constants from three experiments conducted at different temperatures using pseudo homogeneous model as usually stated in the literature [Jagadeesh babu et al., 2011]. For example at a temperature of 353 K it is difficult to mix acetic acid and methanol in liquid form since methanol would be a vapor at this temperature. Also the reactants have to be pre-heated to the desired temperature before the mixing to conduct an isothermal reaction. Moreover a controller for heat input to the reactor is necessary if it is an endothermic reaction or if there are heats of mixing between the newly formed products and the reactants. Therefore it may be a difficult proposition to claim a perfect isothermal reaction data. Hence an alternative to this is proposed in this work that is to provide a step heat input rate to a batch reactor in which the reactants start at room temperature. With the supply of heat there will be temperature dynamics as well as concentration dynamics. But if both temperature verses time and concentration verses time are gathered then that data can be used to optimally determine the four unknown constants of kinetics (k_{f_0}, E_f, k_{b_0}, E_b) from use of Eq. (2.4) by latest optimization tool set such as genetic algorithm in MATLAB.

The gap addressed in this work is to determine the mass transfer coefficient correlations from suitable experiments and use for rate based modeling of distillation and further validation. In this work a batch distillation apparatus consisting of a reboiler, packed column and a condenser is fabricated and used. A binary system of non-reacting liquids and non-azeotropic liquids is chosen and its separation into higher light component in the distillate is studied experimentally and also modeled and simulated using a rate based model approach. Certain assumptions are made in order to make the set of equations solvable. Lab scale experiments were conducted to determine the evaporation mass transfer coefficients of the component liquids in pure form as well as in mixture. Unlike the constant temperature in the reboiler, a constant heat input is applied in order to analyze the performance of the above distillation column with respect to distillate composition, variation of composition along the height of the column. Also the transient of temperature in the reboiler and the time for onset of distillate are obtained experimentally. The model prediction of distillate composition is validated against the experimental data which is found to be good.

The gaps identified in literature and that were addressed are: (1) packed bed rectification column (2) detailed capture of start-up dynamics (3) jacketed rectification column with hot water circulation (4) constant heat input to the reboiler. In the present work, the preliminary experiments on BRD show that it takes a while for distillate to start as also observed for other applications in literature (Peng et al. 2010; Yang et al. 2007; Xu, Afacan, and Chuang 1999).This is because the vapour generated in the reboiler has to heat up the packing and the walls of the column before reaching the condenser and forming the distillate. As a novelty the column in present experiments is provided with a jacket through which hot water can be supplied at a desired value in the range of 40 ^{0}C- 60 ^{0}C. Use of jacketed reboiler was also reported in literature (Jana and Maiti 2013). The purpose of such operating condition as wall heating is to decrease the time for onset of distillate. Alternately the high heat input rate to the reboiler can also be used to achieve the same. But due to coupled phenomena of reaction kinetics and distillation dynamics there may be some optimal combination of heat input rate to the reboiler and the wall temperature of column to obtain high purity of methyl acetate the product in distillate as well as high throughput unlike the temperature controlled BRD (Sørensen and Skogestad 1994). The reflux ratio in the top condenser is maintained as infinity implying that entire distillate is circulated back to the column unlike in literature (Kim, Hong, and Wozny 2002). Total reflux was chosen because it gives the highest possible purity of the lighter component in distillate.

CHAPTER 3
OBJECTIVES OF THE STUDY

Objectives of the Study

1. To evaluate the parameters of pore diffusion model of heterogeneous catalysis at particle scale with various types of boundary conditions at particle-liquid interface: It helps to obtain appropriate values of kinetic constants and parameters
2. To determine kinetic constants of a heterogeneously catalyzed reversible reaction from dynamics in a batch reactor with constant heat input rate: It is to be explored whether non-isothermal data can lead to the estimation of kinetic constants based on pseudo homogenous reaction rate models.
3. To develop and validate evaporation rate based model for binary non reacting mixture in a packed distillation column for steady state condition with total reflux: A case study will be taken up to develop a model and compare it with experimental results regarding the distillate composition.
4. To study experimentally the effect of wall heating on various characteristics such as distillate composition, onset of distillate, time to reach bubble point in reboiler and product purity in distillate in a batch reactive distillation (BRD): The start-up dynamics will be obtained to understand the role of various innovating operations such as wall heating on the onset of distillate and its purity.
5. To develop and validate the model and simulation using rate based approach for four component Reactive Distillation (RD) system i.e., catalytic esterification of acetic acid with methanol leading to methyl acetate and water formation in a batch reactor/reboiler mounted with a packed bed distillation column and total reflux at the top: A novel constant heat input rate method will be applied on this system where solid catalyst like INDION 180 and 190 are utilised. Composition profiles along the column will also be applied.

CHAPTER 4
EXPERIMENTAL STUDIES

Experimental Studies

4.1 Materials and Methods

Esterification of acetic acid with methanol is chosen as the reaction system for the present study. In particular this reaction is studied under the effect of cationic solid resin catalyst such as INDION 190 available commercially. The catalytic esterification reaction goes as $CH_3COOH + CH_3OH \leftrightarrow CH_3COOCH_3 + H_2O$ in liquid state. The catalyst specifications of INDION 180 and INDION 190 are tabulated in Table 4.1.

Table 4.1 Physical properties of INDION 180 and Indion 190 catalysts.

Physical Property	**INDION 190**	**INDION 180**
Manufacturer	Ion Exchange India Limited	Ion Exchange India Limited
Shape	Beads	Beads
Physical Form	Opaque, faint dark grey coloured	Opaque, faint dark grey coloured
Size (µm)	725	725
Apparent Bulk Density (g/cm^3)	0.55-0.60	0.55-0.60
Surface area (m^2/g)	28-32	28-32
Pore Volume (ml/g)	0.32-0.38	0.32-0.38
Max Operating Temperature (^0C)	150	150
Hydrogen ion capacity (meq/g)	4.7	5.0
Matrix Type	Styrene – DVB	Styrene – DVB
p^H range	0-7	0-7
Resin type	Macro porous strong acidic	Macro porous strong acidic
Functional group	$-SO_3^-$	$-SO_3^-$
Ionic group	H^+	H^+

The experimental apparatus used for present study is shown with Fig. 4.1 (a) and Fig. 4.1 (b).

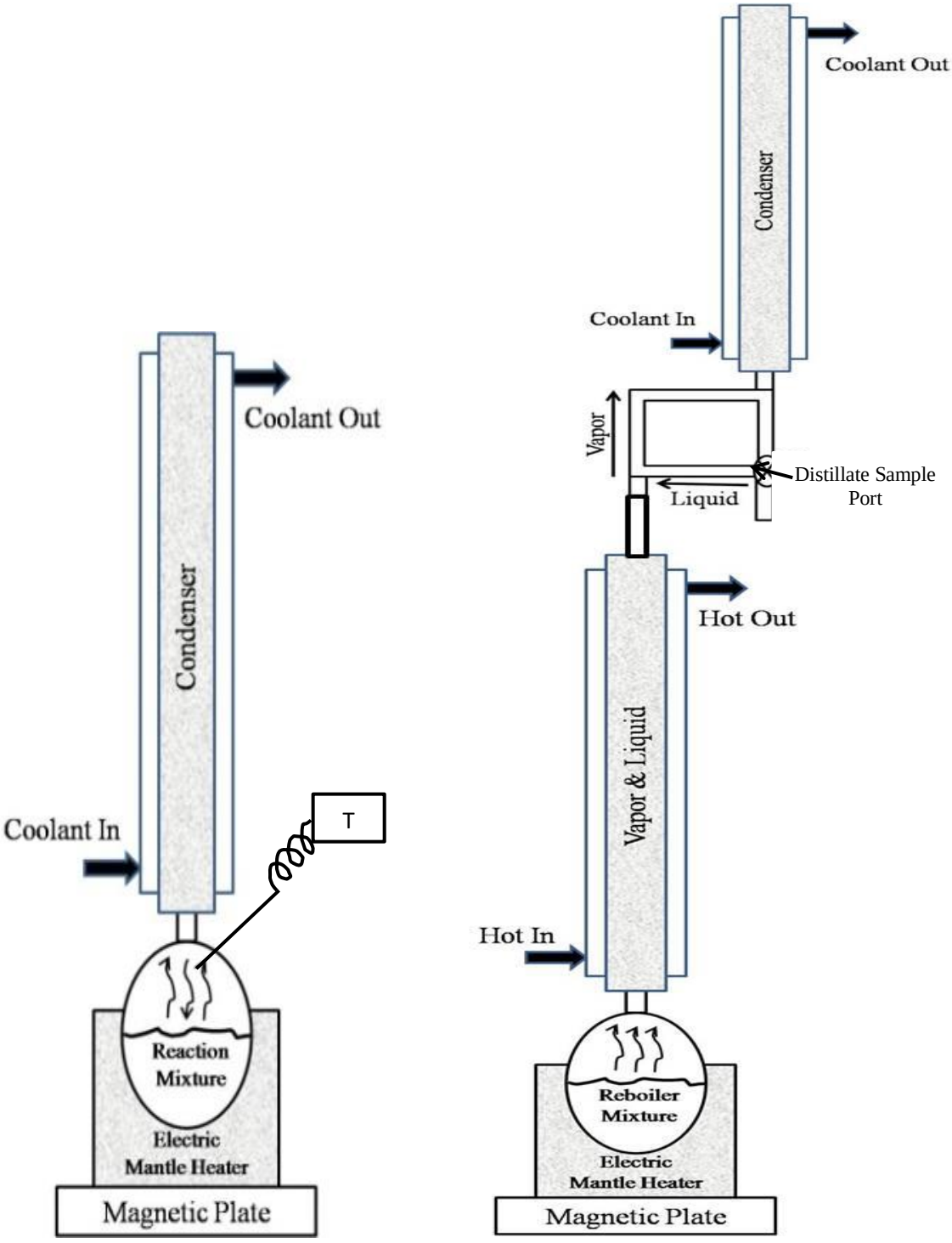

(a) **(b)**

Fig. 4.1 (a) Schematic experimental apparatus for study of kinetics (b) Schematic representation of the experimental apparatus used in this study for BRD.

The apparatus for batch reaction kinetics as in Fig. 4.1 (a) consists of a one litre spherical glass reactor (3-neck round bottom flask) surrounded by a heating mantle and magnetic stirrer plate at the bottom. A condenser with cold water supply at 25 ^{0}C is provided on top so that the vapours are immediately condensed back to the reactor. A PT-100 temperature sensor is also used with 0.1 ^{o}C accuracy to monitor the temperature of the reaction mixture in reboiler. The heat input rate to the reactor can be calculated from the product of voltage supplied and the resulting current of the heater from the measurement with the help of digital voltmeter and ammeter. A magnetic stirrer is present inside the reaction mixture to enable complete mixing of liquids and catalyst particles. The mantle heater is placed over magnetic plate for rotating the magnetic stirrer.

The apparatus is as in Fig. 4.1 (b) for Batch Reactive Distillation (BRD) studies consists of a reboiler surrounded by kettle heater cum a packed column placed above it with provision for circulating hot water in the jacket. At the top a condenser is provided with closed top and circulating coolant water at sufficient flow rate to have complete condensation. The reboiler is fitted with a PT-100 temperature sensor. The electric heater is provided with a voltage variac so that the heat input rate can be adjusted to a desired value in terms of watts which can be calculated from the product of voltage and current passing through the electric heater. An external hot water bath is available to provide hot circulating water to the jacket of the column. The reboiler is a round bottom flask with three neck openings and made of borosil glass. The column is also made of borosil glass with inner diameter of 5 cm and height of 50 cm with packing as raschig rings of about 1 cm hollow cylinders which are made of glass. A perforated plate is provided at the bottom of the column to avoid slippage of packing. At the top of the column suitable glass tube loop is provided so that the vapor goes up into the condenser, gets condensed and passes downward past the two way valve and back into the column. The two way valve is kept in closed condition to have total reflux implying that entire condensate is refluxed back to the column. Only a couple of millilitres (2 ml) of distillate was collected from the sample port of reflux at steady state. The entire apparatus is ensured to have leak proof for vapors.

The experimental procedure for BRD is as follows: Both reactants acetic acid and methanol of 2.5 moles each are poured into the reboiler. Catalyst at a loading of 0.025 g/ml is added. Immediately the variac of electric heater is set to a desired voltage and this marks the beginning of the reaction (time=0). The temperature of the reboiler contents are recorded for every 2 ^{0}C

rise in temperature from the digital display with 0.1 ^{0}C precision. The column outer surface can be provided with three different boundary conditions (1) Hot water circulating along the jacket. (2) Without any hot water and with air filling the jacket space and outermost glass surface of the jacket open to ambient air. (3) Similar condition as in (2) but the outermost surface is covered with insulating cotton. The heating is continued throughout the experiment at constant rate. When the temperature increases in the reboiler it was found that vapor raises and its condensate is also visible in the column. After certain time the vapor enters the top condenser and the condensate flows down back to the column. The time taken for the first distillate drop to form at the condenser and filling the sample port is recorded as the time for onset of distillate. Form this point of time another 20-30 minutes of heating the reboiler is continued so that the thermal equilibrium or bubble point is reached in the reboiler as well as constant distillate flow is observed at the top of the column. A sample is collected from the distillate and stored. In some experimental runs a sample is taken from the reboiler. The operating conditions varied are heat input rates as 50 W,100 W and 150 W approximately. Another variable operating condition is the nature of boundary conditions applied for the column (three different wall temperatures), only air and only air with insulation. The resulting temperature verses time dynamics for a wall temperature of 50 ^{0}C with different heat inputs is also presented in Fig. 4.9. The same procedure was used for conducting distillation of binary non – reacting mixture of benzene and toluene. The composition of the distillate is analysed using gas chromatography (GC). The make and model of the GC were YL 6500 South Korea. There are fifteen samples of distillate to be analysed for methyl acetate. A couple of samples from the reboiler at the end of experiments are also analysed to evaluate the reaction equilibrium constant as a validation or check.

4.2 Kinetics from non-isothermal reaction

The schematic of the experimental set-up is shown in Figure 1. It consists of a spherical glass reactor surrounded by a heating mantle and magnetic stirrer plate at the bottom. A condenser is provided so that the vapours are immediately condensed back to the reactor. A PT-100 temperature sensor is also used with 0.1°C accuracy to monitor the temperature of the reaction mixture. The heat input rate to the reactor can be calculated from the product of voltage supplied and the resulting current of the heater with the help of digital voltmeter and ammeter. A magnetic stirrer is present inside the reactor to enable complete mixing.

Initially, 200 ml of methanol is added to the reactor vessel. This corresponds to 4.95 gmol of methanol. Then 283 ml of acetic acid is added to methanol such that the number of moles of acetic acid is also 4.95 gmol. As per the literature recommendation, 12.075 g of catalyst in the form of INDION 190, a cationic resin catalyst in the form of fine particles, is added. With the help of a stopwatch, the time is recorded and the temperature is also recorded frequently. For every 5°C rise in temperature, a 2 ml sample is withdrawn and titrated against 1 N NaOH solution to obtain the concentration of acetic acid from a further simple calculation. $N_A V_A = N_{NaOH} V_{NaOH}$, where N_A is the normality or concentration of acetic acid, V_A = 2 ml, N_{NaOH} = 1 gmol/l and V_{NaOH} is the volume of titrant in millilitres. Phenolphthalein is used as indicator which turns from colourless to pale pink upon completion of titration or complete neutralisation of acetic acid.

The obtained temperature and concentration dynamics for two different heat input rates of 32 W and 50 W are shown in Fig. 4.2 and Fig. 4.3 . The concentration of acetic acid is on right y-axis and reactor temperature is on left y-axis. Time is represented on the x-axis.

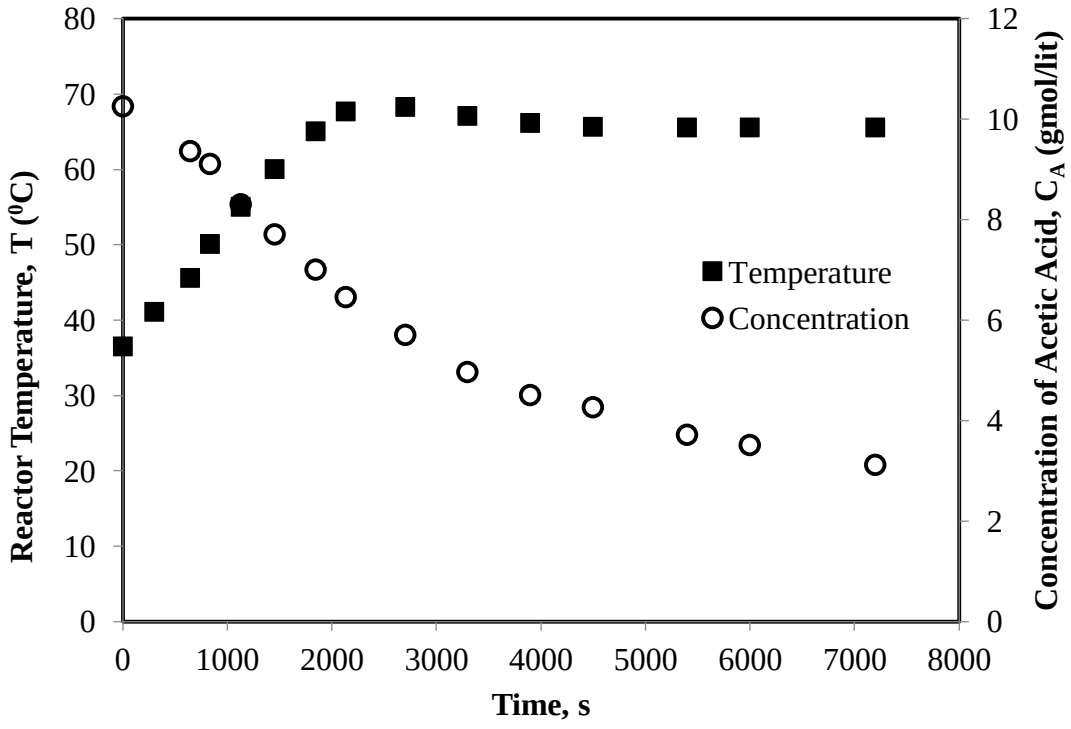

Fig. 4.2 Experimental temperature and concentration dynamics in reactor for 32 W.

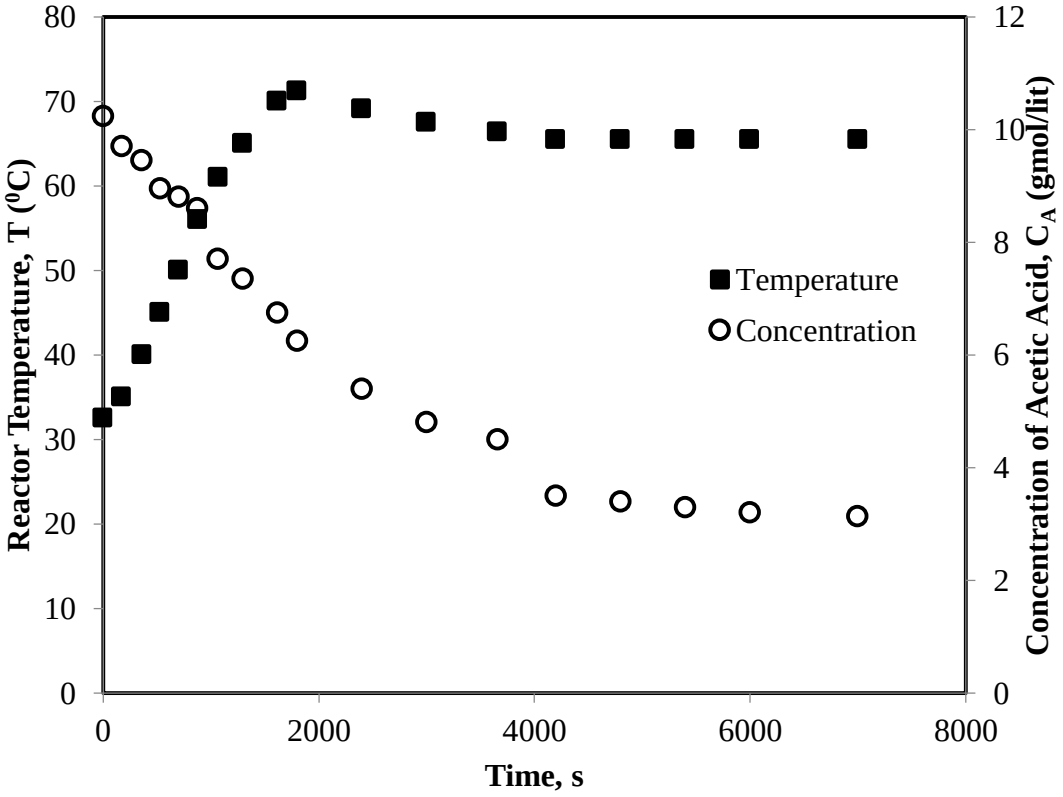

Fig. 4.3 Experimental temperature and concentration dynamics in reactor for 50 W.

4.3 Distillation of non-reacting binary mixture

The present chosen system involves four components out of which two are reactants and two other are products of esterification. Since there would be combined effect of distillation and reaction, it was planned to develop rate based model first for binary non-reacting system. The chosen binary system is a mixture of benzene-toluene. The applicability of rate based model for packed bed distillation can be validated with more rigor for a non-reacting mixture. The reason is that ΔH_R (heat of reaction) and other effects like azeotrope formation at or near atmospheric pressure are not there for benzene-toluene mixture.

It is intended to start with an equimolar mixture if benzene and toluene and obtain higher benzene fractions which is the lighter component at the top of the column. The apparatus is a batch packed column with reflux facility. In the first part of the experimental study the evaporation rate constants of benzene and toluene are obtained. In the second part of the experimental study the dynamics of reboiler temperature and steady state distillate composition are determined for various heat input rates to the reboiler. A digital refractometer is used to

measure the refractive index of benzene-toluene mixtures and the corresponding composition of any sample is determined using a pre-calibrated chart.

4.3.1 Determination of evaporation rate constants

When a mixture of two completely miscible liquids is heated at an infinitesimally small rate then the mixture reaches its bubble point or boiling point in case of pure liquids at steady state. At this bubble point the temperature remains constant for a small evaporated quantity. The procedure adopted is that a clean empty beaker of 50 ml volume filled with a mixture of benzene and toluene is kept on a hot plate until a steady state temperature is reached. The schematic of this experiment is shown in Fig. 4.4.

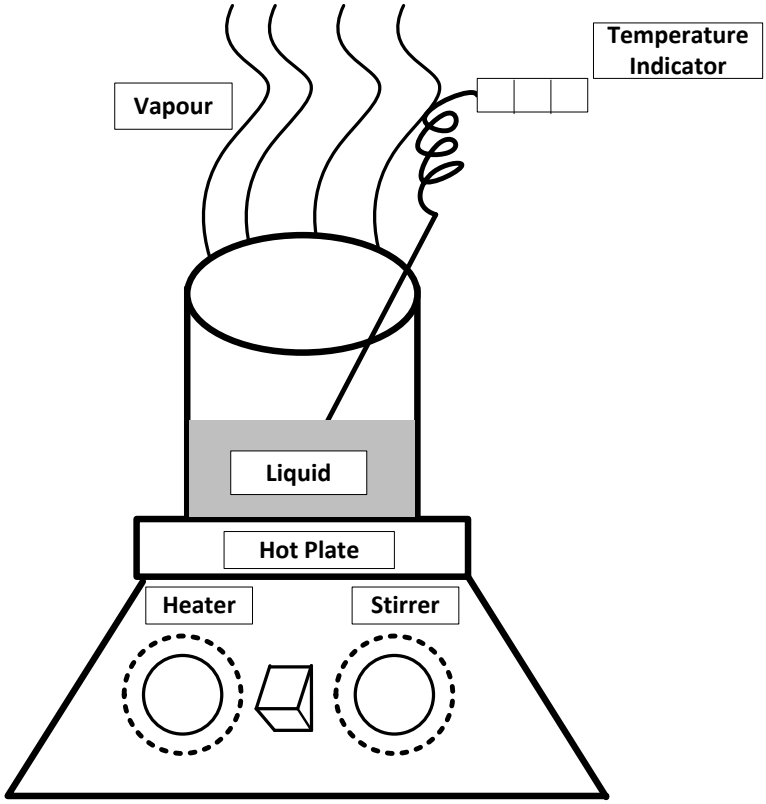

Fig. 4.4 Schematic of a heated beaker used to evaluate the evaporation rate of a liquid.

At this juncture the beaker is shifted onto a digital weighing balance with an accuracy of 1 mg. the time taken for one gram loss in weight of the beaker containing the liquid mixture is noted. This data is tabulated in Table 4.1.

Table 4.2 Experimental data pertaining to the evaporation of benzene-toluene mixture.

Benzene Volume (ml)	Toluene Volume (ml)	Bubble Point Temperature (^oC)	Time taken for one gram loss at Bubble Point (s)
50	0	81.2	27.2
40	10	83.5	25.4
30	20	90.4	22.8
20	30	95.5	22.5
10	40	103.2	24.9
0	50	110.3	26

Let the components be labelled as benzene (A) and toluene (B). To calculate the evaporation mass transfer coefficients of benzene (K_A) and toluene (K_B) the following equations are used similar to the evaporation of pure liquids [Himus and Hinchley, 1924].

Evaporation flux of benzene (A) = $K_A . A_c . a_c . (x_A . p_A^{sat} - y_A . p_t)$ 4.1(a)

Evaporation flux of toluene (B) = $K_B . A_c . a_c . (x_B . p_B^{sat} - y_B . p_t)$ 4.1(b)

Where,

x_A is mole fraction of component 'A' in liquid phase

y_A is mole fraction of component 'A' in vapor phase

K_A is mass transfer coefficient of component 'A' (gmol/m^2.atm.s)

p_A^{sat} is saturated vapor pressure of component 'A' (atm)

x_B is mole fraction of component 'B' in liquid phase

y_B is mole fraction of component 'B' in vapor phase

K_B is mass transfer coefficient of component 'B' (gmol/m^2.atm.s)

p_B^{sat} is saturated vapor pressure of component 'B' (atm)

p_t is Total pressure or atmospheric pressure (atm)

In the above equations Eq. 4.1(a) and Eq. 4.1(b) the mole fractions y_A and y_B of the evaporating liquids in air are assumed negligible and that the mole fractions in the liquid are assumed same as the starting mixture compositions. The evaporation flux in kg/m^2.atm of A and B are evaluated using the following formula.

$$\text{Evaporation flux} = \frac{\Delta m}{\Delta t}\frac{1}{A_{c,b}MW} \qquad 4.2(a)$$

Where,

Δm = mass of evaporated liquid (g)

Δt = time of evaporation (s)

$A_{c,b}$ = cross sectional area of the beaker (m^2)

MW = molecular weight of liquid (g/gmol)

By substituting the result of Eq. 4.2(a) in Eq. 4.1(a) and Eq. 4.1(b) the corresponding evaporation mass transfer coefficients are obtained and plotted in Fig. 4.5 and Fig. 4.6. The p_A^{sat} and p_B^{sat} are the saturation vapor pressures of A & B evaluated using Antoine equation.

$$p_A^{sat} = 10^{\left(4.02232-\frac{1206.53}{220.291+T}\right)} \qquad 4.2(b)$$

$$p_B^{sat} = 10^{\left(4.0854-\frac{1348.77}{219.976+T}\right)} \qquad 4.2(c)$$

Here vapour pressure unit is atm and temperature is in ^{0}C

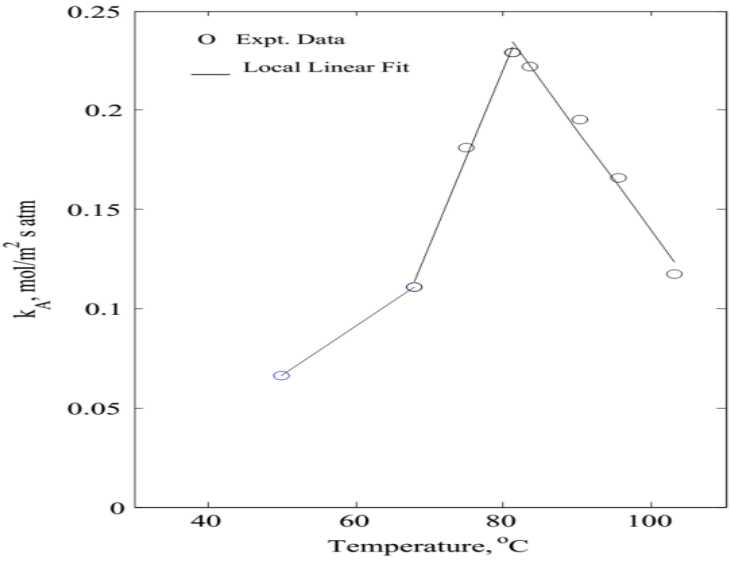

Fig. 4.5 Evaporation mass transfer coefficients of benzene (A) at various temperatures.

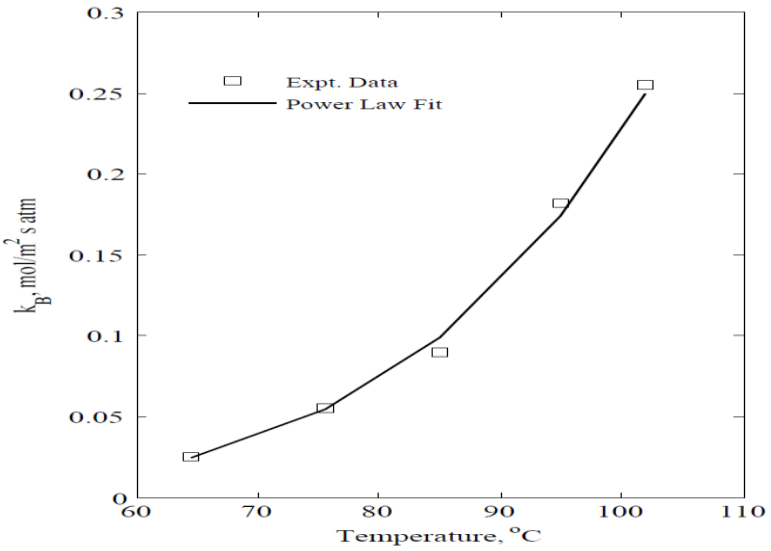

Fig. 4.6 Evaporation mass transfer coefficients of toluene (B) at various temperatures.

It can be observed from Fig. 4.5 that K_A exhibits three different slopes for the entire temperature range of applicability to distillation as such the fitted linear expressions for K_A vs T are as given below in Eq. 4.3(a), Eq. 4.3(b) and Eq. 4.3(c).

$K_A = 0.0025*T + 0.0578$ for $T<68°C$ 4.3(a)

$K_A = 0.009*T – 0.4961$ for $68°C <T<81.2°C$ 4.3(b)

$K_A = -0.005*T+0.6443$ for $T>81.2°C$ 4.3(c)

Whereas the expression obtained for K_B vs T from Fig. 4.6 is of power law model type as given below in Eq. (4.4) with T in ^0C

$$K_B = 1.5339*10^{-11}*T^{5.0844} \quad (4.4)$$

The regression R-square value for all the above fits were very close to 1 which indicates a good fit. For benzene the boiling point is 81.2 °C where as that of toluene is 110.3 °C. Hence as we heat a mixture of benzene-toluene at some point of temperature the benzene is in superheated state thereby increasing p_A^{sat} by large factor exponentially. Hence, when mass transfer coefficient K_A is calculated from Eq. 4.1(a), the magnitude of it drops below that of its value at its normal boiling point since the evaporation flux increases slowly. Therefore, there is a

maximum in mass transfer coefficient of benzene at 81.2 ^{0}C in the given range of temperatures i.e., 50 °C – 110 °C approximately.

4.3.2 Batch distillation under total reflux

Experiments were carried out on binary mixture of benzene and toluene at various reboiler heat input rates. The experimental apparatus used is shown schematically in Fig. 4.1(b). It consists of a round bottom flask of one-liter capacity surrounded with an electric heater. A temperature probe of PT-100 type is provided in the reboiler with a digital display to record the temperature manually. The heater power can be varied by changing the applied voltage with the help of a variac. An ammeter is provided to display the current passing through the heater. By taking the product of applied voltage and current the power input is calculated. A packed column of 0.5m height is provided on the top of the round bottom flask. The packing was made of raschig rings of approximately 1 cm size. Both the packing and the column wall are made of the glass. The top of the column is connected to a vertical condenser with a three-way valve and recycle tubing. The coolant water is available at room temperature of 30 ^{0}C which is circulated in the vertical condenser at a moderate flow rate so that there are very less vapor losses.

For all the experimental runs a mixture of 0.5 mole of benzene and 0.5 mole of toluene is added to the reboiler. It gives a volume of 450 ml. The heater is set to a certain applied voltage with the help of variac. The recorded voltage, current and calculated power are tabulated in Table 4.2 for three runs.

Table 4.3 Experimental data at steady state.

Run No	Voltage (Volts)	Current (Amp)	Power (Watts)
1	104	0.503	52.3
2	144	0.7	100.8
3	175	0.853	149.2

The temperature indicated by a sensor for the reboiler liquid is noted at regular time intervals. Actually the time is noted for every 1 ^{0}C rise in temperature. The obtained temperature dynamics are plotted in Fig. 4.7. It can be observed that there is an initial ramp owing to sensible heat supplied to the liquid. This ramp time decreases as the heat supply rate is increased. The time to reach the steady state or bubble point temperature (94.2 ^{0}C for 0.5 mole fraction of benzene) is noted and plotted in Fig. 4.8. The distillate doesn't appear or formed immediately as the bubble point is reached. It was observed that the hot vapor keeps moving up in the column at a slower rate than the temperature ramp rate of the reboiler liquid. This is because the hot vapor losses heat owing to the sensible heat required for heating the packing and the glass wall for the column. The time at which the first droplet of distillate appeared was also noted as the time of onset of distillation and it is plotted in Fig. 4.9 for various heat input rates.

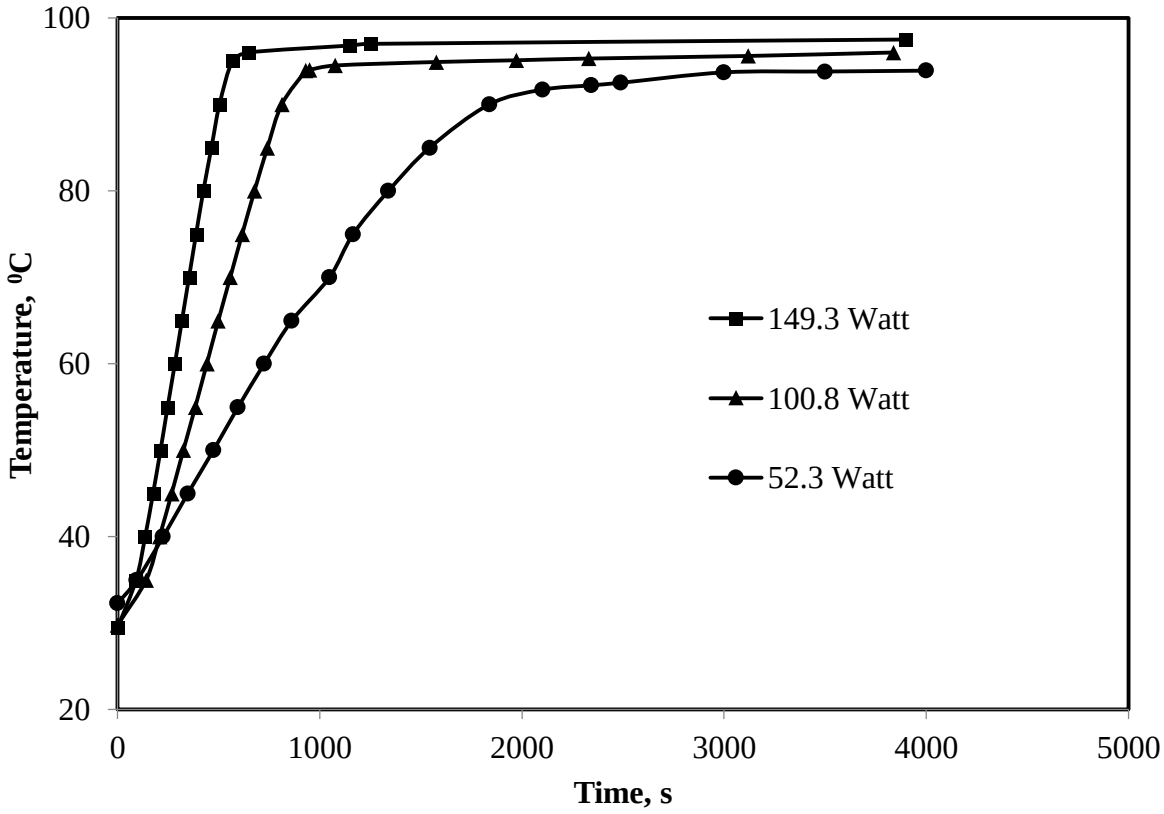

Fig. 4.7 Experimental temperature dynamics for three different heat inputs to the reboiler for mixture of benzene-toluene with a mole fraction of 0.5.

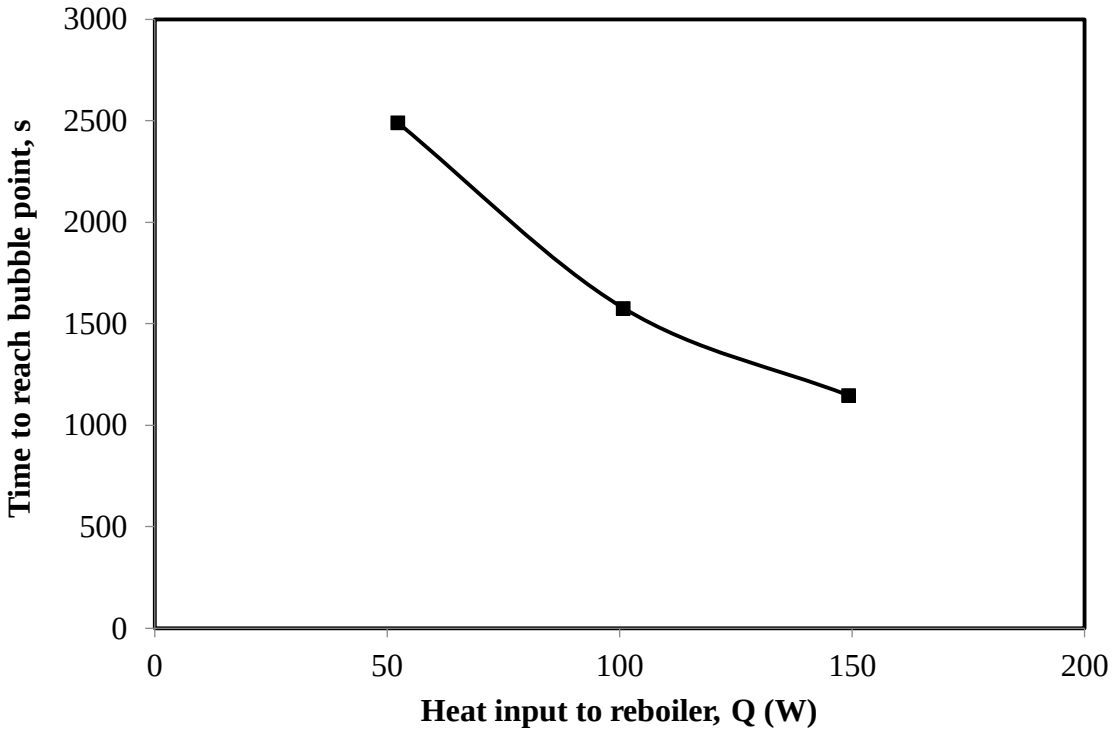

Fig. 4.8 Experimental time to reach the bubble point for three heat inputs to the reboiler.

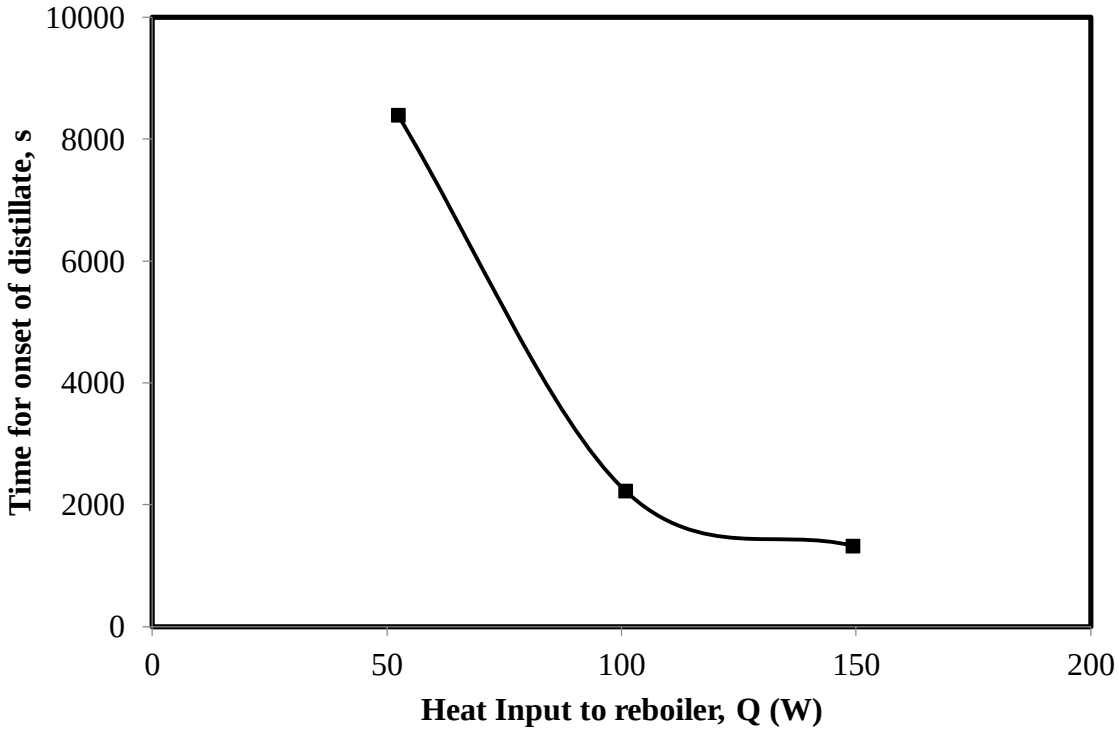

Fig. 4.9 Time for onset of distillation for three heat inputs to the reboiler.

The distillate composition was measured using a digital refractometer and pre-calibrated data is presented in Table 4.4 and as a chart in Fig. 4.10.

Table 4.4 Refractive index of a benzene-toluene mixture

Volume fraction of benzene (A)	Volume fraction of toluene (B)	Refractive Index (R.I.) at 30 °C
1	0	1.4963
0.8	0.2	1.4958
0.6	0.4	1.495
0.4	0.6	1.4942
0.2	0.8	1.493
0	1	1.4919

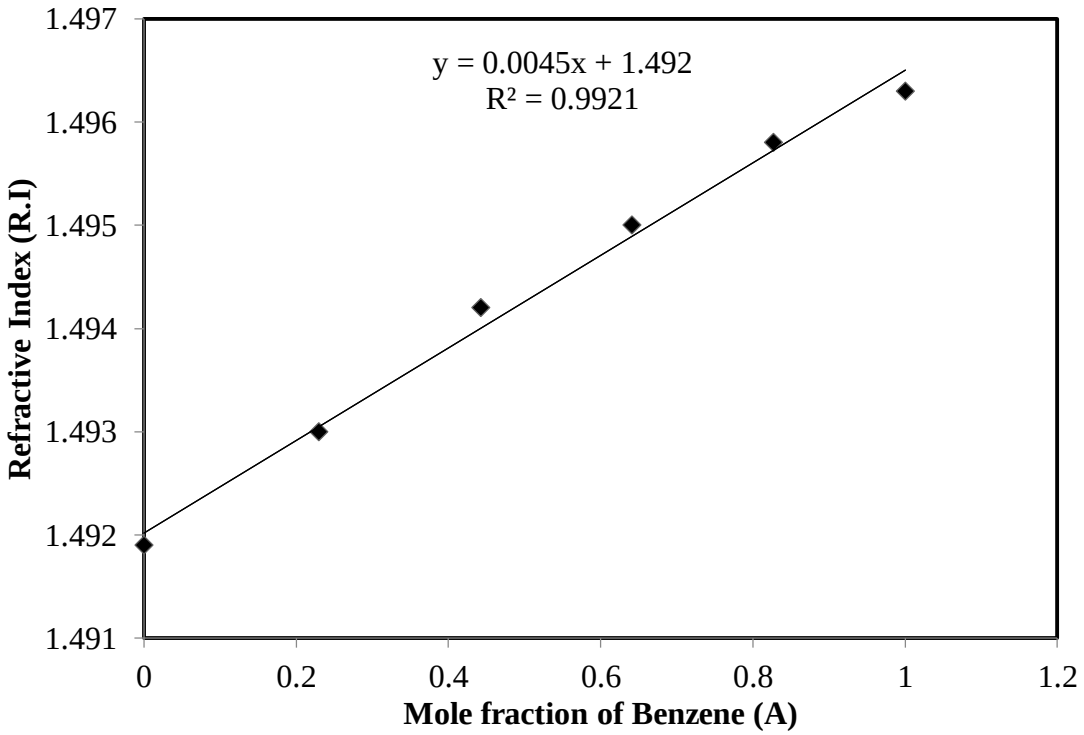

Fig. 4.10 Calibration chart of Refractive Index vs mole fraction of benzene in benzene-toluene mixture at temperature of 30 ^{0}C.

The measured distillate composition in terms of the mole fraction of benzene is plotted for three different heat inputs in Fig. 4.11.

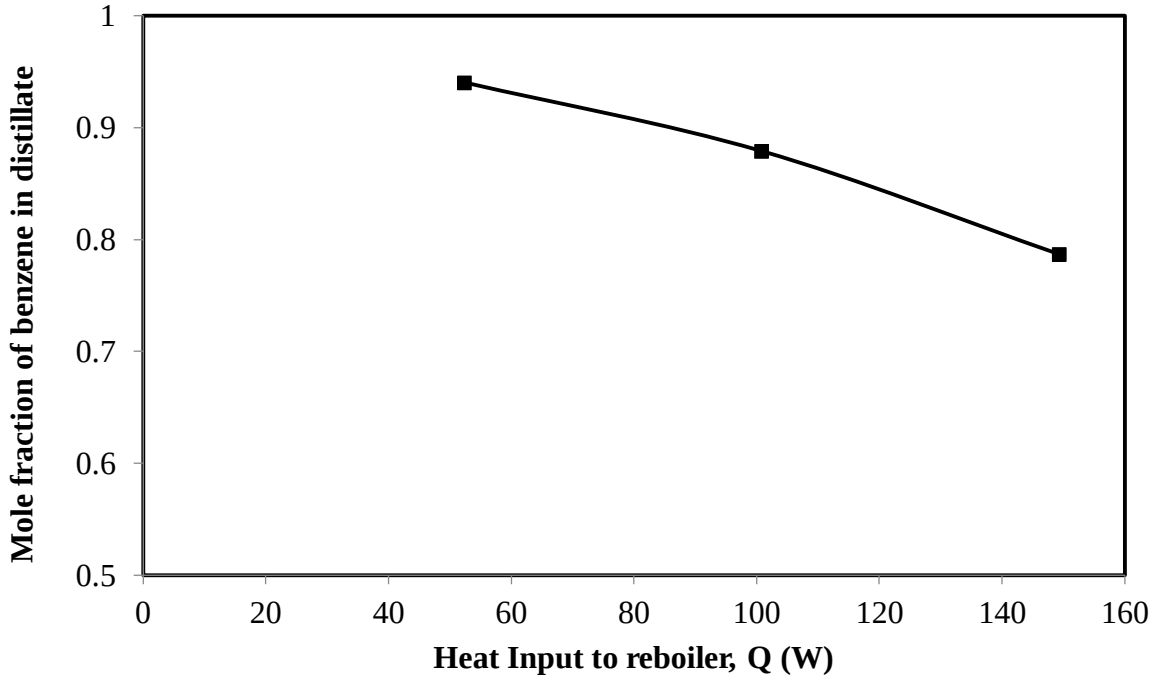

Fig. 4.11 Experimental distillate composition of benzene for three heat inputs to the reboiler at total reflux.

It can be observed from Fig. 4.11 that the distillate purity of benzene is highest for lowest heat input rate. Also the distillate composition seems to decrease monotonically with the applied a heat input rate to the reboiler. Qualitatively lower heat inputs have lower vapor and liquid flow rates leading to high contact residence time in the column giving higher rectification. This particular aspect will be predicted by a steady state rate based model in the chapters 5 & 6.

4.4 Batch reactive distillation - Esterification of Acetic Acid

Esterification of acetic acid with methanol is chosen as the reactive system for the present study. In particular this reaction is studied under the effect of cationic solid resin catalyst such as INDION 190. The kinetics of the above reversible reaction is documented in the literature [Mekala et al., 2013; Patan et al., 2018]. It was reported that the equilibrium constant based on molecular order of the reaction rate is K_e=5.0 approximately. This reaction is known to have very minimal exothermicity. Therefore the K_e value was obtained nearly the same over a temperature range of 40 ^{0}C to 70 ^{0}C. The kinetics of the reaction based on catalyst particle scale is also available from a recent literature [Patan et al., 2018]. The esterification reaction goes as

$CH_3COOH + CH_3OH \leftrightarrow CH_3COOCH_3 + H_2O$ in liquid state. The experimental apparatus used for present study is shown in Fig. 4.1(b). It consists of a reboiler surrounded by kettle heater cum a packed column placed above it with provision for circulating hot water in the jacket. At the top a condenser is provided with closed top and circulating coolant water at sufficient flow rate to have complete condensation. The reboiler is fitted with a PT-100 temperature sensor. The electric heater is provided with a voltage variac so that the heat input rate can be adjusted to a desired value in terms of watts which can be calculated from the product of voltage and current passing through the electric heater. An external hot water bath is available to provide hot circulating water to the jacket of the column. The reboiler is a round bottom flask with three neck openings and made of borosil glass. The column is also made of borosil glass with inner diameter of 5 cm and height of 50 cm with packing as raschig rings of about 1 cm hollow cylinders which are made of glass. A perforated plate is provided at the bottom of the column to avoid slippage of packing. At the top of the column suitable glass tube loop is provided so that the vapor goes up into the condenser, gets condensed and passes downward past the two way valve and back into the column. The two way valve is kept in closed condition to have total reflux implying that entire condensate is refluxed back to the column. Only a couple of milliliters of distillate is collected from the sample port at steady state. The entire apparatus is ensured to have leak proof.

Both the reactants acetic acid and methanol of 2.5 moles each are poured into the reboiler. Catalyst at a loading of 0.025 g/ml is added. Immediately the variac of electric heater is set to a desired voltage and this marks the beginning of the reaction (time=0). The temperature of the reboiler contents are recorded for every 2 ^{0}C rise in temperature from the digital display with 0.1 ^{0}C precision. The column outer surface can be provided with three different boundary conditions (1) Hot water circulating along the jacket. (2) Without any hot water and with air filling the jacket space and outermost glass surface of the jacket open to ambient air. (3) Similar condition as in (2) but the outermost surface is covered with insulating cotton. The heating is continued throughout the experiment at constant rate. When the temperature increases in the reboiler it was found that vapor raises and its condensate is also visible in the column. After certain time the vapor enters the top condenser and the condensate flows down back to the column. The time taken for the first distillate drop to form at the condenser and filling the sample port is recorded as the time for onset of distillate. Form this point of time another 20-30 minutes of heating the reboiler is continued so that the thermal equilibrium or bubble point is reached in the reboiler as well as constant distillate flow is observed at the recycle portion of

the column. A sample is collected from the distillate and stored. In some experimental runs a sample is taken from the reboiler. The operating conditions varied are heat input rates as 50 W,100 W and 150 W. Another variable operating condition is the nature of boundary conditions applied for the column (three different wall temperatures), only air and only air with insulation. The resulting temperature verses time dynamics are presented in Table 4.15 to Table 4.19.

The composition of the distillate is analyzed using gas chromatography (GC). The make and model of the GC were YL 6500 South Korea. A method is created in the GC's computer software so that the peaks of methyl acetate and methanol are obtained clearly and that they are eluted completely. A little more residence time is also provided to obtain acetic acid peak although it may be present in traces only in the distillate. The water found in the reboiler also reaches the distillate in traces amount. Since the GC column is hydrophilic water peak is not observed but its percentage can be evaluated for reboiler mixture from stoichiometric principle applied to the acetic acid liquid. The obtained peak area percentages for the distillate are directly proportional to the weight percentages of all the components. Thus there are fifteen samples of distillate to be analyzed for methyl acetate. A couple of samples from the reboiler at the end of experiments are also analyzed to evaluate the reaction equilibrium constant as a validation or check. A sample GC graph is shown in Fig. 4.12 for reboiler mixture and Fig. 4.13 for distillate sample.

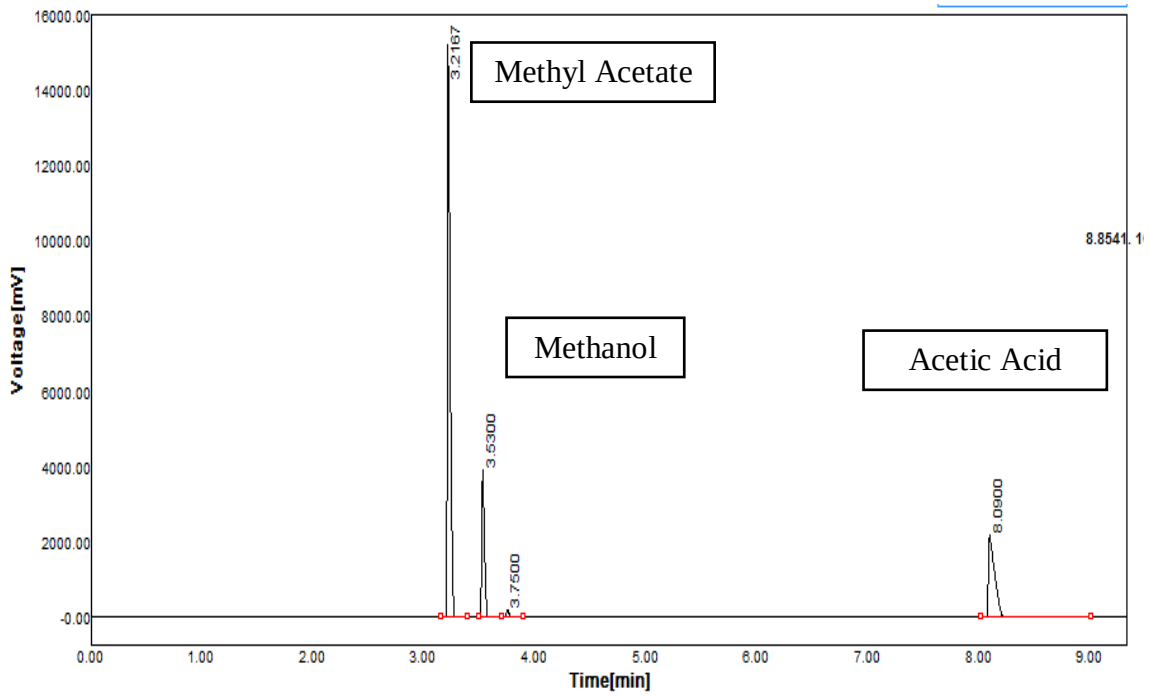

Fig. 4.12 GC peaks obtained for reboiler mixture at steady state (100 W and 50 ^{0}C wall temperature). The four peaks in sequence are for methanol, methyl acetate, water and acetic acid.

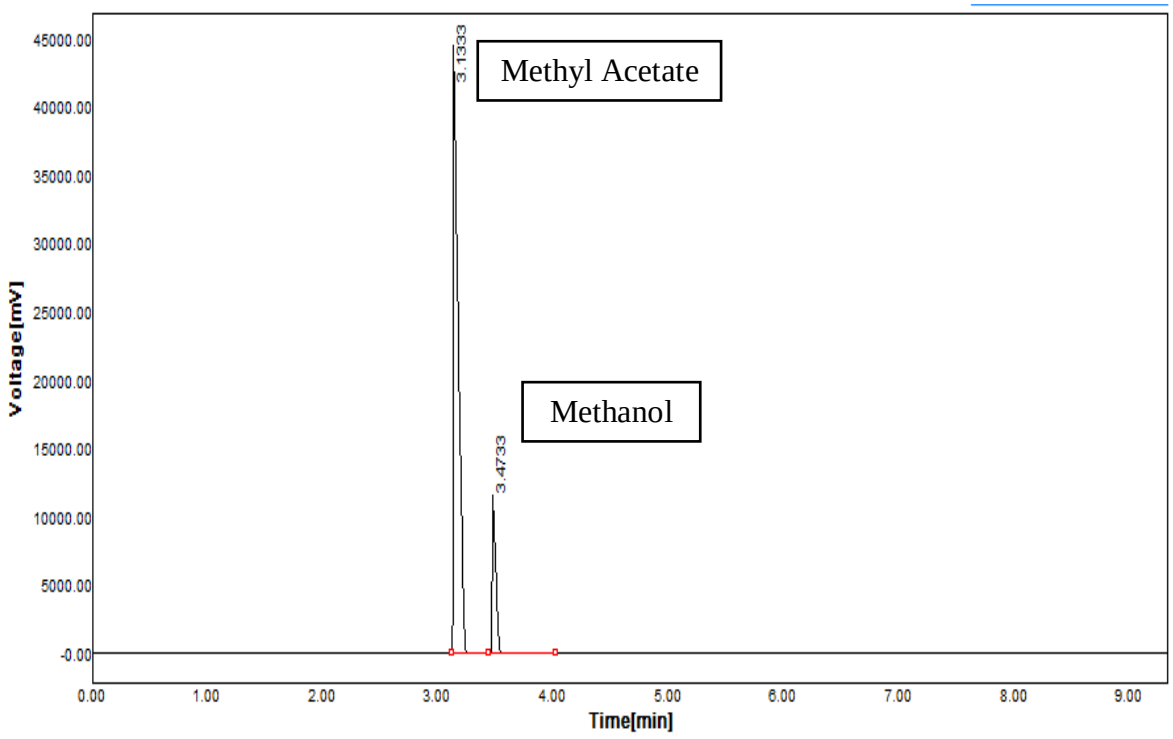

Fig. 4.13 GC peaks obtained for distillate at steady state (100 W and 50 ^{0}C wall temperature). The peaks in sequence are of methanol and methyl acetate.

Table 4.5 Experimental observations for 50 W and Insulated column.

Hot Water temperature on the jacket side of the column: **Insulated Wall**	
Voltage Input to Heater = **100 Volts**	Power Input to Heater P = V*I = **50 Watt**
Current Input to Heater = **0.5 Amp**	
Moles of Component 'A'(Acetic Acid) = **2.5 mole**	Mass of component 'A' = **150 g**
Moles of Component 'B'(Methanol) = **2.5 mole**	Mass of component 'B' = **80 g**
Volume of the mixture = **244 ml**	
Weight of catalyst added (0.025 g/ml) **= 6.1 g**	
Temperature of the water supply to top condenser = **25 ^{0}C**	

Time, s	**T_R, ^{0}C**
0	27.9
91	29
126	30
185	32
236	34
285	36
332	38
378	40
424	42
466	44
510	46
554	48
599	50
641	52
711	55
734	56
793	58
832	60
882	62
936	64
993	66
1053	68
1122	70
1204	72
1233	72.5
1269	73
1320	73.4
1380	73.2
1440	72.9
1500	72.7

Time, s	**T_R, ^{0}C**
1560	72.4
1680	72.1
1800	71.7
1920	71.4
2040	71.2
2160	71
2294*	**70.4**
2400	70.3
2520	70.1
2640	69.7
2760	69.5
2880	69.3
3000	69
3120	68.8
3240	68.7
3360	68.5
3480	68.4
3600	68.4
3720	69.4
3840	69.1
3960	68.1
4080	68.8
4200	68.8
4320	68.8
4440	68.6
4560	68.6
4680	68.6
4800	68.6
4920	68.6
***Onset of Distillate**	

Table 4.6 Experimental observations for 100 W and Insulated column.

Hot Water temperature on the jacket side of the column: **Insulated Wall**	
Voltage Input to Heater = **150 Volts**	Power Input to Heater P = V*I = **100 Watt**
Current Input to Heater = **0.667 Amp**	
Moles of Component 'A'(Acetic Acid) = **2.5 mole**	Mass of component 'A' = **150 g**
Moles of Component 'B'(Methanol) = **2.5 mole**	Mass of component 'B' = **80 g**
Volume of the mixture = **244 ml**	
Weight of catalyst added (0.025 g/ml) **= 6.1 g**	
Temperature of the water supply to top condenser = **25 ^{0}C**	

Time, s	**T_R, ^{0}C**
0	28.1
67	29
92	30
128	32
156	34
183	36
207	38
230	40
253	42
275	44
296	46
317	48
338	50
358	52
378	54
398	56
419	58
441	60
460	62
481	64
503	66
525	68
547	70
559	71
572	72
589	73
605	74
623	75

Time, s	**T_R, ^{0}C**
643	76
690	76.3
720	76.1
780	75.7
840	75.3
960	74.7
1040*	**74.4**
1080	74.1
1200	73.4
1320	72.5
1440	71.9
1560	71.3
1680	70.8
1800	70.4
1920	70
2040	69.6
2160	69.2
2280	69
2340	68.9
2400	68.8
2520	68.5
2580	68.4
2640	68.3
2700	68.2
2760	68.1
2880	68
***Onset of Distillate**	

Table 4.7 Experimental observations for 150 W and Insulated column.

Hot Water temperature on the jacket side of the column: **Insulated Wall**	
Voltage Input to Heater = **200 Volts**	Power Input to Heater P = V*I = **150 Watt**
Current Input to Heater = **0.75 Amp**	
Moles of Component 'A'(Acetic Acid) = **2.5 mole**	Mass of component 'A' = **150 g**
Moles of Component 'B'(Methanol) = **2.5 mole**	Mass of component 'B' = **80 g**
Volume of the mixture = **244 ml**	
Weight of catalyst added (0.025 g/ml) **= 6.1 g**	
Temperature of the water supply to top condenser = **25 ^{0}C**	

Time, s	**T_R, ^{0}C**
0	28.6
75	30
100	32
120	34
137	36
153	38
169	40
182	42
194	44
209	46
222	48
235	50
247	52
260	54
272	56
285	58
298	60
309	62
322	64
333	66
346	68
358	70

Time, s	**T_R, ^{0}C**
370	72
384	74
400	76
448	77.7
480	77.6
540	77.2
595*	**76.8**
690	76
780	75.4
840	75.2
900	74.8
960	74.5
1080	74
1200	73.6
1320	73.5
1440	73.3
1560	73.2
1680	73.2
1800	73.2
1920	73.3
***Onset of Distillate**	

Table 4.8 Experimental observations for 50 W and column at Room Temperature.

Hot Water temperature on the jacket side of the column: **Room Temperature**	
Voltage Input to Heater = **100 Volts**	Power Input to Heater P = V*I = **50 Watt**
Current Input to Heater = **0.5 Amp**	
Moles of Component 'A'(Acetic Acid) = **2.5 mole**	Mass of component 'A' = **150 g**
Moles of Component 'B'(Methanol) = **2.5 mole**	Mass of component 'B' = **80 g**
Volume of the mixture = **244 ml**	
Weight of catalyst added (0.025 g/ml) **= 6.1 g**	
Temperature of the water supply to top condenser = **25 ^{0}C**	

Time, s	T_R, ^{0}C
0	26.4
117	28
182	30
239	32
290	34
340	36
387	38
437	40
483	42
532	44
578	46
626	48
674	50
721	52
772	54
825	56
880	58
941	60
1001	62
1067	64
1144	66
1227	68
1337	70
1401	71
1560	71.7
1680	71.3
1800	70.5
1980	70
2040	69.8
2220	69.2
2280	69.1

Time, s	T_R, ^{0}C
2400	68.8
2520	68.5
2640	68.2
2760	67
2880	67.8
3000	67.7
3120	67.5
3240	67.3
3360	67.2
3480	67.1
3600	67
3720	66.8
3840	66.7
3960	66.7
4080	66.5
4200	66.4
4320	66.3
4440	66.1
4680	66
4800	65.8
5040	65.7
5400	65.5
5760	65.3
6000	65.2
6360	64.9
6600	64.8
6840	64.8
7080	64.5
7200	64.5
No Onset	

Table 4.9 Experimental observations for 100 W and column at Room Temperature.

Hot Water temperature on the jacket side of the column: **Room Temperature**	
Voltage Input to Heater = **150 Volts**	Power Input to Heater P = V*I = **100 Watt**
Current Input to Heater = **0.667 Amp**	
Moles of Component 'A'(Acetic Acid) = **2.5 mole**	Mass of component 'A' = **150 g**
Moles of Component 'B'(Methanol) = **2.5 mole**	Mass of component 'B' = **80 g**
Volume of the mixture = **244 ml**	
Weight of catalyst added (0.025 g/ml) **= 6.1 g**	
Temperature of the water supply to top condenser = **25 ^{0}C**	

Time, s	**T_R, ^{0}C**
0	27.7
72	29
95	30
128	32
158	34
184	36
209	38
232	40
256	42
278	44
301	46
322	48
346	50
366	52
388	54
409	56
432	58
455	60
477	62
500	64
524	66
550	68
580	70
594	71
608	72
626	73

Time, s	**T_R, ^{0}C**
645	74
664	75
690	75.9
720	75.8
780	75.4
840	75.1
900	74.7
960	74.3
1080	73.7
1180*	**73.1**
1200	73
1320	72.5
1440	71.8
1560	71.2
1680	70.8
1800	70.3
1920	70
2040	69.6
2160	69.4
2280	69.1
2400	68.8
2520	68.8
2640	68.4
2760	68.2
3000	68.1
***Onset of Distillate**	

Table 4.10 Experimental observations for 150 W and column at Room Temperature.

Hot Water temperature on the jacket side of the column: **Room Temperature**	
Voltage Input to Heater = **200 Volts**	Power Input to Heater P = V*I = **150 Watt**
Current Input to Heater = **0.75 Amp**	
Moles of Component 'A'(Acetic Acid) = **2.5 mole**	Mass of component 'A' = **150 g**
Moles of Component 'B'(Methanol) = **2.5 mole**	Mass of component 'B' = **80 g**
Volume of the mixture = **244 ml**	
Weight of catalyst added (0.025 g/ml) **= 6.1 g**	
Temperature of the water supply to top condenser = **25 ^{0}C**	

Time, s	**T_R, ^{0}C**
0	28
61	29
80	30
103	32
123	34
139	36
154	38
168	40
183	42
196	44
209	46
222	48
235	50
247	52
260	54
272	56
285	58
297	60
309	62
321	64
334	66
344	68
359	70
372	72
387	74
403	76

Time, s	**T_R, ^{0}C**
420	77.9
450	77.8
490	77.4
540	77
600	76.5
645*	**76.2**
660	75.9
750	74.9
870	73.8
990	72.9
1080	72.4
1200	71.8
1320	71.4
1440	70.9
1560	70.4
1680	70.1
1800	69.8
1920	69.5
2040	69.2
2160	69
2280	68.8
2400	68.6
2520	68.4
2580	68.3
2640	68.3
***Onset of Distillate**	

Table 4.11 Experimental observations for 50 W and column at 40 ^{0}C.

Hot Water temperature on the jacket side of the column: **40 ^{0}C**	
Voltage Input to Heater = **100 Volts**	Power Input to Heater P = V*I = **50 Watt**
Current Input to Heater = **0.5 Amp**	
Moles of Component 'A'(Acetic Acid) = **2.5 mole**	Mass of component 'A' = **150 g**
Moles of Component 'B'(Methanol) = **2.5 mole**	Mass of component 'B' = **80 g**
Volume of the mixture = **244 ml**	
Weight of catalyst added (0.025 g/ml) **= 6.1 g**	
Temperature of the water supply to top condenser = **25 ^{0}C**	

Time, s	**T_R, ^{0}C**
0	27
91	28
134	29
166	30
222	32
273	34
323	36
372	38
424	40
473	42
528	44
583	46
643	48
705	50
767	52
825	54
899	56
970	58
1037	60
1117	62
1156	63
1196	64
1244	65

Time, s	**T_R, ^{0}C**
1283	66
1320	65.9
1344	67
1374	68
1410	68.6
1480	69
1528	69.6
1560	70
1620	69.8
1710	67.4
1800	66.4
1920	65.2
2040	65.8
2160	64.8
2280	64.2
2400	63.9
2520	64.4
2640	64.4
2760	64.4
2880	64.5
3000	64.5
No Onset	

Table 4.12 Experimental observations for 100 W and column at 40 ^{0}C.

Hot Water temperature on the jacket side of the column: **40 ^{0}C**	
Voltage Input to Heater = **150 Volts**	Power Input to Heater P = V*I = **100 Watt**
Current Input to Heater = **0.667 Amp**	
Moles of Component 'A'(Acetic Acid) = **2.5 mole**	Mass of component 'A' = **150 g**
Moles of Component 'B'(Methanol) = **2.5 mole**	Mass of component 'B' = **80 g**
Volume of the mixture = **244 ml**	
Weight of catalyst added (0.025 g/ml) **= 6.1 g**	
Temperature of the water supply to top condenser = **25 ^{0}C**	

Time, s	T_R, ^{0}C
0	25.5
47	26
73	27
92	28
112	29
124	30
153	32
179	34
203	36
227	38
249	40
271	42
294	44
316	46
336	48
358	50
379	52
402	54
422	56
443	58
462	60
486	62
511	64
540	66
568	68
601	70
622	71
643	72

Time, s	T_R, ^{0}C
665	73
684	74
698	75
716	76
780	75.1
840	74.3
900	73.5
1020	72
1080	71.5
1140	71
1200	70.4
1320	69.9
1380	69.7
1440	69.5
1560	69.6
1680	68.6
1800	68
1980	67.8
2100	67.4
2340	66.4
2520	66.1
2640	66
2700	66.1
2880	65.6
3000	65.4
3120	65.4
No Onset	

Table 4.13 Experimental observations for 150 W and column at 40 ^{0}C.

Hot Water temperature on the jacket side of the column: **40 ^{0}C**	
Voltage Input to Heater = **200 Volts** Current Input to Heater = **0.75 Amp**	Power Input to Heater P = V*I = **150 Watt**
Moles of Component 'A'(Acetic Acid) = **2.5 mole**	Mass of component 'A' = **150 g**
Moles of Component 'B'(Methanol) = **2.5 mole**	Mass of component 'B' = **80 g**
Volume of the mixture = **244 ml**	
Weight of catalyst added (0.025 g/ml) **= 6.1 g**	
Temperature of the water supply to top condenser = **25 ^{0}C**	

Time, s	**T_R, ^{0}C**
0	26.4
53	28
78	30
97	32
113	34
129	36
143	38
157	40
171	42
184	44
197	46
210	48
222	50
234	52
246	54
259	56
272	58
287	60
300	62
315	64
327	66
339	68
351	70
361	72
373	74
387	76
400	78
450	78.6
480	78.4
540	77.8

Time, s	**T_R, ^{0}C**
600	76.6
720	74.7
780	74.2
840	74.4
900	72.8
960	71.8
1020	71.7
1080	71.3
1140	71
1200	70.8
1260	70.5
1320	70.2
1380	69.9
1440	69.8
1500	69.6
1560	69.5
1620	69.5
1680	69.5
2100	69.3
2280	68.9
2400	68.6
2460	68.5
2520	68.4
2640	68.3
2760	68.1
2940	68
3000	68
3360	67.3
3480	67.3
No Onset	

Table 4.14 Experimental observations for 50 W and column at 50 ^{0}C.

Hot Water temperature on the jacket side of the column: **50 ^{0}C**	
Voltage Input to Heater = **100 Volts**	Power Input to Heater P = V*I = **50 Watt**
Current Input to Heater = **0.5 Amp**	
Moles of Component 'A'(Acetic Acid) = **2.5 mole**	Mass of component 'A' = **150 g**
Moles of Component 'B'(Methanol) = **2.5 mole**	Mass of component 'B' = **80 g**
Volume of the mixture = **244 ml**	
Weight of catalyst added (0.025 g/ml) **= 6.1 g**	
Temperature of the water supply to top condenser = **25 ^{0}C**	

Time, s	**T_R, ^{0}C**
0	26.8
110	28
183	30
240	32
292	34
342	36
390	38
436	40
482	42
530	44
576	46
622	48
670	50
716	52
768	54
818	56
871	58
930	60
989	62
1053	64
1126	66
1209	68
1314	70

Time, s	**T_R, ^{0}C**
1380	71
1560	72.2
1800	71.6
1860	71.4
1920	71.1
1980	71
2040	70.7
2100	70.4
2160	70.3
2220*	**70.2**
2280	70
2340	69.8
2400	69.6
2520	69.4
2640	69.1
2760	68.8
2880	68.5
3000	68.3
3120	68.1
3240	67.8
3360	67.7
3420	67.7
***Onset of Distillate**	

Table 4.15 Experimental observations for 100 W and column at 50 ^{0}C.

Hot Water temperature on the jacket side of the column: **50 ^{0}C**	
Voltage Input to Heater = **150 Volts**	Power Input to Heater
Current Input to Heater = **0.667 Amp**	P = V*I = **100 Watt**
Moles of Component 'A'(Acetic Acid) = **2.5 mole**	Mass of component 'A' = **150 g**
Moles of Component 'B'(Methanol) = **2.5 mole**	Mass of component 'B' = **80 g**
Volume of the mixture = **244 ml**	
Weight of catalyst added (0.025 g/ml) **= 6.1 g**	
Temperature of the water supply to top condenser = **25 ^{0}C**	

Time, s	**T_R, ^{0}C**
0	28
68	29
87	30
125	32
154	34
178	36
201	38
223	40
245	42
266	44
290	46
309	48
331	50
351	52
370	54
387	56
410	58
432	60
456	62
480	64
518	66
546	68
561	69
572	70

Time, s	**T_R, ^{0}C**
586	71
602	72
618	73
634	75
648	76
681	77
746*	**74.6**
780	74.3
840	73.6
900	73
960	72.3
1020	71.9
1140	71.4
1200	71.2
1320	70.7
1440	70
1560	69.8
1680	69.6
1800	69.3
1920	69.2
2040	69.6
2319	69
2400	69.2
***Onset of Distillate**	

Table 4.16 Experimental observations for 150 W and column at 50 ^{0}C.

Hot Water temperature on the jacket side of the column: **50 ^{0}C**	
Voltage Input to Heater = **200 Volts**	Power Input to Heater P = V*I = **150 Watt**
Current Input to Heater = **0.75 Amp**	
Moles of Component 'A'(Acetic Acid) = **2.5 mole**	Mass of component 'A' = **150 g**
Moles of Component 'B'(Methanol) = **2.5 mole**	Mass of component 'B' = **80 g**
Volume of the mixture = **244 ml**	
Weight of catalyst added (0.025 g/ml) **= 6.1 g**	
Temperature of the water supply to top condenser = **25 ^{0}C**	

Time, s	**T_R, ^{0}C**
0	27.1
49	28
68	29
80	30
102	32
119	34
136	36
151	38
167	40
181	42
195	44
212	46
234	48
249	50
262	52
276	54
289	56
301	58
313	60
325	62
338	64
360	68
379	70

Time, s	**T_R, ^{0}C**
397	73
412	75
430	76
459	80
467	86
489	84
512*	**82**
540	80.7
660	80.3
810	78.2
840	77.8
960	76.4
1080	75.6
1200	74.9
1320	74.5
1440	74.1
1560	73.7
1680	74.2
1800	74.7
1920	74.6
2040	74.4
***Onset of Distillate**	

Table 4.17 Experimental observations for 50 W and column at 60 ^{0}C.

Hot Water temperature on the jacket side of the column: **60 ^{0}C**	
Voltage Input to Heater = **100 Volts** Current Input to Heater = **0.5 Amp**	Power Input to Heater P = V*I = **50 Watt**
Moles of Component 'A'(Acetic Acid) = **2.5 mole**	Mass of component 'A' = **150 g**
Moles of Component 'B'(Methanol) = **2.5 mole**	Mass of component 'B' = **80 g**
Volume of the mixture = **244 ml**	
Weight of catalyst added (0.025 g/ml) **= 6.1 g**	
Temperature of the water supply to top condenser = **25 ^{0}C**	

Time, s	**T_R, ^{0}C**
0	26.7
113	28
186	30
242	32
296	34
354	36
392	38
437	40
482	42
527	44
573	46
619	48
667	50
716	52
766	54
816	56
871	58
927	60
986	62
1050	64
1122	66

Time, s	**T_R, ^{0}C**
1205	68
1305	70
1367	71
1457	72
1560	72.1
1594*	**72**
1680	71.8
1800	71.4
1920	70.1
2040	70
2160	69.9
2280	69.6
2400	69.2
2520	68.9
2640	68.7
2760	68.3
2880	68.1
3000	67.8
3120	67.8
3240	67.7
***Onset of Distillate**	

Table 4.18 Experimental observations for 100 W and column at 50 ^{0}C.

Hot Water temperature on the jacket side of the column: **60 ^{0}C**	
Voltage Input to Heater = **150 Volts**	Power Input to Heater P = V*I = **100 Watt**
Current Input to Heater = **0.667 Amp**	
Moles of Component 'A'(Acetic Acid) = **2.5 mole**	Mass of component 'A' = **150 g**
Moles of Component 'B'(Methanol) = **2.5 mole**	Mass of component 'B' = **80 g**
Volume of the mixture = **244 ml**	
Weight of catalyst added (0.025 g/ml) **= 6.1 g**	
Temperature of the water supply to top condenser = **25 ^{0}C**	

Time, s	**T_R, ^{0}C**
0	27.7
50	29
71	30
102	32
129	34
153	36
176	38
198	40
219	42
240	44
260	46
279	48
300	50
318	52
336	54
355	56
374	58
398	60
424	62
450	64
482	66.7
518	70.1
551	72
575	75

Time, s	T_R, ^{0}C
583	80
603	82
711*	**77**
720	76.9
780	75.3
840	74.4
900	73.8
960	73.2
1080	73.5
1200	73.5
1320	73.6
1502	73.3
1560	73.5
1740	71.2
1860	71.1
1980	71.4
2160	72.1
2340	72.1
2520	69
2580	69.6
2640	70.2
2700	70.3
2760	70.4
***Onset of Distillate**	

Table 4.19 Experimental observations for 150 W and column at 60 ^{0}C.

Hot Water temperature on the jacket side of the column: **60 ^{0}C**	
Voltage Input to Heater = **200 Volts**	Power Input to Heater
Current Input to Heater = **0.75 Amp**	P = V*I = **150 Watt**
Moles of Component 'A'(Acetic Acid) = **2.5 mole**	Mass of component 'A' = **150 g**
Moles of Component 'B'(Methanol) = **2.5 mole**	Mass of component 'B' = **80 g**
Volume of the mixture = **244 ml**	
Weight of catalyst added (0.025 g/ml) **= 6.1 g**	
Temperature of the water supply to top condenser = **25 ^{0}C**	

Time, s	**T_R, ^{0}C**
0	27.4
49	28
84	30
106	32
124	34
140	36
155	38
170	40
183	42
196	44
209	46
221	48
233	50
244	52
256	54
267	56
279	58
291	60
302	62
314	64
325	66
336	68
348	70
359	72
372	74
385	76
402	78
419	78.6
458	79
473*	**79.1**
Time, s	**T_R, ^{0}C**

546	78.5
600	78.7
690	78.7
720	78.5
780	78.2
840	78.1
900	77.9
960	77.8
1020	77.8
1080	77.8
1140	77.8
1200	77.8
1260	77.8
1380	77.8
1500	77.8
1560	78
1680	78.1
1800	78.2
***Onset of Distillate**	

The obtained temperature verses time dynamics of the reboiler mixture are plotted in Figure 4.14 (a-e) corresponding to five different boundary conditions for the column and each plot further contains three curves corresponding to three different heat inputs.

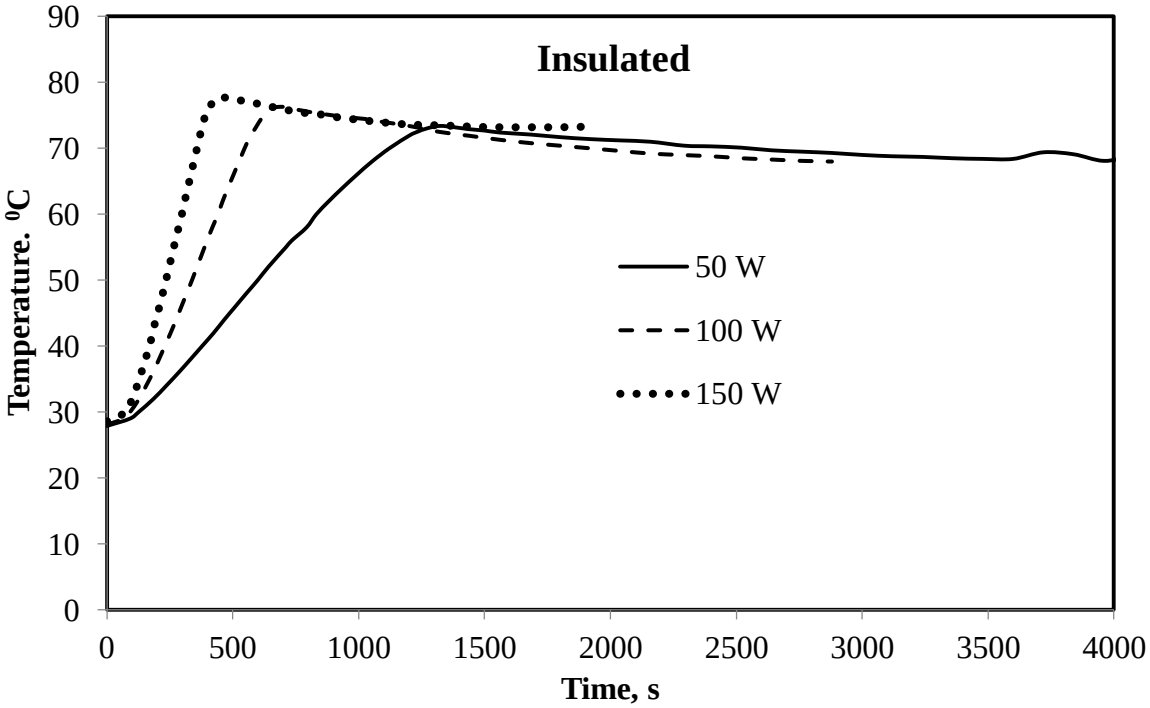

(a)

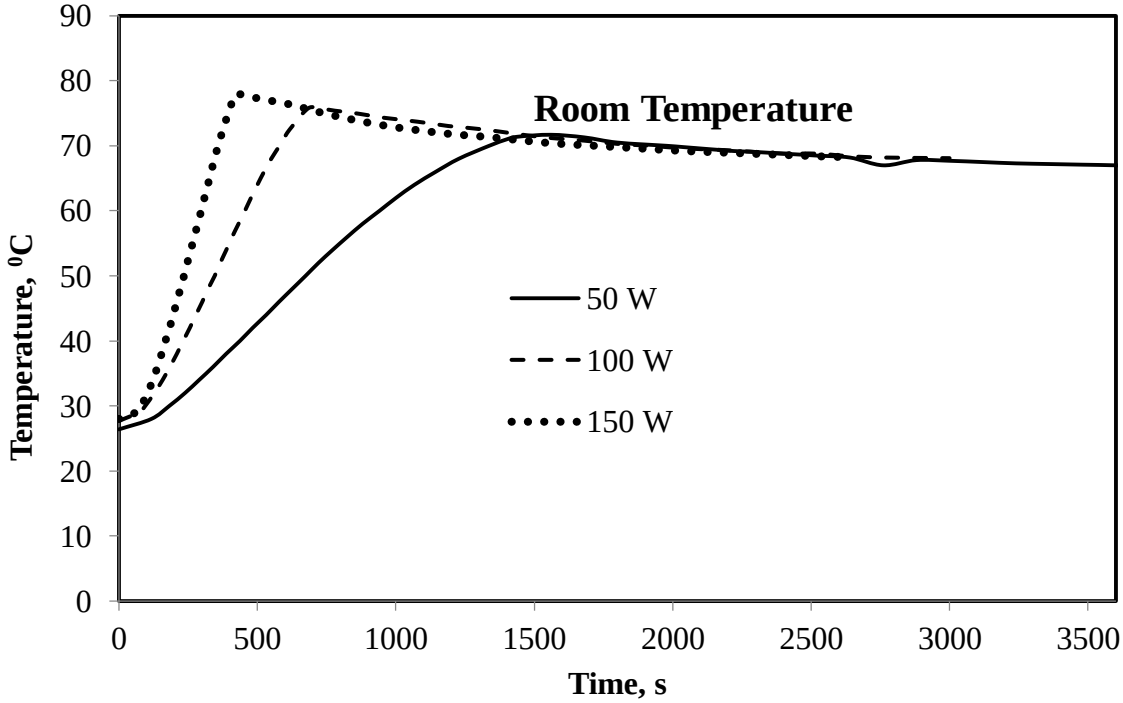

(b)

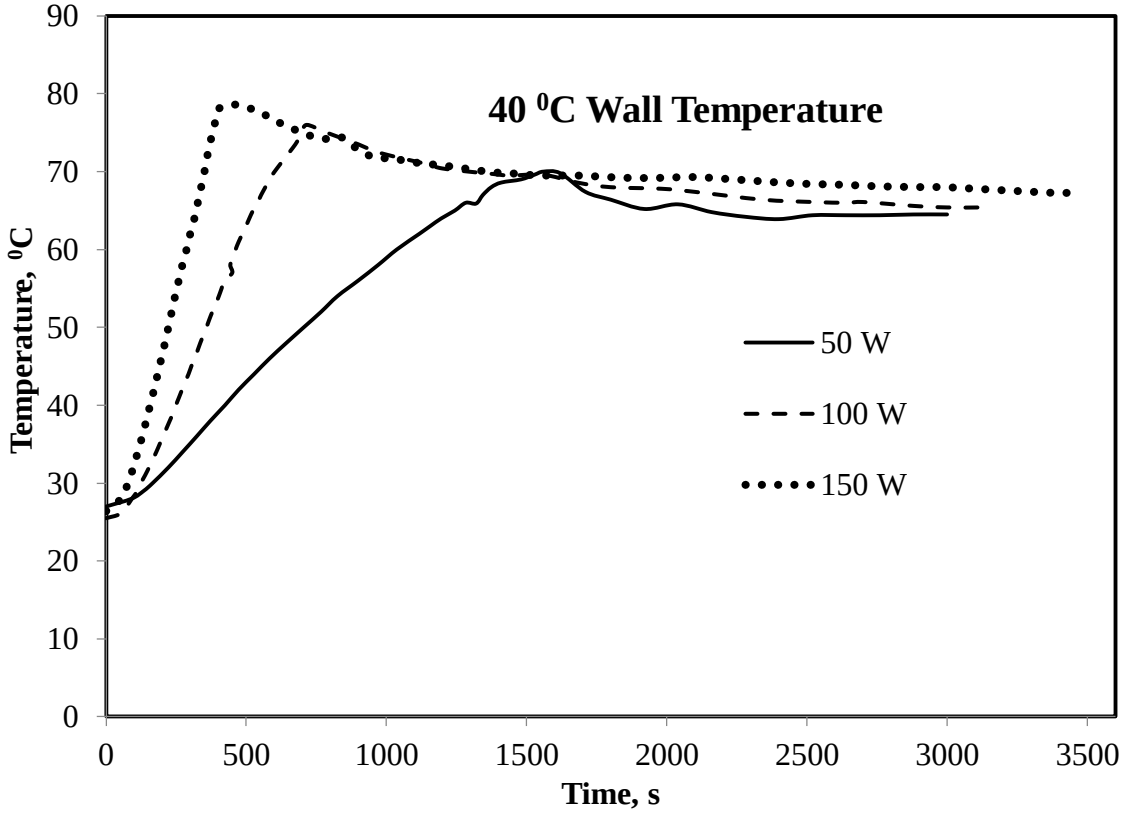
40 0C Wall Temperature
Temperature, 0C
Time, s
50 W
100 W
150 W
0
10
20
30
40
50
60
70
80
90
0
500
1000
1500
2000
2500
3000
3500

(c)

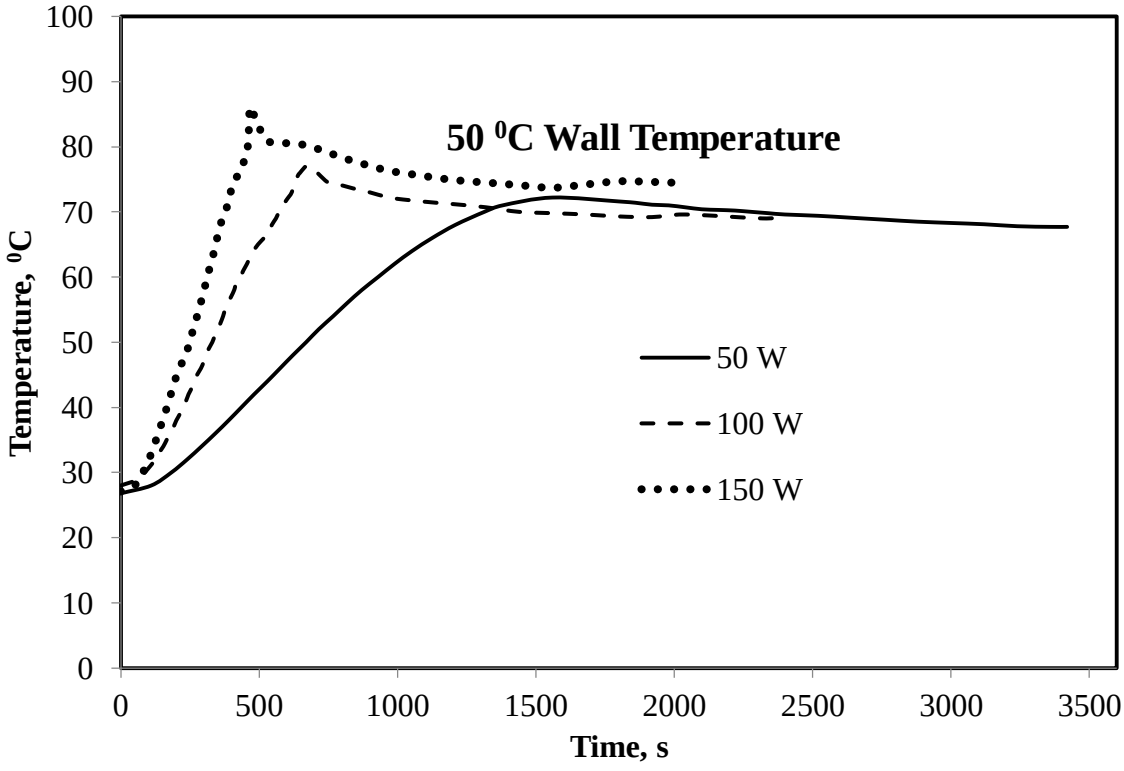
50 0C Wall Temperature
Temperature, 0C
Time, s
50 W
100 W
150 W
0
10
20
30
40
50
60
70
80
90
100
0
500
1000
1500
2000
2500
3000
3500

(d)

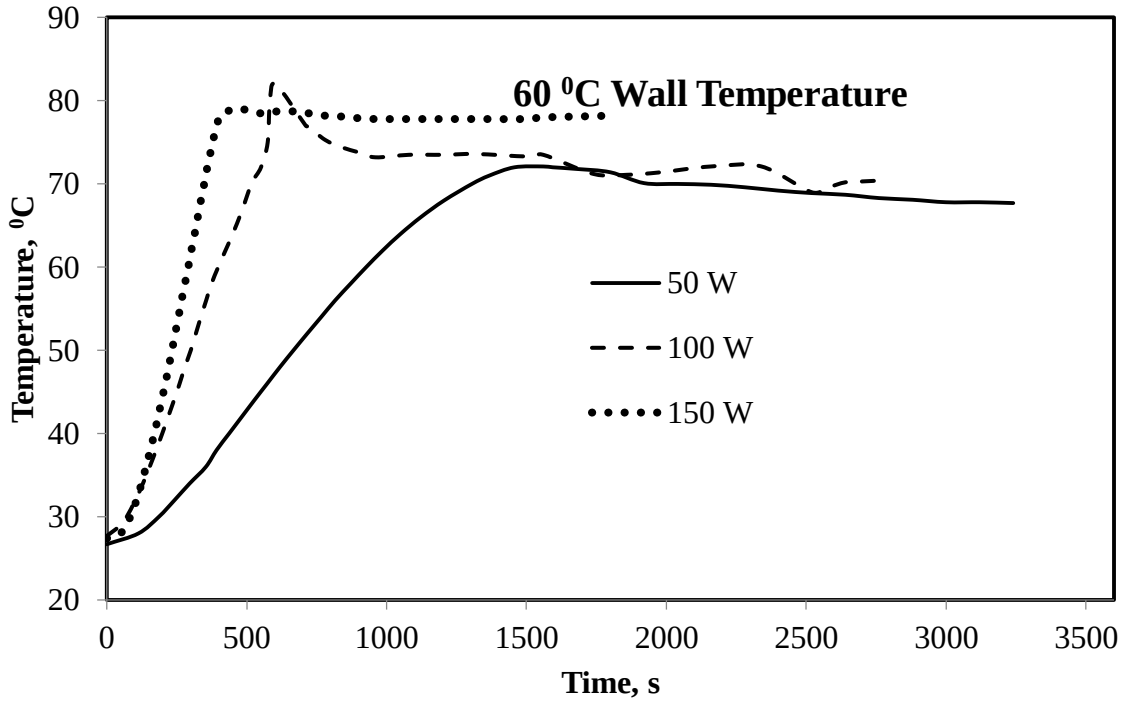

(e)

Fig. 4.14 Experimental temperature dynamics of reboiler with (a) Insulated wall condition (b) Wall at room temperature (c) wall at 40 ^{0}C (d) wall at 50 ^{0}C (e) wall at 60 ^{0}C.

The observed times for onset of distillate for various wall heating and reboiler heating are presented in Table 4.20.

Table 4.20 Experimental data on onset of distillate.

Q (W) / **T_{wall} (^{0}C)**	50	100	150
40	No onset	No onset	No onset
50	2220 sec	746 sec	512 sec
60	1594 sec	711 sec	473 sec
Ambient (28 ^{0}C)	No onset	1180 sec	645 sec
Insulated	2294 sec	1040 sec	595 sec

It can be observed that as the heat input rate Q increases the t_{onset} decreases. Similarly as T_{wall} increases the t_{onset} decreases.

Although smaller t_{onset} implies small start-up time, it is not sure whether the obtained distillate of such condition contains highest purity of methyl acetate. The measured methyl acetate weight percentages inferred from GC analyses of samples in the distillate for the above 15 different operating conditions are tabulated in Table 4.21.

Table 4.21 Distillate compositions in weight percent

Q (W) / **T_{wall} (^{0}C)**	50	100	150
40	No distillate	No distillate	No distillate
50	83.48 %	81.37 %	80.69 %
60	81.22 %	81.9 %	82.06 %
Ambient (28 ^{0}C)	No distillate	81.92 %	81.62 %
Insulated	84.85 %	82.14 %	82.42 %

It can be observed that the combination of insulated wall and 50 W heat input rate gives the highest distillate purity in terms of methyl acetate. If we compare this with batch reactor which has the methyl acetate weight percentage as 30 %. BRD is advantageous for acetic acid esterification with methanol to obtain methyl acetate as product. Therefore by providing rectification column higher purity methyl acetate product is obtained. It is the advantage of BRD as noted in the introduction also. In the perspective of industrial application a suitable combination of heat input rate and wall condition can be used. For theoretical analysis or process intensification, a model can be developed which can optimize the height of the column desired for various finite distillate flow rate or finite reflux ratio. Further the packing characteristics such as specific surface area can also be explored by model.

CHAPTER 5
MATHEMATICAL MODELLING AND SIMULATION

Mathematical Modelling and Simulation

5.1 Pore diffusion model – Improvised for heterogeneous esterification

The basic geometry created in the COMSOL Multiphysics is a catalyst particle surrounded with certain volume of the stationary reactant mixture. This kind of geometry is possible when the RPM of the stirrer inside the reactor is high such that the relative velocity between the catalyst particle and the reactant – product solution is almost equal to zero. The density difference between catalyst particle and solution mixture is comparatively very small and hence there will be a uniform dispersion of catalyst particles. This actually signifies that convection term in the major governing equation i.e., convection – diffusion – reaction equation is negligible. The catalyst particles surrounded by reactant-product liquid solution and the associated geometry in comsol is shown in Fig. 5.1. The dimension of the catalyst sphere is d_p = 725 µm and liquid cube's edge length is l = 0.001705 m. Hence the volume l^3 can be determined from total reactant volume divided by the number of particles.

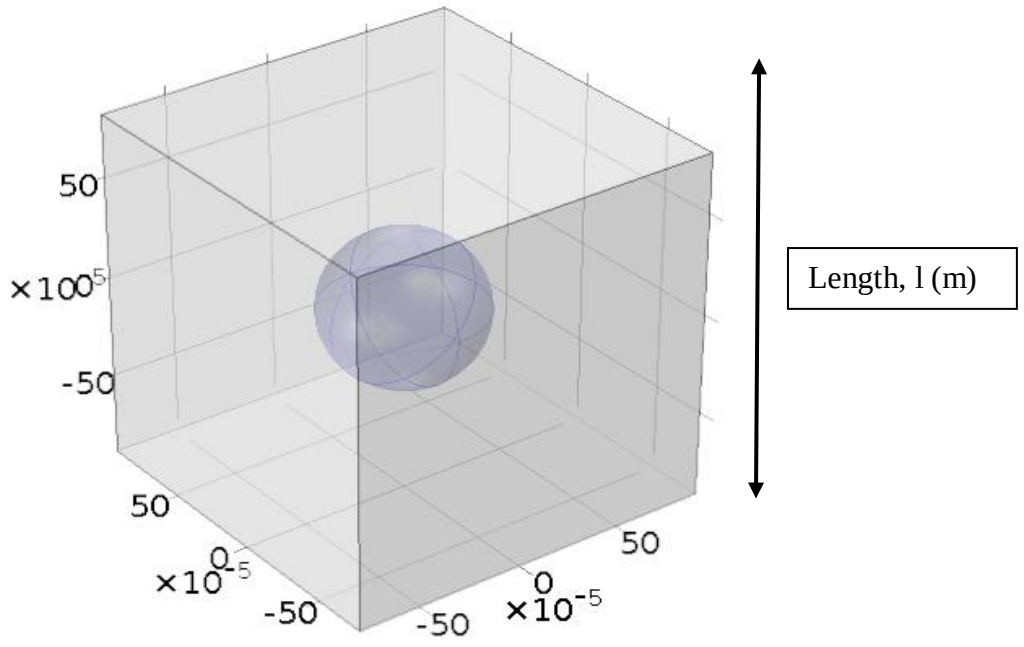

Fig. 5.1 Geometry in COMSOL Multiphysics simulation for the catalyst particle surrounded by a cube of reactant liquid mixture. Units of length is in meters.

Governing Equations

The mathematical model that is used for this system is distributed parameter model involving time and space as independent variables and concentration as dependent variable. Further conversion X_A of the acetic acid for the case 1:1 feed is estimated. The generic form of reaction – diffusion equation for species A inside the catalyst particle whose pore volume fraction is equal to ε is as follows in Eq. (5.1). The reaction is a reversible one as A +B ←→C+D

$$\frac{\partial C_A}{\partial t} - D_{A2}\nabla^2 C_A = -\varepsilon k_{f2}\left[C_A C_B - \frac{C_C C_D}{K_e}\right] \tag{5.1}$$

Where k_{f2} and k_{b2} are the forward and backward rate constants inside the catalyst particle and ε is the available pore volume for the reaction to occur inside the catalyst particle.

The generic form of reaction –diffusion equation in surrounding liquid phase is given as follows

$$\frac{\partial C_A}{\partial t} - D_{A1}\nabla^2 C_A = -k_{f1}\left[C_A C_B - \frac{C_C C_D}{K_e}\right] \tag{5.2}$$

These k_{f2} and k_{b2} are different from k_{f1} and k_{b1} because the availability of H^+ ion in catalyst pores is high than actually released into bulk liquid.

Boundary conditions and initial conditions

At the center of the particle, owing to symmetry

$$r = 0, \quad \frac{\partial C_A}{\partial r} = 0 \tag{5.3}$$

At surface of the particle, there will be concentration continuity as in Eq. (5.4) and either flux continuity as below in Eq. (5.5) or C_A = constant (Dirichlet condition) in bulk liquid

$$r = R_p, \; C_{A,in} = C_{A,out} \tag{5.4}$$

$$r=R_p, \; -D_{A1}\frac{dC_A}{dr} = -D_{A2}\frac{dC_A}{dr} \tag{5.5}$$

At the faces of the cube, symmetry or equivalently no-flux condition is applied as $\underline{\nabla}_n C_A = 0$ (normal derivative of concentration is zero).

At $t = 0$, $C_A = C_{Ao}$, $0 < r < R_p$ and in the bulk liquid (5.6)

Since 1:1 mole ratio of A and B are taken as reactant mixture, it suffices to solve for species A only and rest of them are related through stoichiometry as in Eq. (2.1) $C_B = C_A$, $C_C = C_{A0} - C_A$ and $C_D = C_{A0} - C_A$. The overall conversion in the reactor liquid is $X_A = 1-C_A/C_{A0}$.

Simulation Tool

COMSOL Multiphysics was finite element method (FEM) based simulation software applicable for many kinds of engineering. It consists of different types of physics modules and selection of each module is application specific. The module we chose for the problem was transport of dilute species since convection zero owing to 1:1 or equimolar counter diffusion [Mekala et al., 2013]. A robust solution of partial differential equations Eq. (5.1) and Eq. (5.2) can be obtained using comsol and hence it is considered as powerful software package. It can be used in conjunction with MATLAB too. The algorithm for this section is presented in appendix.

5.1.1 Determination of Rate Constants

5.1.1.1 Homogeneous rate constant

The conversion of acetic acid Vs time (X_A vs t) for esterification without catalyst at various temperatures is plotted in the figure Fig. 5.2. The data is from the literature [Mekala et al., 2013].

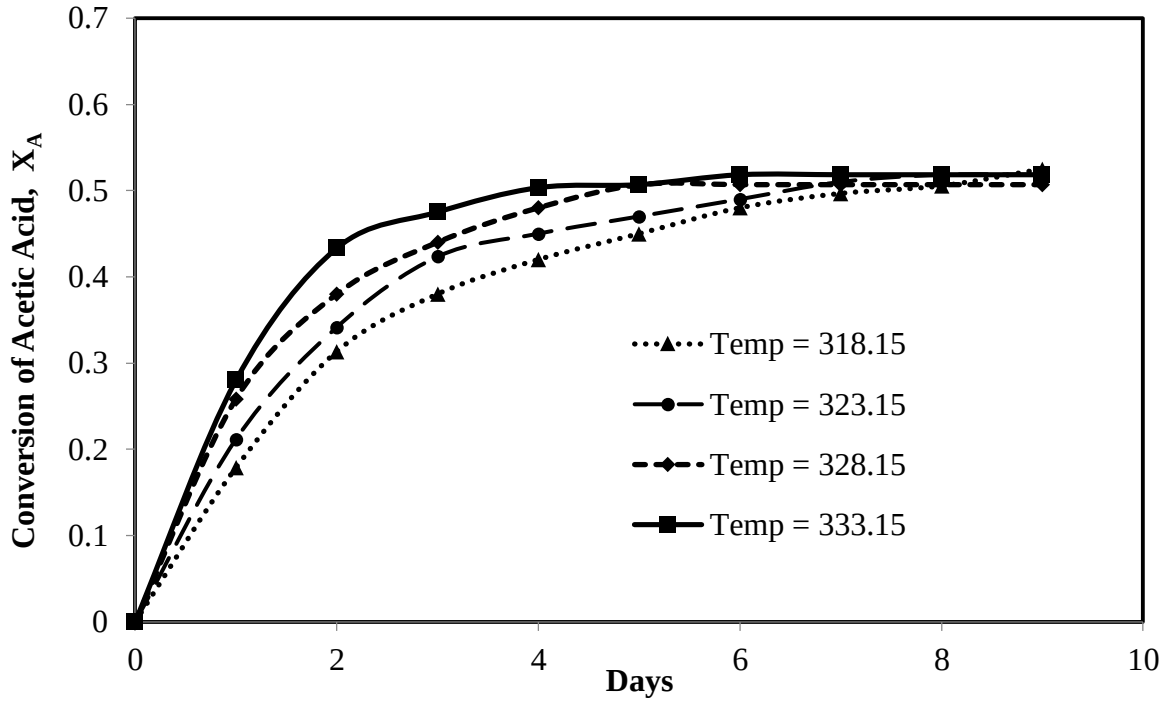

Fig. 5.2 Experimental conversion of acetic acid without catalyst at different temperatures.

The rate of homogeneous reaction is given by

$$\frac{dC_A}{dt} = -k_{f1}\left(C_A C_B - \frac{C_C C_D}{K_e}\right) \tag{5.7}$$

Where 'k_{f1}' is forward reaction rate constant and K_e is the equilibrium constant.

Since the experiments were conducted with equimolar ratio 1:1 of A & B, the above equation with $X_A = 1 - C_A/C_{A0}$ reduces to

$$\frac{dX_A}{dt} = k_{f1} * C_{A0}\left((1-X_A)^2 - \frac{X_A^2}{K_e}\right) \tag{5.8}$$

By evaluating the rate of conversion $\frac{dX_A}{dt}$ at t=0 which is the initial slopes of the curves in Fig. 5.2, it provides the value of $k_{f1} * C_{A0}$, since $X_A = 0$ at t=0. Further k_{f1} can be calculated at different temperatures (T) and thereby Arrhenius expression $k_{f1_0} e^{\frac{-E_{f1}}{RT}}$ can be fitted and k_{f1_0} and E_{f1} can be obtained.

5.1.1.2 Heterogeneous rate constant

Simulation of Eq. (5.1) and Eq. (5.2) were done in order to optimize the value of k_{f2} as in Eq (5.1). Diffusivities of all species is assumed constant as $D_{A1} = 3*10^{-9}$ m^2/sec in the bulk liquid and $D_{A2}=1*10^{-9}$ m^2/sec inside the catalyst particle since different diffusivities would complicate solving equations for all species. Reaction kinetics is used from [Mekala et al., 2013]. The average concentration of A in the liquid phase is used to evaluate the overall conversion of A. As described in Table 2.1, the plot between the error =absolute ($\beta_{sim} - \beta_{expt}$) and the guess value of k_{f2} is represented in Fig. 5.3 for one situation.

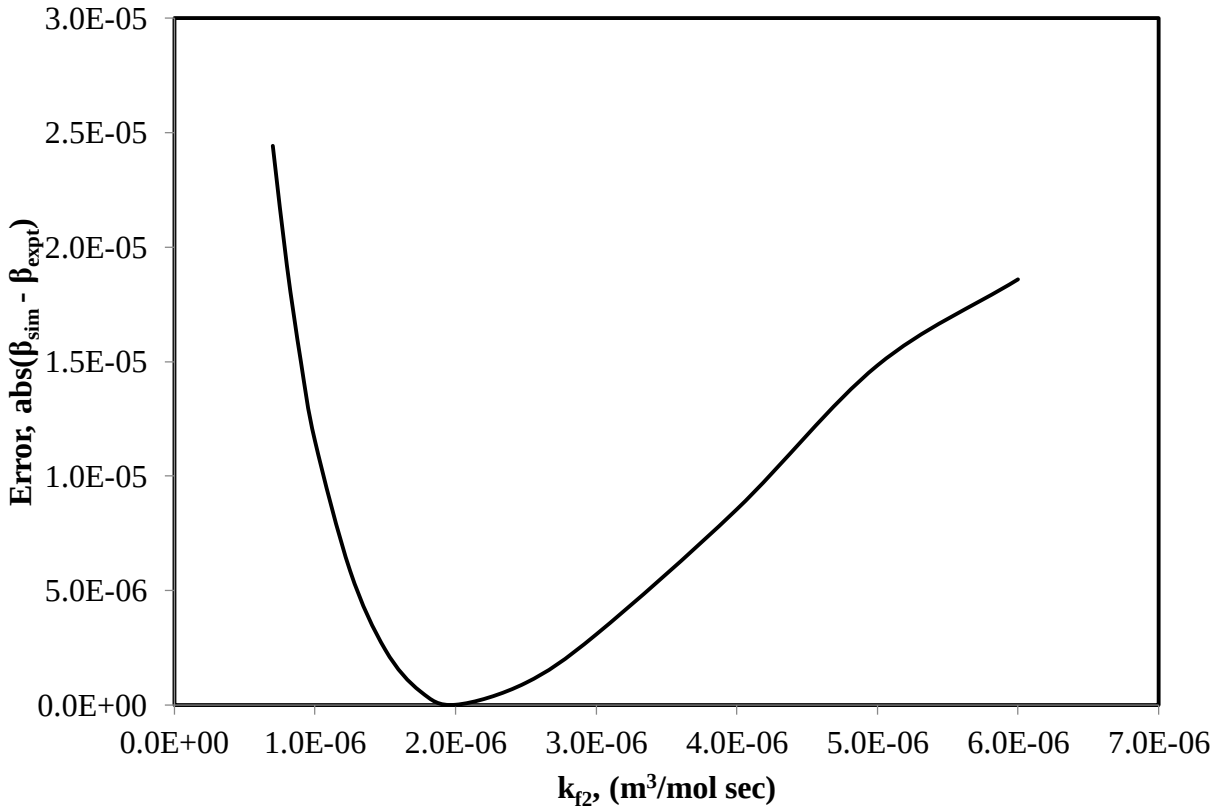

Fig. 5.3 Error plot for evaluating optimum k_{f2} at a temperature of 343.15 K using comsol solution for reaction-diffusion equation.

The values of k_{f1} and k_{f2} obtained from all the three models described in Table 2.1 are tabulated in Table 5.1. The kinetic rate constant k_{f1} corresponds to bulk liquid phase where as k_{f2} corresponds to inside the catalyst. We had two types of approaches for determining liquid phase or macro scale k_{f1} which correspond to using the initial rate only or by curve fitting. The similarity of the constants is due to the similar procedure adopted as per Table 2.1 for the sub parts of the problem where the modeling approach was mentioned.

Table 5.1 Rate constant values for all the three models at different temperatures.

Temperature (K)	**Type of Model**	**k_{f1} (l/mol.min)**	**k_{f2} (l/mol.min)**
323.15	Model 1	0.0000165	0.0603
	Model 2	0.000414	0.1443
	Model 3	0.000414	0.0603
333.15	Model 1	0.0000237	0.0895
	Model 2	0.000673	0.1494
	Model 3	0.000673	0.0895
343.15	Model 1	0.0000333	0.1298
	Model 2	0.001064	0.1544
	Model 3	0.001064	0.1298
353.15	Model 1	0.0000460	0.1843
	Model 2	0.001638	0.1592
	Model 3	0.001638	0.1843

The rate constants k_{f1} and k_{f2} are further fitted to Arrhenius rate law as $k = k_0*\exp(-E/R*T)$. The linear fit for k_{f2} Vs 1/T obtained from Model 1, Model 2 and Model 3 are plotted in Fig. 5.4 (a) and Fig. 5.4(b).

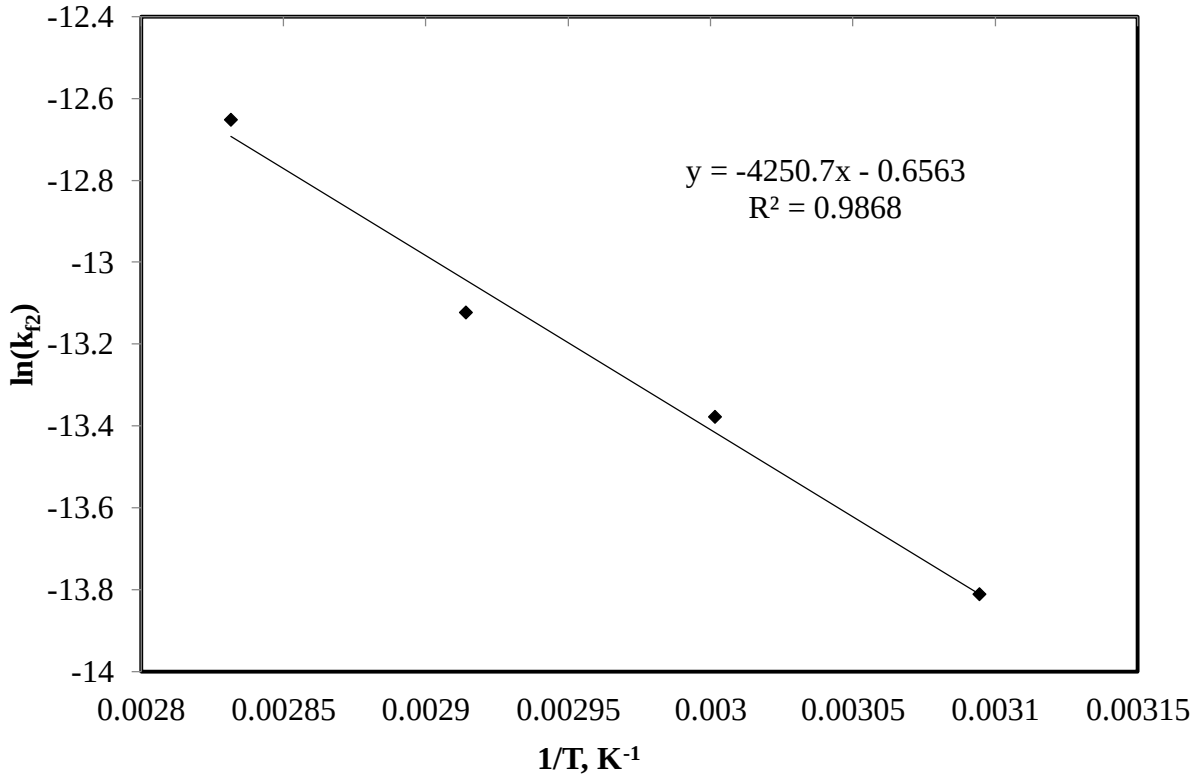

(a)

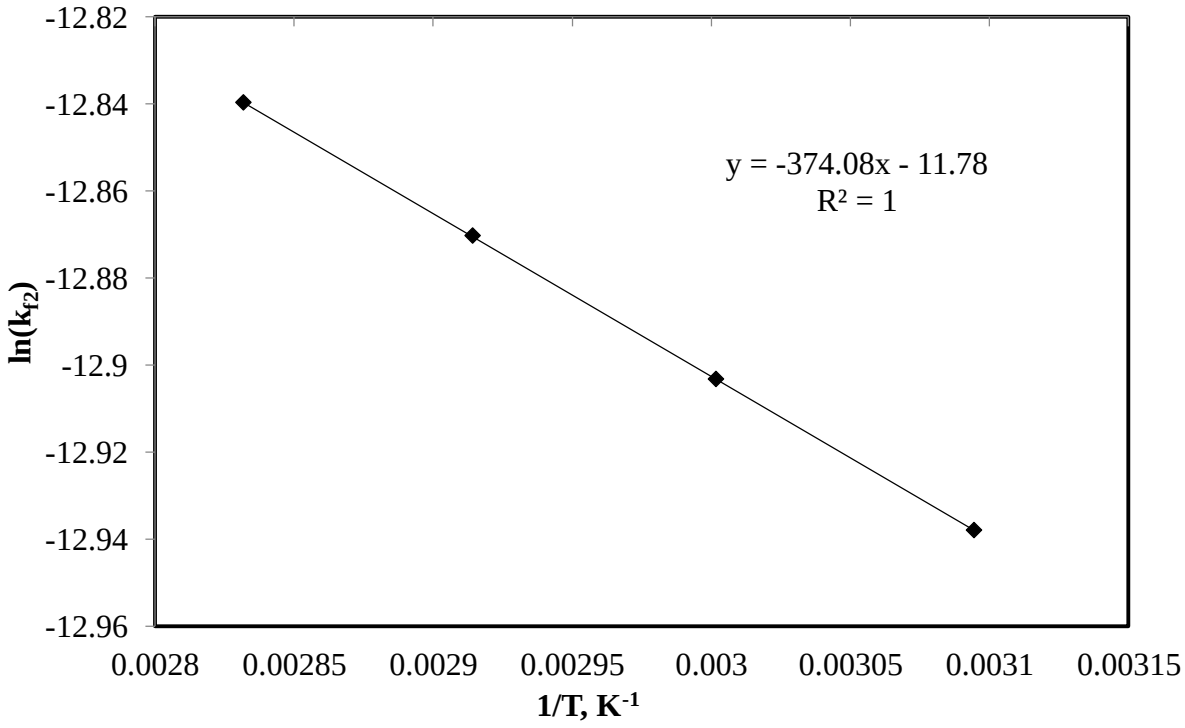

(b)

Fig. 5.4 Arrhenius plot for reaction rate constant inside the catalyst pores (a) For Model 1 and Model 3 (b) For model 2.

The values of pre-factor k_0 and activation energy E are tabulated in Table 5.2 for k_{f1} and k_{f2} for each of the models of Table 2.1.

Table 5.2 k_0 and E values for k_{f1} and k_{f2} for all three models.

Type of Model	Rate Constant, k_{f1}		Rate Constant, k_{f2}	
	Pre Exponential factor, k_{f1_0} (l/mol min)	Activation Energy, E_{f1} (J/mol)	Pre Exponential factor, k_{f2_0} (l/mol min)	Activation Energy, E_{f2} (J/mol)
Model 1	2.9659	32511.89	31126.02	35341.15
Model 2	4465	43507	0.46	3115
Model 3	4465	43507	31126.02	35341.15

5.2 Determination of kinetic constants from non-isothermal data

By taking the rate law as in Eq. (2.7) with input as both temperature (T) vs. time (*t*) and Concentration (C_A) vs. time (*t*), an objective function or error is defined as standard deviation between experimental C_A and predicted C_A over the entire time range defined as in Eq. (5.9).

$$Error = \sqrt{\frac{\sum_{i=1}^{n}\left(C_{A,pred,i}-C_{A,expt,i}\right)^2}{n}} \tag{5.9}$$

Here $C_{A,pred}$ is estimated by numerical integration of the differential equation by central difference method. Genetic algorithm of MATLAB is used to determine the four unknown constants by minimizing the error of Eq. (5.9).

5.3 Dynamic Model for reaction kinetics based on constant heat supply

A model was also developed to predict the start-up dynamics for a BRD system with constant heat supply. In this Eq. (2.7) is integrated by finite difference method in MATLAB. The algorithm invokes that maximum temperature attained in the reboiler is equal to the bubble point of the mixture which is determined using ASPEN software.

The bubble point temperature of a mixture of Acetic acid (A), Methanol (B), Methyl acetate (C) and Water (D) assuming from an initial 1:1 mole ratio of Acetic acid and Methanol is obtained from ASPEN as in Eq. (5.10)

$$T_{BP} = 59.993 + 24.5x_A + 13.938x_A^2 + 70.836x_A^3 \quad (5.10)$$

Now, the mixture temperature is assumed to vary with time owing to sensible heating as in Eq. 5.11(b). As per the literature the esterification reaction of the present system is having negligible ΔH_R.

$$\frac{-dC_A}{dt} = k_{f_0} e^{\frac{-E_f}{RT}} C_A^2 - k_{b_0} e^{\frac{-E_b}{RT}} (C_{A_0} - C_A)^2 \quad 5.11(a)$$

$$\frac{dT}{dt} = \frac{Q}{\sum n_i c_{pi}} \quad 5.11(b)$$

As soon as the temperature hits bubble point T_{BP}, the value of temperature is not updated. But there is a simultaneous reaction occurring which shifts the mole fraction x_A of acetic acid. Hence certain dynamics are anticipated in T(t) and $C_A(t)$. The result from this model will predict both temperature and concentration dynamics in the reactor as a coupled initial value problem.

5.4 Rate based model for distillation of binary non-reacting mixture

The aim here is to develop a steady state model where the reboiler composition is specified, heat input rate to reboiler is specified and distillate composition has to be predicted for total reflux condition in the column as shown in Fig. 4.1 (b). Some assumptions had to be made in order to arrive at a reasonable output. They are:

- The steady state temperature in the reboiler is assumed equal to the bubble point temperature in ^{0}C which is a linear function as $T_R = 109.6\text{-}30.8*X_{AR}$. this assumption is applied for all three heat input rates.
- The vapor generation rates of A and B in the reboiler are assumed to be proportional to the mole fractions in the liquid or the mole fraction of benzene ensuing from the vapor in reboiler is considered equal to 0.5 which is the initial mole fraction in the reboiler contents.
- A linear temperature profile is assumed along the height of the column. The expression is $T(z) = T_R\text{-}(z/H)(T_R\text{-}T_C)$ where T_C is the column temperature at top most point. It is assumed as T_C=65 °C. Here H is the height of the column.

By considering shell of thickness 'dz' as in Fig. 5.5 and performing material balance and component balance, the following set of differential equations were obtained for composition and molar flow rate variations along the height of the column.

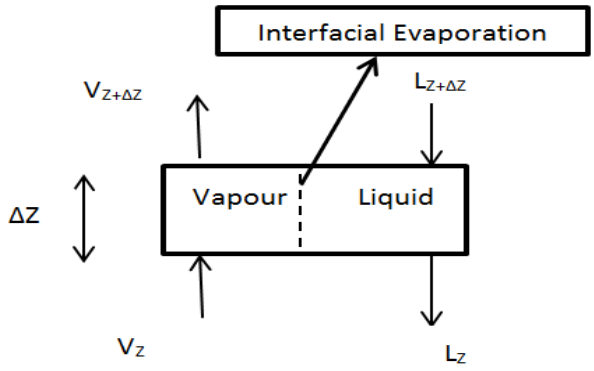

Fig. 5.5 Shell of thickness dz for material and component balance.

$$\frac{dV}{dz} = \frac{dL}{dz} \tag{5.12}$$

Where V and L are vapor and liquid molar flow rates. z is vertical height above reboiler. z = 0 corresponds to bottom and z = H corresponds to top of the column.

At infinite reflux distillate flow rate almost tends to zero and Eq.(5.10) gives V = L.

Component Balance for 'A' in vapor phase using evaporation rate based model gives,

$$\frac{d(y_A.V)}{dz} = K_A.A_c.a_c.(x_A.p_A^{sat} - y_A.p_t) \tag{5.13}$$

The RHS of Eq. 5.13 represents that the rate of evaporation of a component is proportional to the driving force as per the non – equilibrium suggested by Raoult's law. To recollect Raoult's law it says that $x_A.p_A^{sat} - y_A.p_t$ at equilibrium. Taking their difference as non – equilibrium the present proposal is a simple model.

Component Balance for 'B' in vapor phase

$$\frac{d(y_B.V)}{dz} = K_B.A_c.a_c.(x_B.p_B^{sat} - y_B.p_t) \tag{5.14}$$

Component Balance for 'A' in liquid phase

$$\frac{d(x_A.L)}{dz} = K_A.A_c.a_c.(x_A.p_A^{sat} - y_A.p_t) \tag{5.15}$$

Component Balance for 'B' in liquid phase

$$\frac{d(x_B.L)}{dz} = K_B.A_c.a_c.(x_B.p_B^{sat} - y_B.p_t) \quad (5.16)$$

In the present study at steady state, the reboiler temperature is assumed to be at bubble point of the mixture which is given by

$$T_R = 109.6 - 30.8\, x_{AR} \quad (5.17)$$

Temperature variation in the column is assumed to vary linearly from reboiler to the condenser as below

$$T(z) = T_R-(T_R-T_C)*(z/H) \quad (5.18)$$

At first node at the bottom of the column the vapor molar flow rates are related to the heat input rate as below

$$Q = V_A.\lambda_A + V_B.\lambda_B \quad (5.19)$$

The vapor generation rates of A and B in the reboiler are assumed to be proportional to the mole fraction in the liquid as below

$$V_A = V * x_{AR} \quad 5.20(a)$$

$$V_A = V * (1 - x_{AR}) \quad 5.20(b)$$

The saturated vapor pressures of Benzene (A) and Toluene (B) from Antoine equation are as in Eq. 21(a) and Eq. 21(b).

$$p_A^{sat} = 10^{\left(4.02232-\frac{1206.53}{220.291+T}\right)}, \text{ atm} \quad 5.21(b)$$

$$p_B^{sat} = 10^{\left(4.0854-\frac{1348.77}{219.976+T}\right)}, \text{ atm} \quad 5.21(b)$$

Where T is in ^{0}C

In the above Eq. (5.12) to Eq. (5.21) the notation for various symbols is as follows

'Q' is heat supplied to reboiler (Watts)

'L' is the molar flow rate of liquid from column to the reboiler (mol/sec)

'L_A' is the molar flow rate of component 'A' in liquid from column to the reboiler (mol/sec)

'L_B' is the molar flow rate of component 'B' in liquid from column to the reboiler (mol/sec)

'V' is the molar flow rate of the vapor from reboiler in to the column (mol/sec)

'V_A' is the molar flow rate of component 'A' in vapor from reboiler in to the column (mol/sec)

'V_B' is the molar flow rate of component 'B' in vapor from reboiler in to the column (mol/sec)

'x_A' mole fraction of component 'A' in liquid phase at a location z in the column

'y_A' mole fraction of component 'A' in vapor phase at a location z in the column

'x_{AR}' mole fraction of component 'A' in reboiler

'K_A' mass transfer coefficient of component 'A' (gmol/m^2.atm.s) as in Fig. 4.5

'A_c' Cross sectional area of the column (m^2)

'a_c' specific surface area available inside the column in the form of raschig rings (m^2/m^3) ~100 m^2/m^3 for raschig rings.

'p_A^{sat}' saturated vapor pressure of component 'A' at a location z inside the column (atm) as per Antoine equation

'x_B' mole fraction of component 'B' in liquid phase at a location z in the column

'y_B'mole fraction of component 'B' in vapor phase at a location z in the column

'x_{BR}' mole fraction of component 'B' in reboiler

'K_B' mass transfer coefficient of component 'B' (gmol/m^2.atm.s) as in Fig. 4.6

'p_B^{sat}'saturated vapor pressure of component 'B' at a location z inside the column (atm) as per Antoine equation

'p_t' Total pressure or atmospheric pressure (atm)

'λ_A' Latent heat of vaporization of component 'A'

'λ_B' Latent heat of vaporization of component 'B'

Simulation

The set of differential equations from Eq. (5.12) to Eq. (5.16) are solved numerically using explicit Euler forward finite difference method. It should be noted that the molar flow rate of vapor 'V' is in upward direction and molar flow rate of liquid 'L' is in downward direction. About 51 nodes are placed at equi-distance along the height of the column. This gives 50 segments of 1 cm each. The algorithm for this section is presented in appendix.

5.5 Application of rate based model for batch reactive distillation (BRD)

The modeling procedure is similar to section 5.4 for binary non reacting mixture in packed column but with reaction incorporated in reboiler as in Fig. 4.1(b). By this modelling approach it was intended to approach the distillate composition obtained in a BRD simulation with experiments. The trend of y_D (distillate mole fraction of Methyl acetate) with respect to change in heat supply rate to reboiler and packing's specific surface area were sought for.

By considering shell of thickness 'dz' as in Fig. 5.5 and performing material balance and component balance, the following set of differential equations were obtained for composition and molar flow rate variations along the height of the column.

$$\frac{dV}{dz} = \frac{dL}{dz} \tag{5.19}$$

Where V and L are vapor and liquid flow rates. z is vertical height above reboiler. z = 0 corresponds to bottom and z = H corresponds to top of the column.

At infinite reflux distillate flow rate almost tends to zero and Eq.(5.19) gives V = L.

Component Balance for 'A' in vapor phase using evaporation rate based model gives,

$$\frac{d(y_A.V)}{dz} = K_A.A_c.a_c.(x_A.p_A^{sat} - y_A.p_t) \tag{5.20}$$

The RHS of Eq. 5.13 represents that the rate of evaporation of a component is proportional to the driving force as per the non – equilibrium suggested by Raoult's law. To recollect Raoult's law it says that $x_A.p_A^{sat} - y_A.p_t$ at equilibrium. Taking their difference as non – equilibrium the present proposal is a simple model.

Component Balance for 'B' in vapor phase

$$\frac{d(y_B.V)}{dz} = K_B.A_c.a_c.(x_B.p_B^{sat} - y_B.p_t) \tag{5.21}$$

Component Balance for 'C' in vapor phase

$$\frac{d(y_C.V)}{dz} = K_C.A_c.a_c.(x_C.p_C^{sat} - y_C.p_t) \tag{5.22}$$

Component Balance for 'D' in vapor phase

$$\frac{d(y_D.V)}{dz} = K_D.A_c.a_c.(x_D.p_D^{sat} - y_D.p_t) \tag{5.23}$$

Component Balance for 'A' in liquid phase

$$\frac{d(x_A.L)}{dz} = K_A.A_c.a_c.(x_A.p_A^{sat} - y_A.p_t) \quad (5.13)$$

Component Balance for 'B' in liquid phase

$$\frac{d(x_B.L)}{dz} = K_B.A_c.a_c.(x_B.p_A^{sat} - y_A.p_t) \quad (5.24)$$

Component Balance for 'C' in liquid phase

$$\frac{d(x_C.L)}{dz} = K_C.A_c.a_c.(x_C.p_C^{sat} - y_C.p_t) \quad (5.25)$$

Component Balance for 'D' in liquid phase

$$\frac{d(x_D.L)}{dz} = K_D.A_c.a_c.(x_D.p_D^{sat} - y_D.p_t) \quad (5.26)$$

In the present study at steady state, the reboiler temperature is assumed to be at bubble point of the mixture which is given by

$$T_{BP} = 59.99. + 24.5x_{AR} + 13.938x_{AR}^2 + 70.836x_{AR}^3 \quad (5.27)$$

At first node at the bottom of the column the vapor molar flow rates are related to the heat input rate as below

$$Q = V_A.\lambda_A + V_B.\lambda_B + V_C.\lambda_C + V_D.\lambda_D \quad (5.28)$$

The above equation can be rearranged to relate vapour flow rate from the reboiler to the column and heat input to the reboiler as follows

$$V = \frac{Q}{x_{AR}.\lambda_A + x_{BR}.\lambda_B + x_{CR}.\lambda_C + x_{DR}.\lambda_D} \quad (5.29)$$

The vapor generation rates of A, B, C and D in the reboiler are assumed to be proportional to the mole fraction in the liquid as below

$$V_A = x_{AR}.V \quad (5.30a)$$

$$V_B = x_{BR}.V \quad (5.30b)$$

$$V_C = x_{CR}.V \quad (5.30c)$$

$$V_D = x_{DR}.V \quad (5.30d)$$

The saturated vapor pressures of Acetic acid (A), Methanol (B), Methyl acetate (C) and Water (D) from Antoine equation are as in Eq. 21(a-d).

$$p_A^{sat} = 10^{-5}.exp^{\left(22.1 - \frac{3654.62}{T - 45.39}\right)}, \text{ atm} \quad 5.31(a)$$

$$p_B^{sat} = 10^{-5}.exp^{\left(23.5 - \frac{3643.3}{T - 33.43}\right)}, \text{ atm} \quad 5.31(b)$$

$$p_C^{sat} = 10^{-5}.exp^{\left(21.5 - \frac{2662.78}{T - 53.46}\right)}, \text{ atm} \quad 5.31(c)$$

$$p_D^{sat} = 10^{-5}.exp^{\left(23.22-\frac{3835.18}{T-45.34}\right)}, \text{ atm} \qquad 5.31(d)$$

In the above equations the notation for various symbols is as follows

'Q' is heat supplied to reboiler (Watts)

'L' is the molar flow rate of liquid from column to the reboiler (mol/sec)

'L_A' is the molar flow rate of component 'A' in liquid from column to the reboiler (mol/sec)

'L_B' is the molar flow rate of component 'B' in liquid from column to the reboiler (mol/sec)

'L_C' is the molar flow rate of component 'C' in liquid from column to the reboiler (mol/sec)

'L_D' is the molar flow rate of component 'D' in liquid from column to the reboiler (mol/sec)

'V' is the molar flow rate of the vapor from reboiler in to the column (mol/sec)

'V_A' is the molar flow rate of component 'A' in vapor from reboiler in to the column (mol/sec)

'V_B' is the molar flow rate of component 'B' in vapor from reboiler in to the column (mol/sec)

'V_C' is the molar flow rate of component 'C' in vapor from reboiler in to the column (mol/sec)

'V_D' is the molar flow rate of component 'D' in vapor from reboiler in to the column (mol/sec)

'x_A' mole fraction of component 'A' in liquid phase at a location z in the column

'y_A' mole fraction of component 'A' in vapor phase at a location z in the column

'x_{AR}' mole fraction of component 'A' in reboiler

'K_A' mass transfer coefficient of component 'A' (gmol/m^2.atm.s)

'A_c' Cross sectional area of the column (m^2)

'a_c' specific surface area available inside the column in the form of raschig rings (m^2/m^3) ~100 m^2/m^3 for raschig rings.

'p_A^{sat}' saturated vapor pressure of component 'A' at a location z inside the column (atm)

'x_B' mole fraction of component 'B' in liquid phase at a z location in the column

'y_B'mole fraction of component 'B' in vapor phase at a z location in the column

'x_{BR}' mole fraction of component 'B' in reboiler

'K_B' mass transfer coefficient of component 'B' (gmol/m^2.atm.s)

'p_B^{sat}'saturated vapor pressure of component 'B' at a z location inside the column (atm)

'x_C' mole fraction of component 'C' in liquid phase at a z location in the column

'y_C' mole fraction of component 'C' in vapor phase at a z location in the column

'x_{CR}' mole fraction of component 'C' in reboiler

'K_C' mass transfer coefficient of component 'C' (gmol/m^2.atm.s)

'p_C^{sat}' saturated vapor pressure of component 'C' at a location z inside the column (atm)

'x_D' mole fraction of component 'D' in liquid phase at a location z in the column

'y_D' mole fraction of component 'D' in vapor phase at a location z in the column

'x_{DR}' mole fraction of component 'D' in reboiler

'K_D' mass transfer coefficient of component 'D' (gmol/m^2.atm.s)

'p_D^{sat}' saturated vapor pressure of component 'D' at a location z inside the column (atm)

'p_t' Total pressure or atmospheric pressure (atm)

'λ_A' Latent heat of vaporization of component 'A'

'λ_B' Latent heat of vaporization of component 'B'

'λ_C' Latent heat of vaporization of component 'C'

'λ_D' Latent heat of vaporization of component 'D'

Simulation

The set of differential equations from Eq. (5.19) to Eq. (5.26) are solved numerically using explicit Euler forward finite difference method. It should be noted that the molar flow rate of vapor 'V' is in upward direction and molar flow rate of liquid 'L' is in downward direction. About 51 nodes are placed at equi-distance along the height of the column. This gives 50 segments of 1 cm each. The algorithm for this section is presented in Appendix.

CHAPTER 6
RESULTS AND DISCUSSION

Results and Discussion

6.1 Particle scale simulation of pore diffusion model and validation

Simulations were carried out with all the models described in Table 2.1 of section 2.1 and the results are discussed as follows.

Concentration distribution inside and outside catalyst particle

The spatial concentration distribution at an instant of time during the dynamic simulation inside the geometry consisting of two domains i.e., one inside the catalyst and the other bulk of the liquid is shown in Fig. 6.1 with the help of slice in the comsol software. As we know the conversion is high in the region inside the catalyst particle as compared to bulk of the liquid, the region inside the particle has lower concentration of the reactant species and in particular that of acetic acid (A). To bring out a clear picture of the concentration distribution in both the domains the concentration profile from one face of the cell to the other face passing through the catalyst at different times is shown in Fig. 6.1.

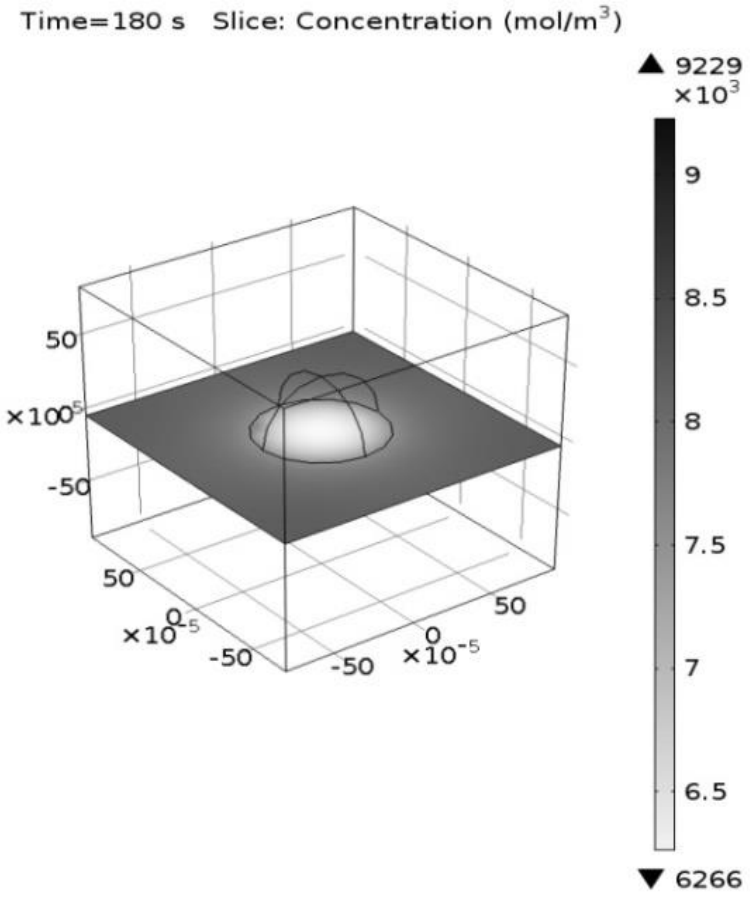

Fig. 6.1 Spatial concentration distribution inside the catalyst particle and around it in the solution at an instant of time 180 s during dynamic simulation.

6.1.1 Validation of model

The rate constants evaluated for all the three models as in Table 5.1 are used to determine the conversion of acetic acid at various temperatures and validated with that of experimental conversion of acetic acid vs time. It was noticed that model 3 is in good agreement with that of experimental values. Model 3 is further validated to see the effect of conversion with respect to that of intrinsic parameters like different temperatures (323.15 – 353.15 K), different catalyst loading (0.01-0.05 gm/cc) and different particle size (400 – 1000 µm) and is listed in subsequent figures.

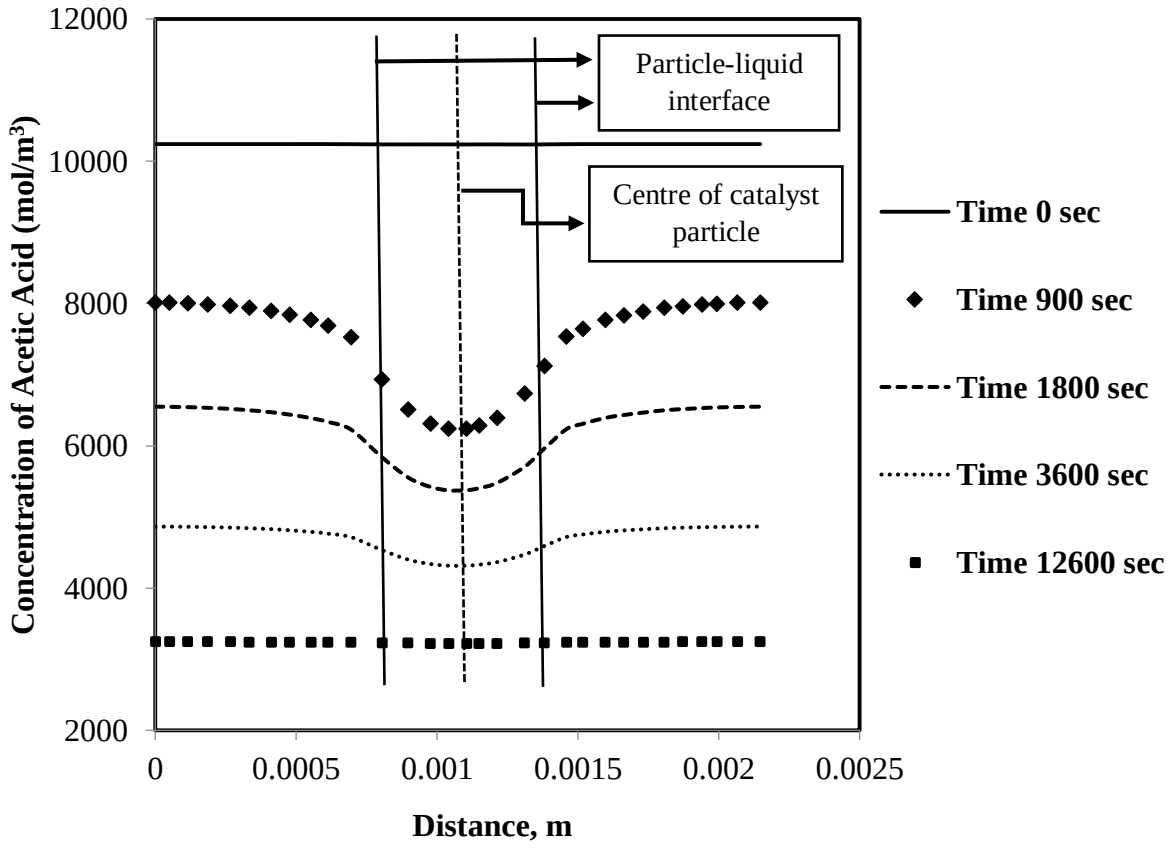

Fig. 6.2 Concentration profiles along an arc length from one face of cell to opposite face passing through the catalyst at different times.

6.1.1.1 Effect of temperature

Temperature is considered to be as major intrinsic parameters for the evaluation of reaction kinetics. Increase in temperature brings out an instinctive thought that there will be increase in conversion caused either by increase in probability of collision between molecules or by fast diffusion of molecules towards active site of the catalyst where there are sufficient amount of H^+ ions to catalyze before giving rise to respective products. Another approach to compare mathematically is by Arrhenius expression which says that with increase of temperature the exponential value increases thereby the rate constant value increases. Increase in rate constant increases the rate of reaction as it is holds direct proportional relationship. All the three models were used to validate with respect to experimental investigations carried out at three different temperatures 333.15 K, 343.15 K, and 353.15 K for a particle diameter of 725 µm and catalyst loading of 0.025 gm/cc and are shown in Fig. 6.3, Fig. 6.4, and Fig. 6.5. It was observed that conversion reached equilibrium value very fast at high temperatures. The proposal of three models were evaluated and it appears that evaluating the initial rate of reaction from two data points (Time = 0 and Time = 15 min) has resulted in lesser k_{f1} value and thereby it lead to error in the prediction as can be seen from Fig. 6.3, 6.4 and 6.5. To explain further it is the difference between linear interpolation and cubic interpolation that has resulted in different numerical values of the parameter k_{f1}.

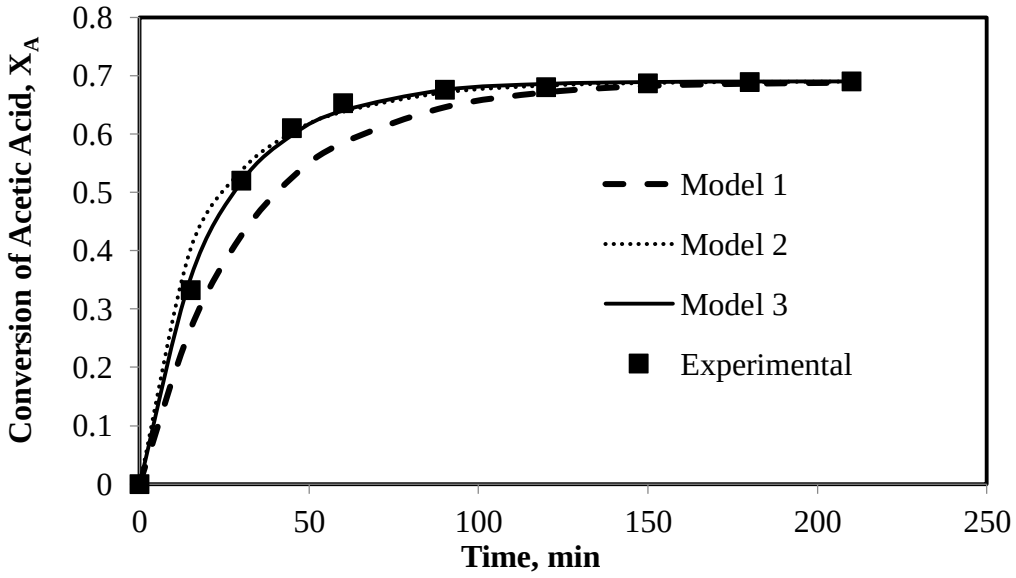

Fig. 6.3 Kinetics of acetic acid conversion for temperature of 353.15 K at constant catalyst loading of 0.025 g/cc and particle diameter of 725 µm as calculated from experimental data and predicted by the simulation.

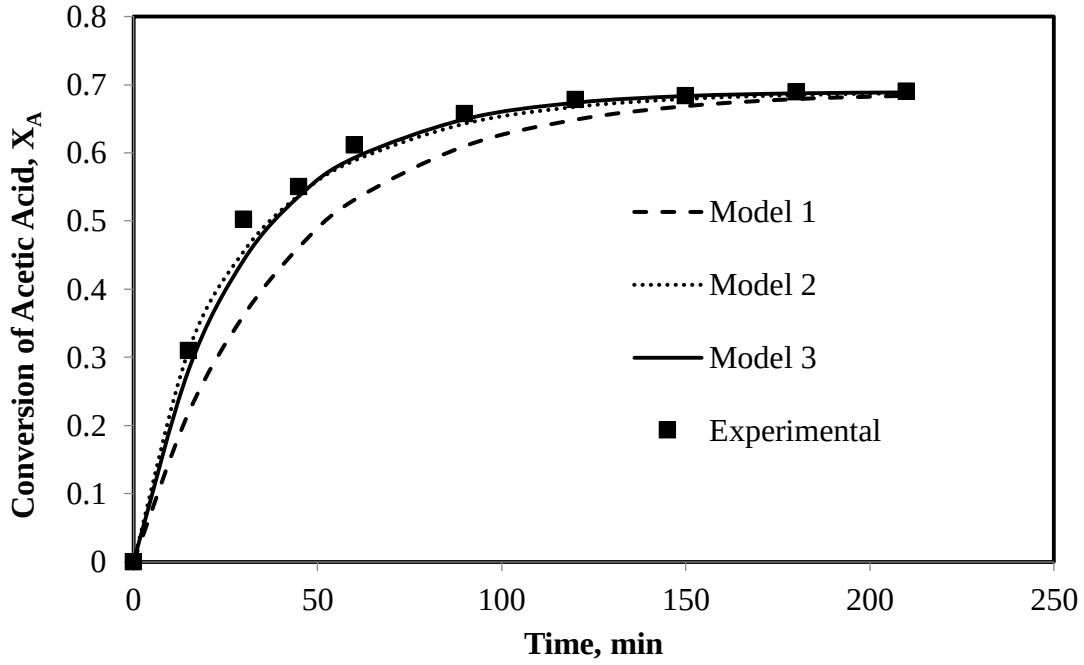

Fig. 6.4 Kinetics of acetic acid conversion for temperature of 343.15 K at constant catalyst loading of 0.025 g/cc and particle diameter of 725 µm as calculated from experimental data and predicted by the simulation.

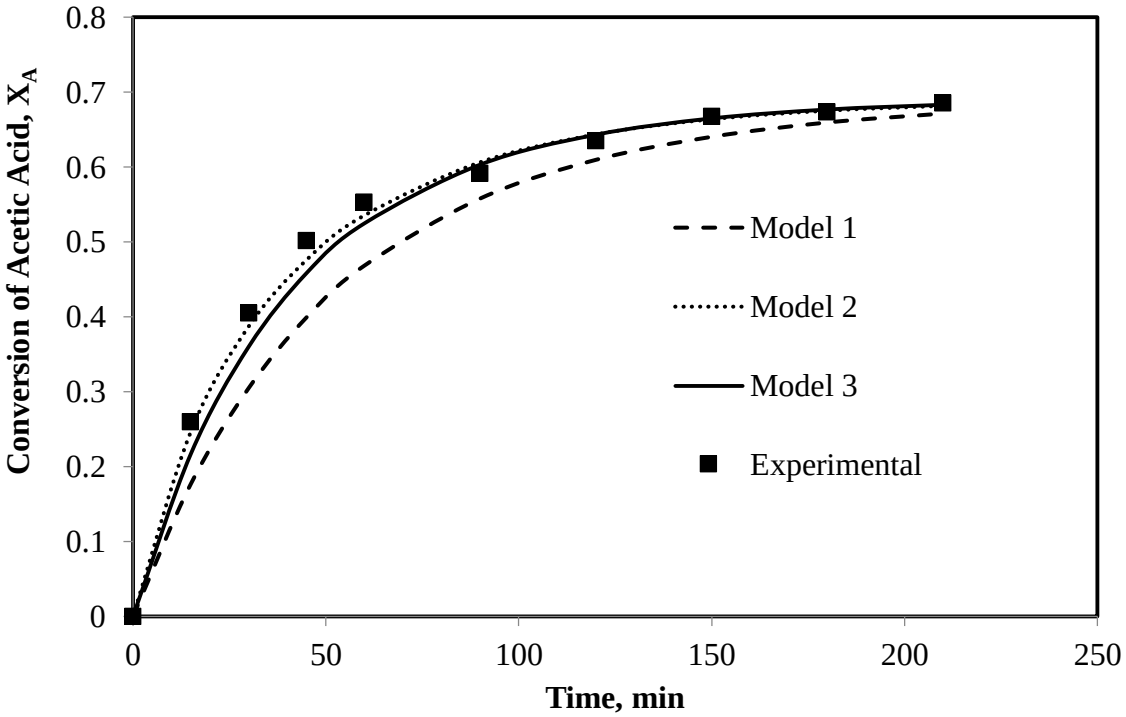

Fig. 6.5 Kinetics of acetic acid conversion for temperature of 333.15 K at constant catalyst loading of 0.025 g/cc and particle diameter of 725 µm as calculated from experimental data and predicted by the simulation.

Further, model 3 which is in good agreement with that of experimental results is plotted separately to account the effect of conversion with respect to variation in temperature and is shown in Fig. 6.6. These results enlighten that temperature controls the reaction to major extent and as it increases the time taken by the system to reach equilibrium is decreased.

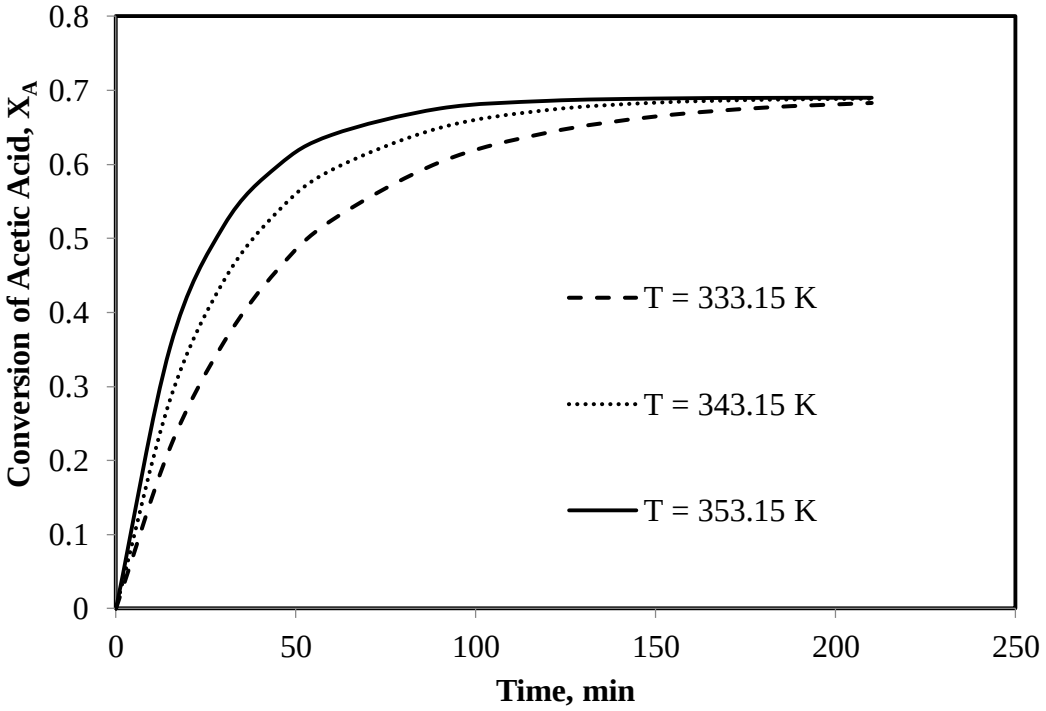

Fig. 6.6 Kinetics of acetic acid conversion for different temperatures at constant catalyst loading of 0.025 g/cc and particle diameter of 725 µm as predicted by the simulation using Model 3.

6.1.1.2 Effect of particle diameter

The particle diameter effect keeping the same catalyst loading is also simulated. The results were obtained for three different particle sizes for a constant catalyst loading of 0.025 gm/cc and at a temperature of 343.15 K.

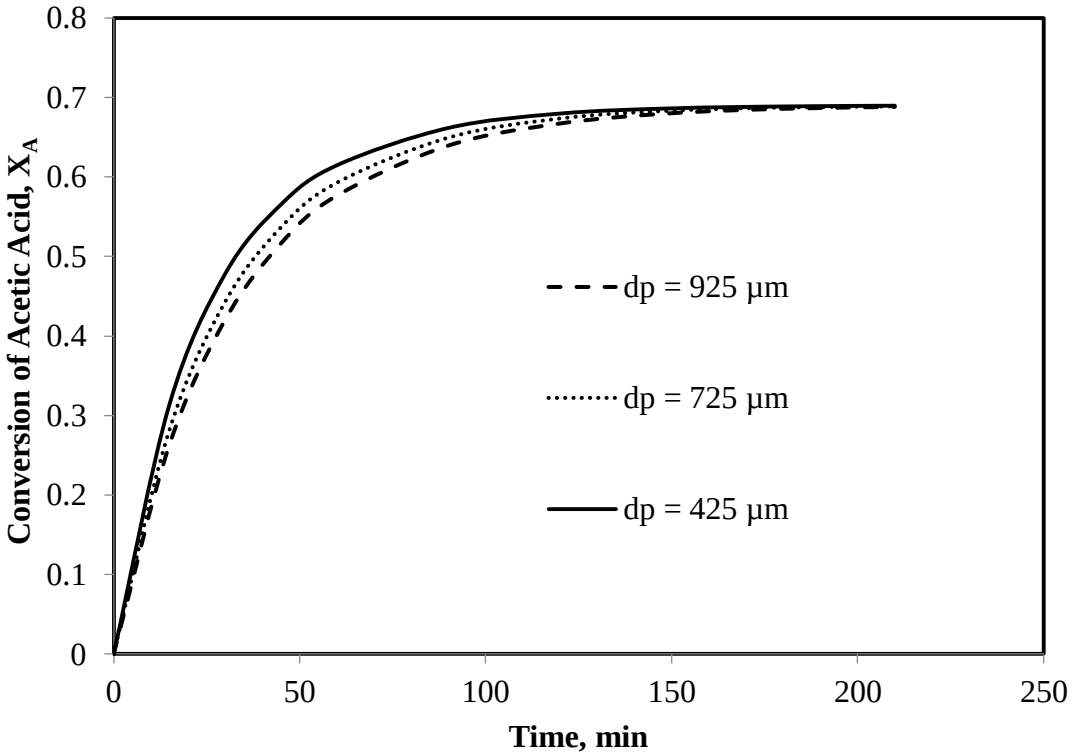

Fig. 6.7 Kinetics of acetic acid conversion for various particle sizes at constant loading of 0.025 g/cc as predicted by the simulation using k_{f1} evaluated with MATLAB and k_{f2} evaluated with COMSOL Multiphysics.

Interestingly there is no much variance in the kinetics owing particle size. This must be substituted with conventional explanation that reaction rate is proportional to $1/R_p$ i.e., lower the particle size higher is the conversion and it must be attributed when the reaction takes place at the surface of the catalyst in a heterogeneous reaction. In the present case particle pore volume is also utilized and hence the entire volume of catalyst particles is same as long as the catalyst loading is same. But the resultant dependency of the reaction rate over the catalyst particle size can be obtained by solving the reaction – diffusion equation inside the catalyst particle. Fig. 6.7 shows the simulated results of kinetics of acetic acid conversion for different particle sizes and at a constant catalyst loading of 0.025 gm/cc and at a temperature of 343.15 K.

6.1.1.3 Effect of catalyst loading

Simulations were also carried out at different catalyst loading for a temperature of 343.15 K and at a particle size of 725 µm. The kinetics effect with respect to catalyst loading is shown in Fig. 6.8. When the amount of catalyst loading is increased for a particular size of particle the reaction rate increases because of more H^+ ions available for the catalysis and gives rise to constituent products. Increase in catalyst loading has a linear increase in conversion may be an erroneous conclusion. If catalyst loading is considered then particle size also needs to be addressed.

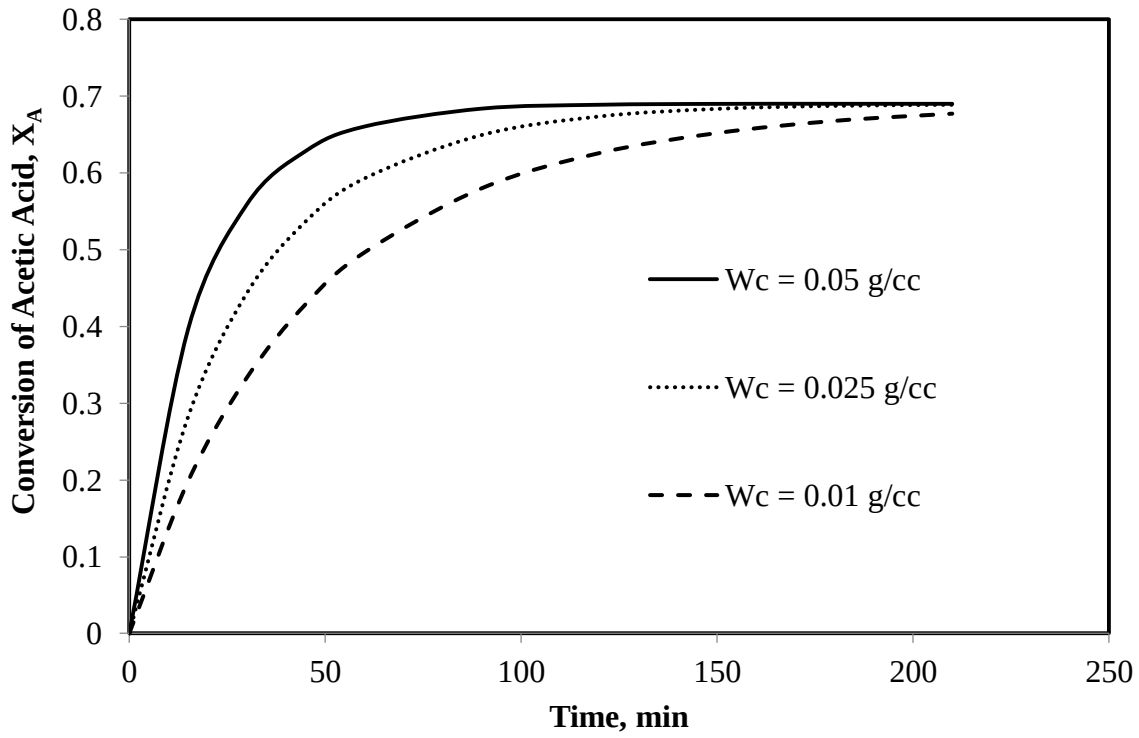

Fig. 6.8 Kinetics of acetic acid conversion for various catalyst loading with particle diameter of 725 µm as predicted by the simulation using k_{f1} evaluated with MATLAB and k_{f2} evaluated with COMSOL Multiphysics.

6.2 Predicted rate constants for pseudo homogeneous model from non-isothermal data

By taking the rate law as in Eq (2.7) with input as both T vs. time (t) and C_A vs. time (t), an objective function or error is defined as standard deviation between experimental C_A and predicted C_A over the entire time range defined as in Eq. (5.9). Here $C_{A,pred}$ is estimated by numerical integration of the differential equation by central difference method:

Genetic algorithm of MATLAB is used to determine the four unknown constants by minimizing the error of Eq. (5.9) as given in Table 6.1 for two different heat inputs. The constraints used during the optimization of parameters are that all the four constants have to be positive.

Table 6.1 Kinetic constants for pseudo homogenous model for two different heat inputs.

Q (W)	k_{f0} (L/gmol.s)	E_f (J/gmol)	K_{b0} (L/gmol.s)	E_b (J/gmol)
32	7.43	34,309	2.98	38,519
50	7.02	33,424	2.99	36,345

It can be noticed that the prediction of present result has repeatability.

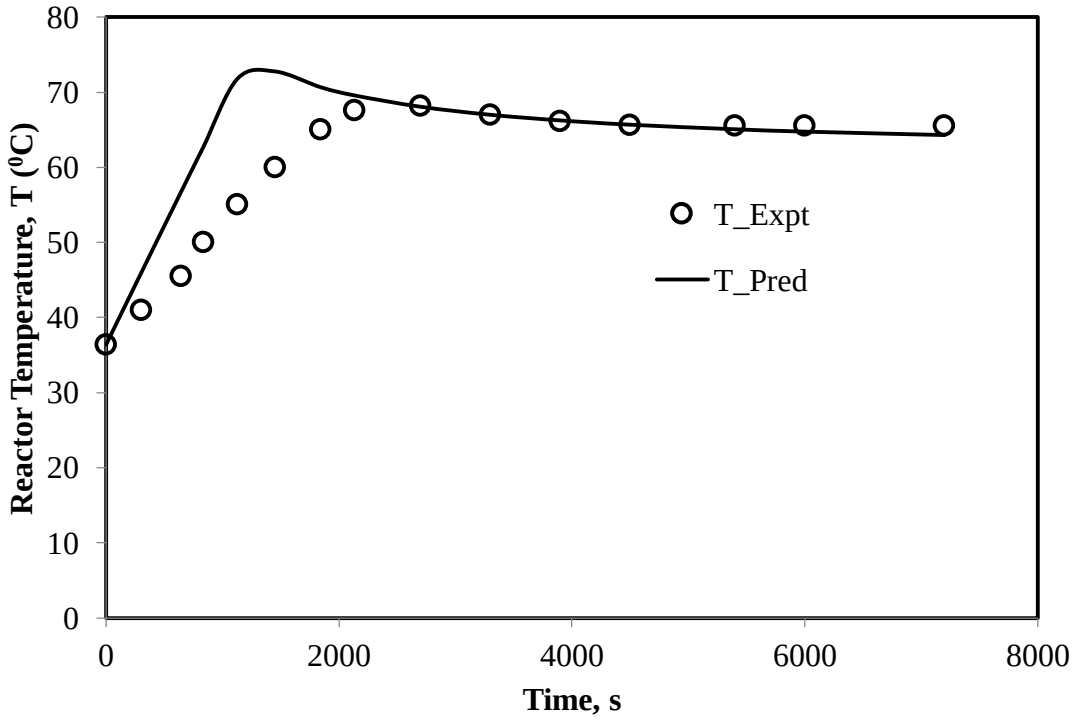

(a)

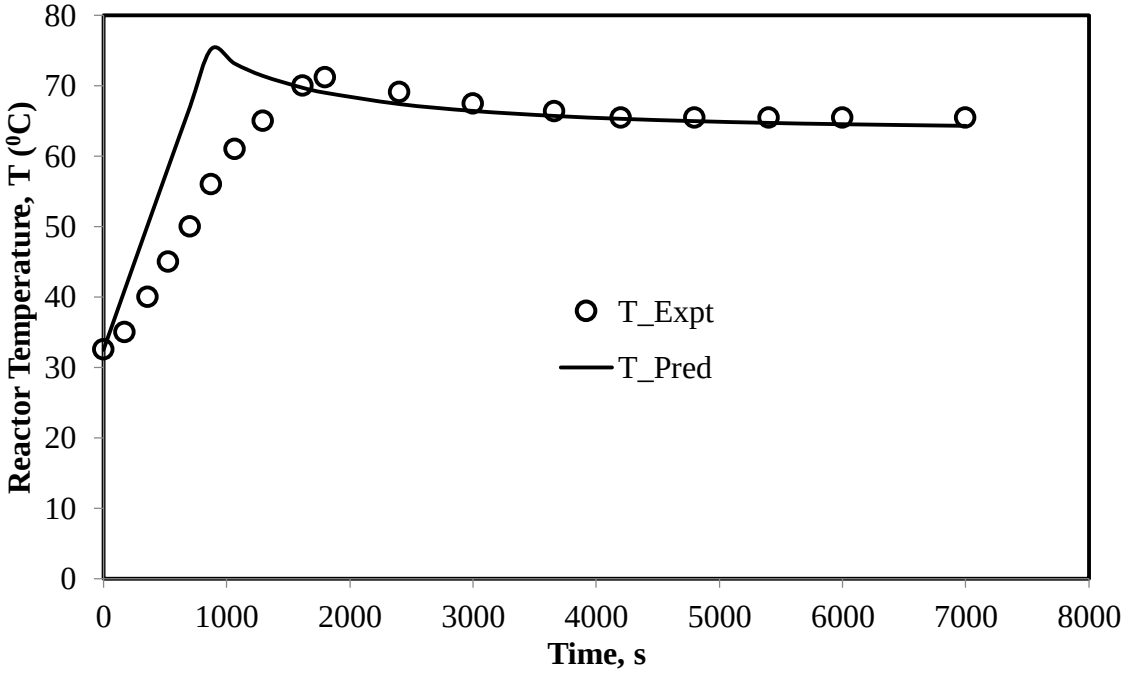

(b)

Fig. 6.9 Reboiler temperature dynamics for different heat inputs: (a) 32 W, (b) 50 W.

For the initial ramp region of T vs t, the predicted value is higher than experimental values. This may be because in experiments there is some cooling taking place due to evaporation and condensation on surface of mixture in the reactor.

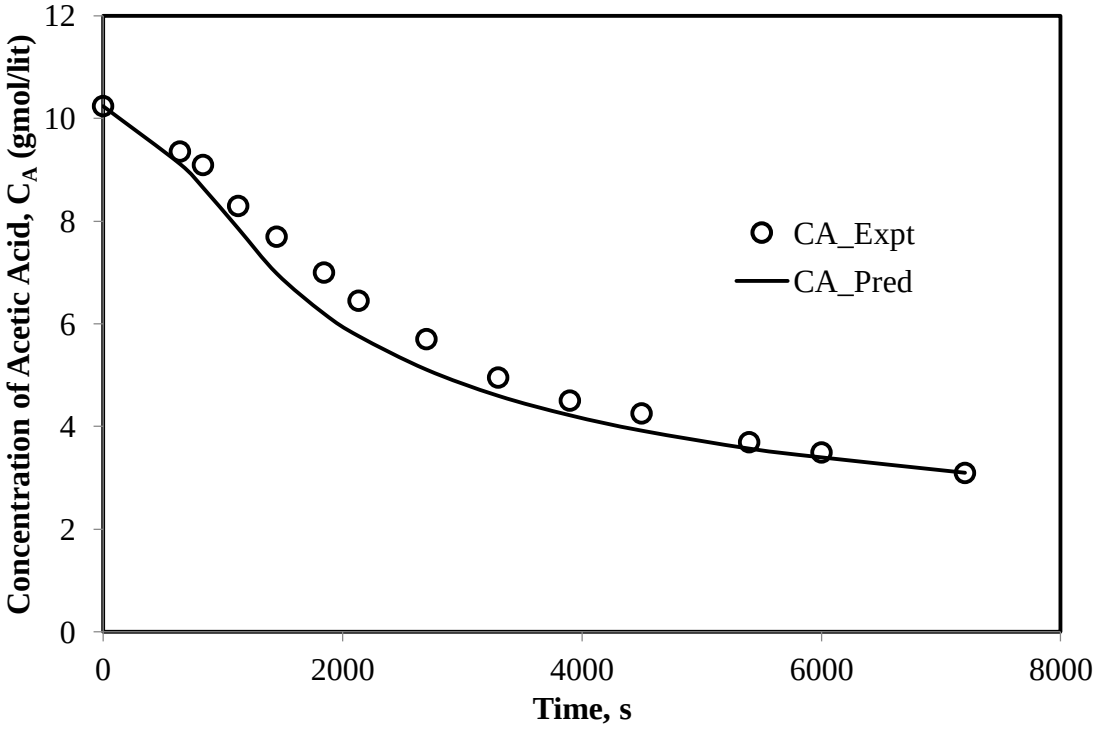

(a)

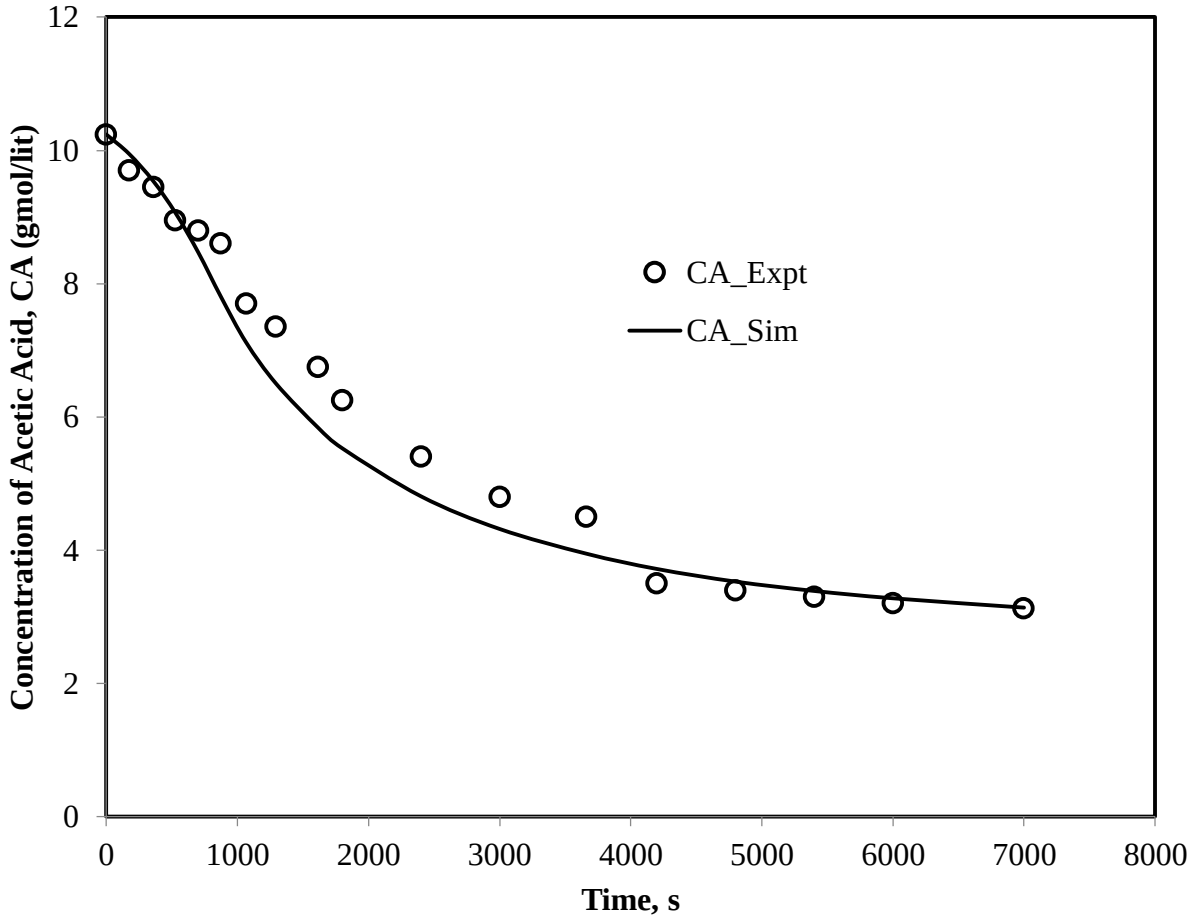

(b)

Fig. 6.10 Experimental and predicted concentration dynamics of acetic acid for two different heat inputs: (a) 32 W, (b) 50 W.

6.3 Prediction of distillate composition in non-reacting system

The obtained results are presented in Fig. 6.11 for temperature versus local height in the column, Fig. 6.12 for benzene (A) mole fraction x_A in liquid along the height of the column, Fig. 6.13 for benzene (A) mole fraction y_A in vapor along the height of the column and Table 6.2 indicating the composition of distillate at total reflux obtained from simulation and experiments. The good comparison between experimental distillate composition and simulated value matched very well for the binary non-reacting mixture. Therefore, the model equations of binary system can be extended for the present system of four components along with reaction in the reboiler. Thus the validation for the binary system helped the purpose of applying rate based model for the four component system with more confidence.

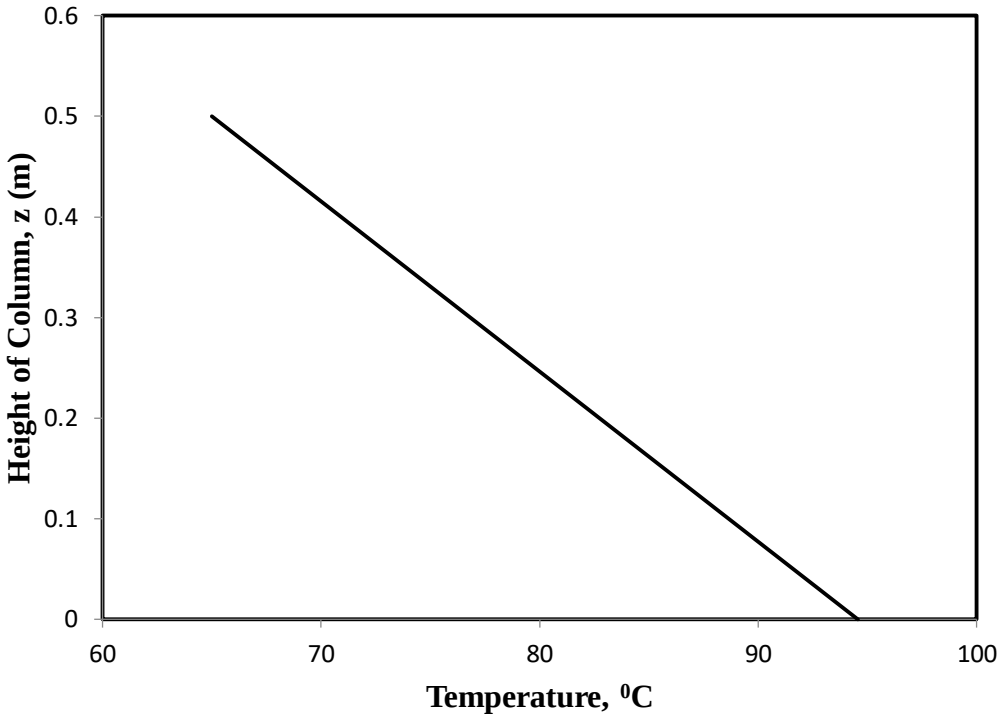

Fig. 6.11 Temperature variation along the height of the column at steady state

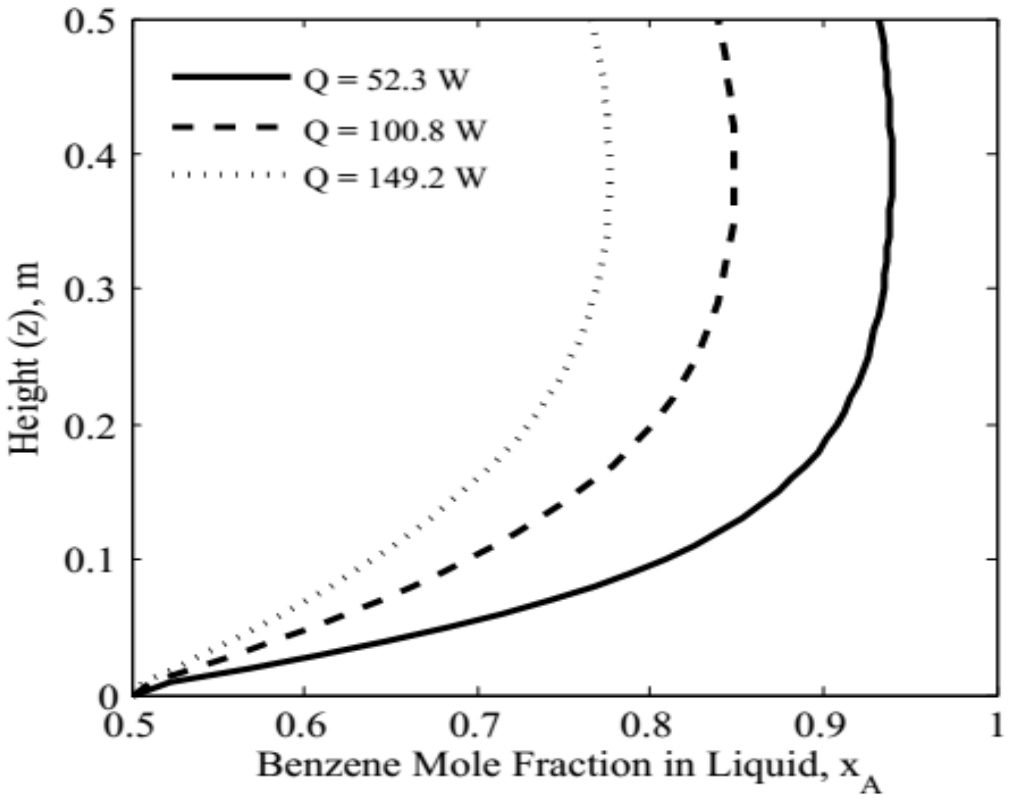

Fig. 6.12 Benzene mole fraction in liquid along the height of the column.

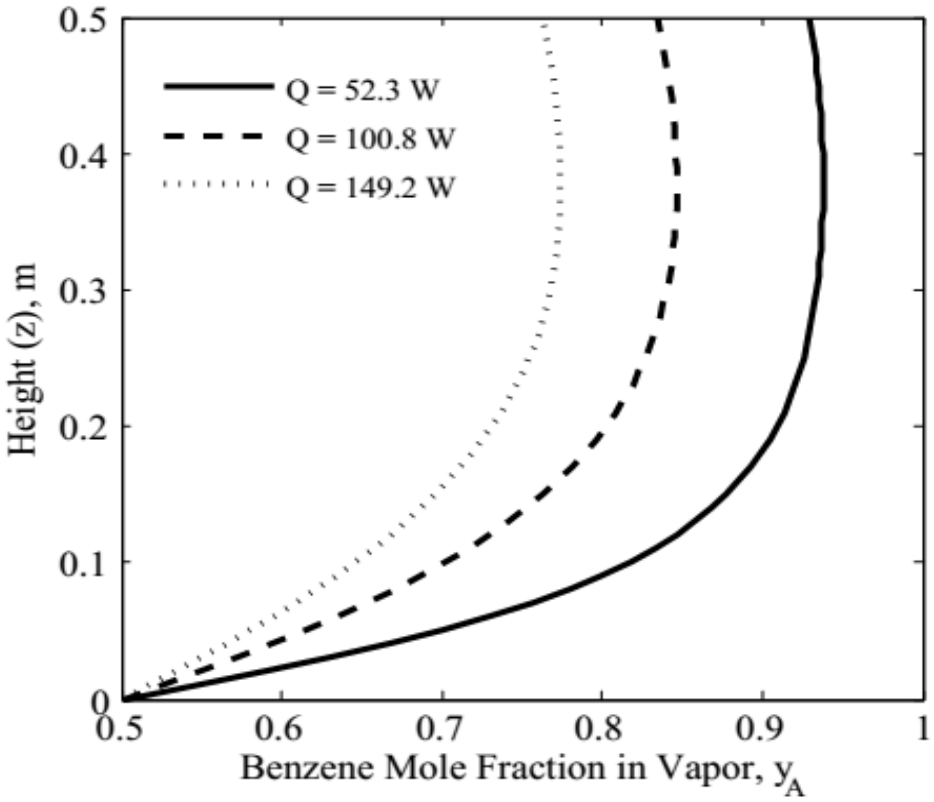

Fig. 6.13 Benzene mole fraction in vapor along the height of the column.

Table 6.2 Simulation results as compared to experimental data.

Run No.	Heat input rate to Reboiler (Watts)	y_{A,D_expt}	y_{A,D_sim}	$L_{condensor}$ (mol/s)	$L_{A,condenser}$ (mol/s)
1	52.3	0.94	0.93	0.0016	0.0015
2	100.8	0.88	0.835	0.0025	0.0021
3	149.2	0.79	0.763	0.0037	0.0028

In Fig. 6.12 and Fig. 6.13, the difference in vapor and liquid mole fractions of the components mainly depends on vapor and liquid flow rates. Since we are using a small heat input rate the distillation or the rectification seems to occur at a quasi-steady state implying that the streams leaving each node in the finite difference method of simulation are nearly at equilibrium. One important analysis taken up is the evaluation of local relative volatility in the column at various locations as compared to the equilibrium value. The local relative volatility αsimulation is obtained from the definition $(y_A/(1-y_A))/(x_A/(1-x_A))$ and αequilibrium is obtained from ratio of

saturation pressures of A and B at the prevailing local temperature as P_A^{sat}/P_B^{sat}. These two are compared in Fig. 6.14.

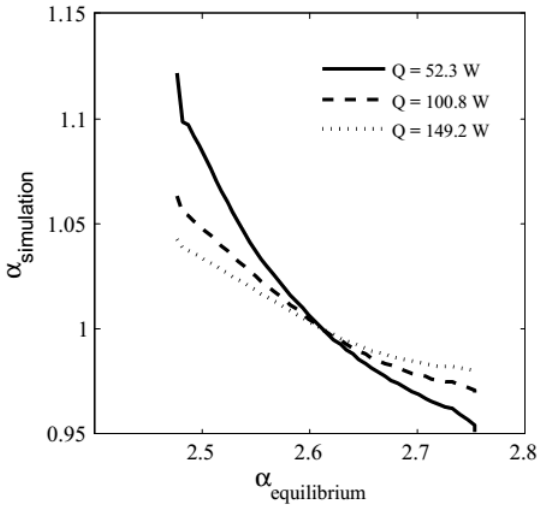

Fig. 6.14 Local relative volatility as obtained from steady state simulation composition and from temperature.

The data evaluated and plotted in Fig. 6.14 is from Fig. 6.12 and Fig. 6.13. Usually relative volatility of 1 implies azeotrope situation. But owing to the rate based model approach of simulation, such an azeotrope situation is overcome. Owing to the quasi steady state as mentioned earlier, the relative volatility is close to 1. It also can be inferred that half of the column height itself is sufficient to obtain the maximum possible rectification. Also the temperature variation in the column is assumed to be linear as per Eq.(5.16). Hence it could be a minor factor that the intersection point of Fig. 6.14 is due to such an assumption and also the reason for relative volatility less than 1. It indicates that the more volatile benzene is rectified majorly near the reboiler itself and after half a height of the column there is no much rectification.

6.4 Prediction of distillate composition in esterification reaction carried out in BRD apparatus

Fig. 4.14 (a-e) depict a similar trend with mechanism as shown schematically in Fig. 6.16.

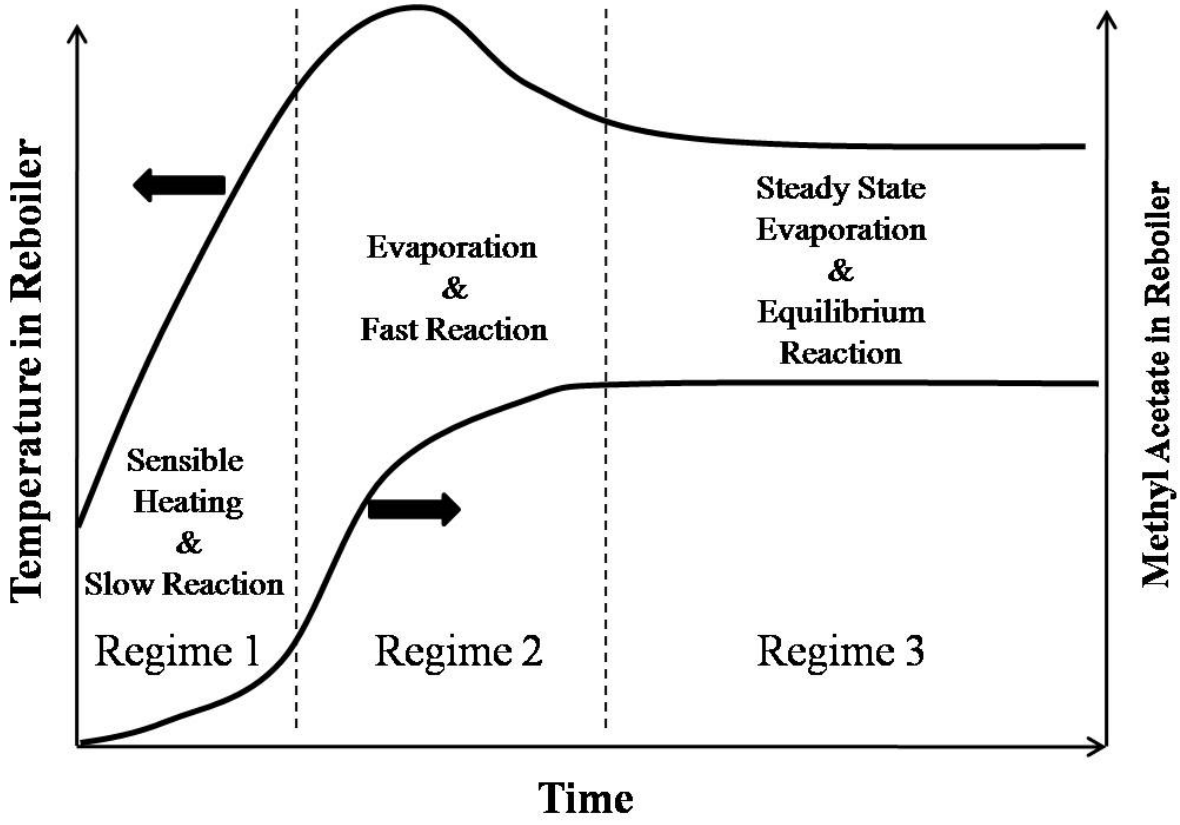

Fig. 6.15 Schematic representation of temperature dynamics and corresponding phenomena occurring in the reboiler.

The regime 1 corresponds to sensible heating of the reactant mixture. The starting temperature of all the experiments was around 25-28 ^{0}C. As the temperature increases and with the presence of catalyst, reaction occurs leading to the formation of products namely methyl acetate and water. It is here important to note the boiling points of the four components approximately as methanol-64^{0}C, acetic acid-118^{0}C, methyl acetate-57 ^{0}Cand water-100^{0}C at atmospheric pressure. As the product methyl acetate begins to form the mixture temperature tends to decrease since the bubble point temperature is lowered. Simultaneously there is evaporation from the reboiler mixture. Therefore there is drop in temperature owing to evaporative cooling i.e., the required latent heat for vapour formation has to be lost by the liquid. Thus in regime 2 there is reaction and evaporation in the reboiler. As the heating proceeds vapour is condensed at the top of the column to form condensate which flows back to the reboiler and thereby cooling its contents by a little bit. Hence in regime 3 there is steady state evaporation, steady

state condensate reflux, thermal equilibrium and reaction equilibrium in the reboiler. Therefore by the end of regime 3 both reaction and distillation reach a steady state. The observed average reboiler steady state temperature was around 66-72 ^{0}C. In general higher heat input rates have slightly higher steady state temperatures.

It was observed that distillate did not form for few operating conditions. It is because the vapour condenses completely within the column before reaching the top condenser. The interface location of maximum vapour height for low and high heat inputs and with wall temperature as 40 ^{0}C is shown schematically in Fig. 6.17 (a) and Fig. 6.17 (b).

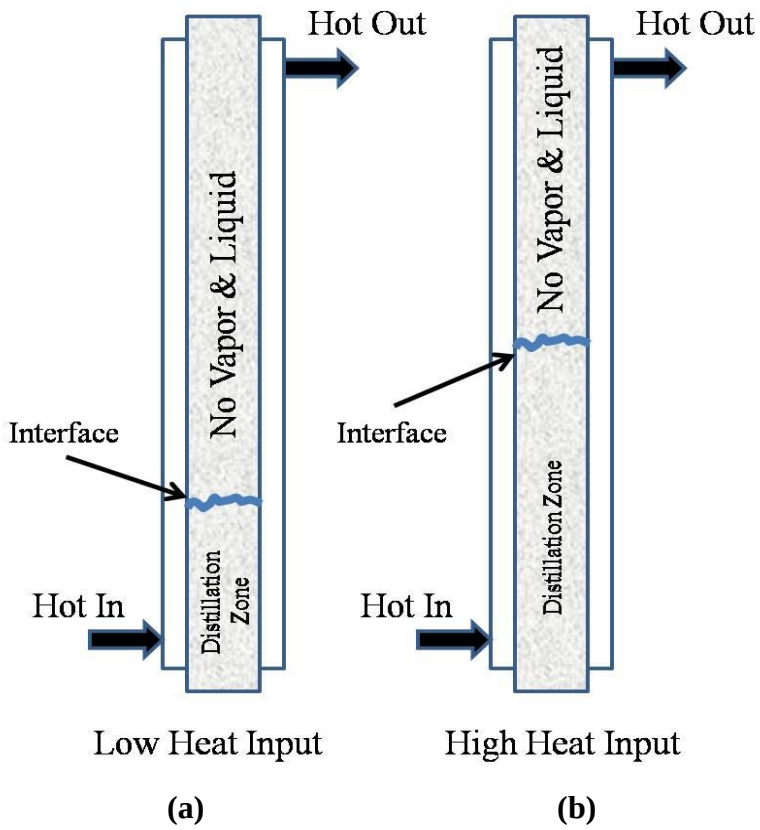

Fig. 6.16 (a) Vapour-air interface for low heat input rate and (b) Vapour-air interface for high heat input rate.

Out of 15 operating conditions four of them did not yield any distillate because of the above mentioned reason. The recorded time for onset of distillate is tabulated in Table 4.5.

Based on the reaction kinetics [Patan et al., 2018] and the temperature dynamics of reboiler for an insulated condition with three different heat inputs (50 W, 100 W and 150 W), the mole fraction of methyl acetate dynamics is simulated and compared with various isothermal conditions as shown in Fig. 6.17 (a-c).

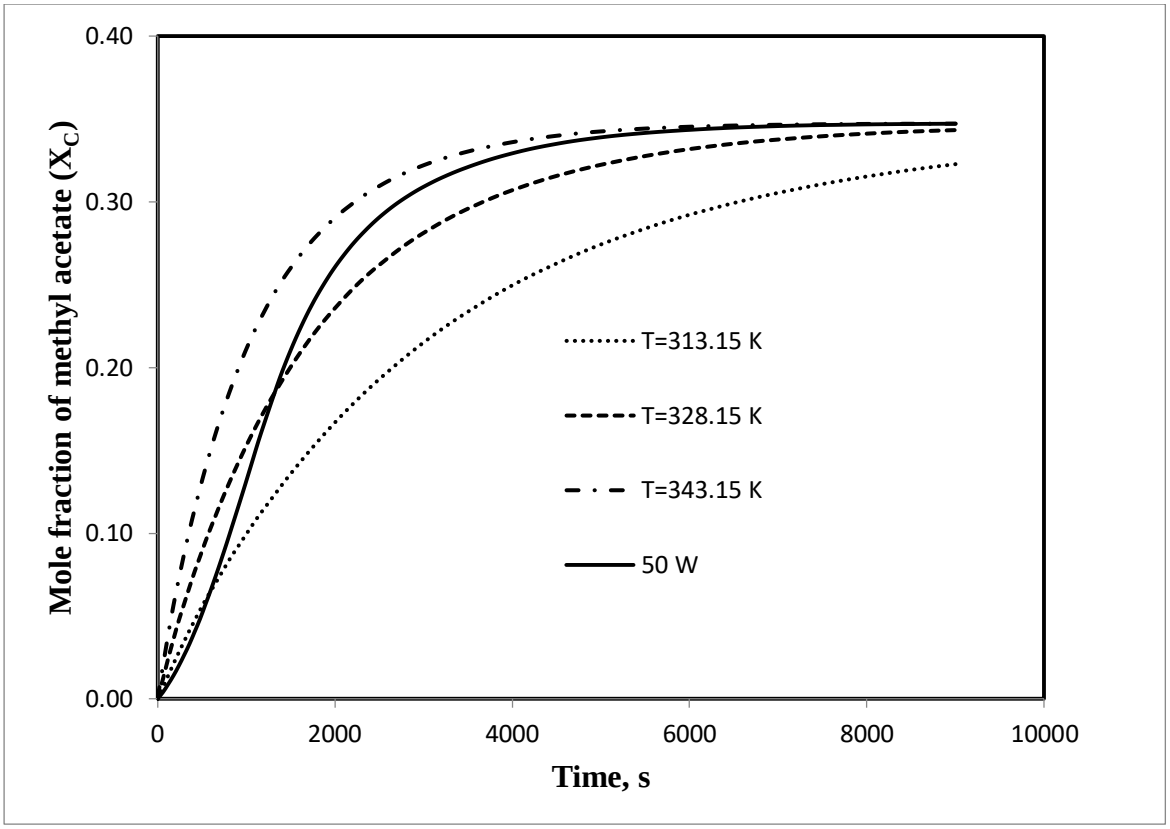
0.40
0.30
0.20
0.10
0.00
Mole fraction of methyl acetate (X_C)
0
2000
4000
6000
8000
10000
Time, s
T=313.15 K
T=328.15 K
T=343.15 K
50 W

(a)

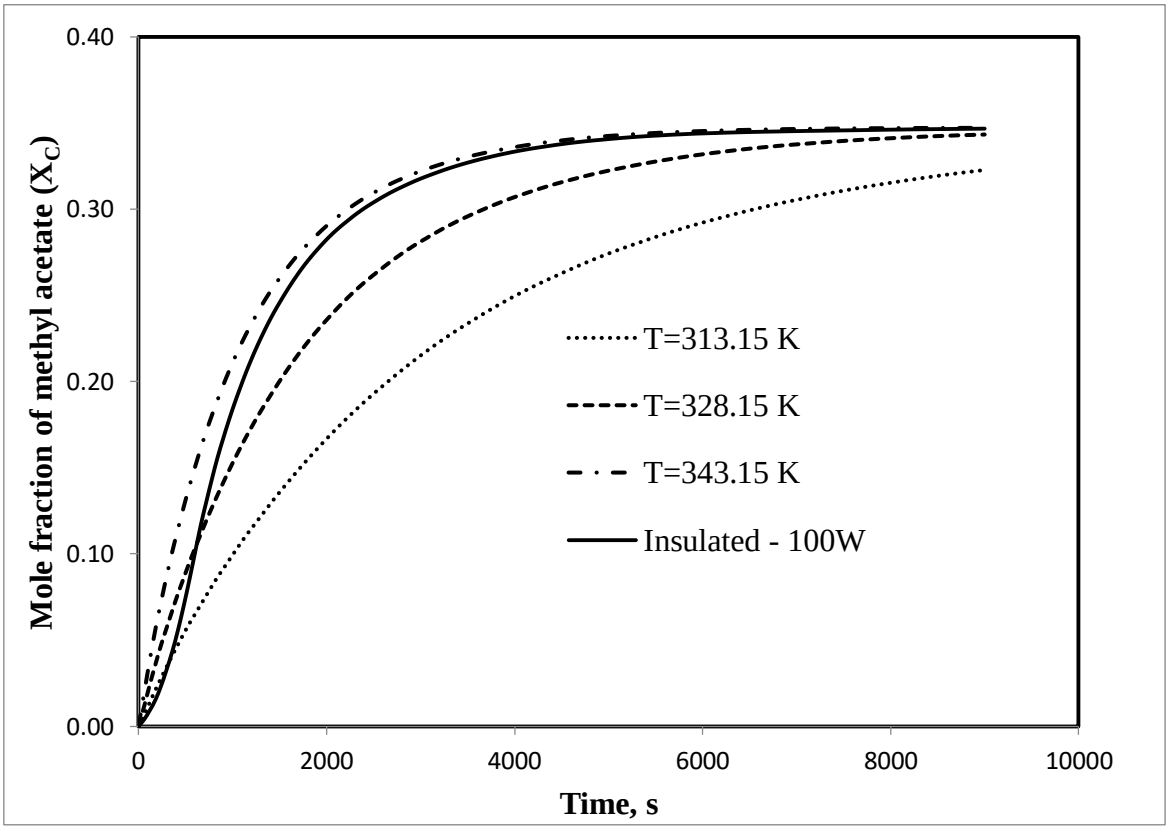
0.40
0.30
0.20
0.10
0.00
Mole fraction of methyl acetate (X_C)
0
2000
4000
6000
8000
10000
Time, s
T=313.15 K
T=328.15 K
T=343.15 K
Insulated - 100W

(b)

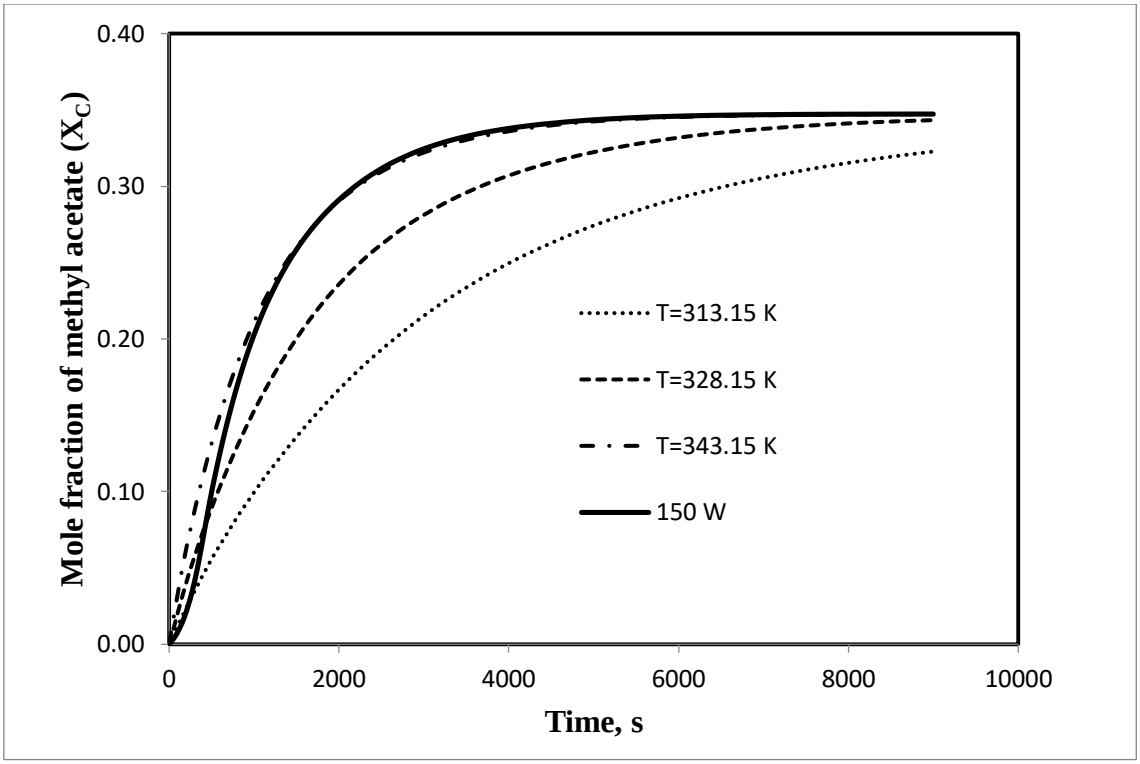

(c)

Fig. 6.17 Dynamics of mole fraction of methyl acetate (solid line) in the reboiler obtained from kinetics for (a) Insulated 50 W (b) Insulated 100 W (c) Insulated 150W and compared with isothermal conditions.

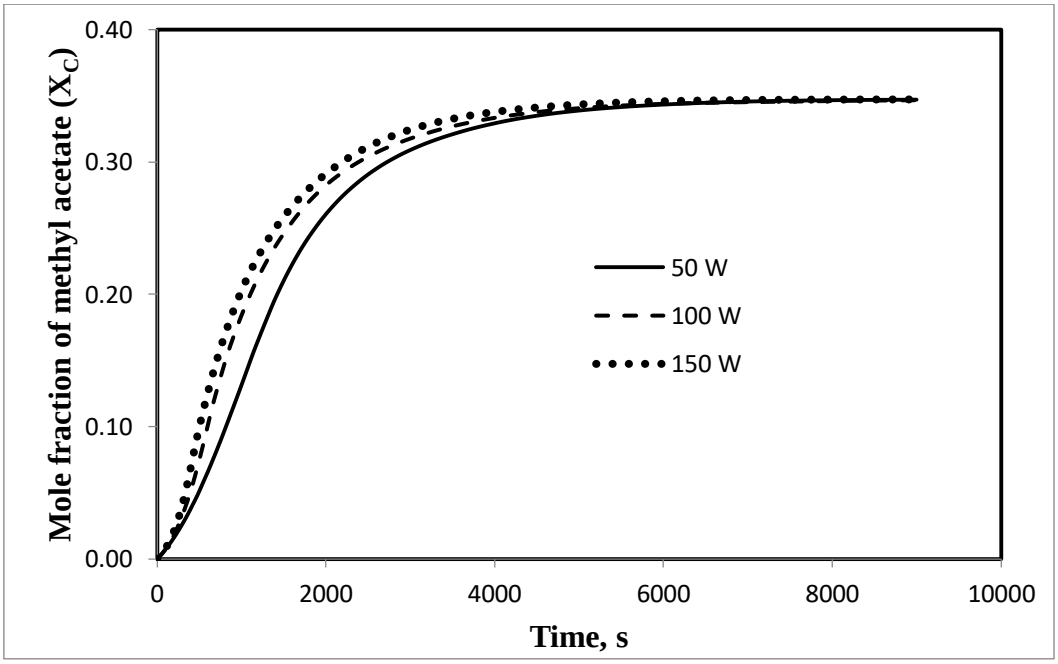

Fig. 6.18 Comparative dynamics of mole fraction of methyl acetate in the reboiler obtained from kinetics for insulated conditions with three different heat inputs.

It can be observed from Fig. 6.17(a-c) that the mole fraction dynamics of the product verses time is highly sensitive to a temperature difference of 10 K. Whereas the dynamics as per Fig. 6.18 the effect of heat input rate variation is less. Another advantage with constant heat supply is that the product formation is slightly of second order type than a fast first order type for isothermal condition.

The mole fraction of methyl acetate in the reboiler at the onset of distillate (at transient from regime 1 to regime 2) is obtained from simulation using the literature kinetics and presented in Table 6.3.

Table 6.3 Simulated Mole fraction of methyl acetate in reactor at onset of distillation

Q (W) / **T_{wall} (^{0}C)**	50	100	150
40	-	-	-
50	0.269	0.136	0.098
60	0.211	0.131	0.093
Ambient (28 ^{0}C)	-	0.208	0.136
Insulated	0.278	0.190	0.124

It can be observed from Table 6.3 that the onset of distillate takes place early for high heat input rate to the reboiler and for higher wall temperature of the rectification column.

Table 6.4 Experimental and simulated mole fractions in distillate of BRD for different heat inputs.

	Q = 50 W	**Q = 100 W**	**Q = 150 W**	**Q = 32 W**
Mole fraction of 'C' in distillate from experiment, $y_{C,D}$	0.686	0.6538	0.6437	
Mole fraction of 'C' in distillate from simulation, $y_{C,D}$	0.7054	0.6519	0.6339	**~1.0**
Adjusted a_c value m^2/m^3	60	90	120	**~90**

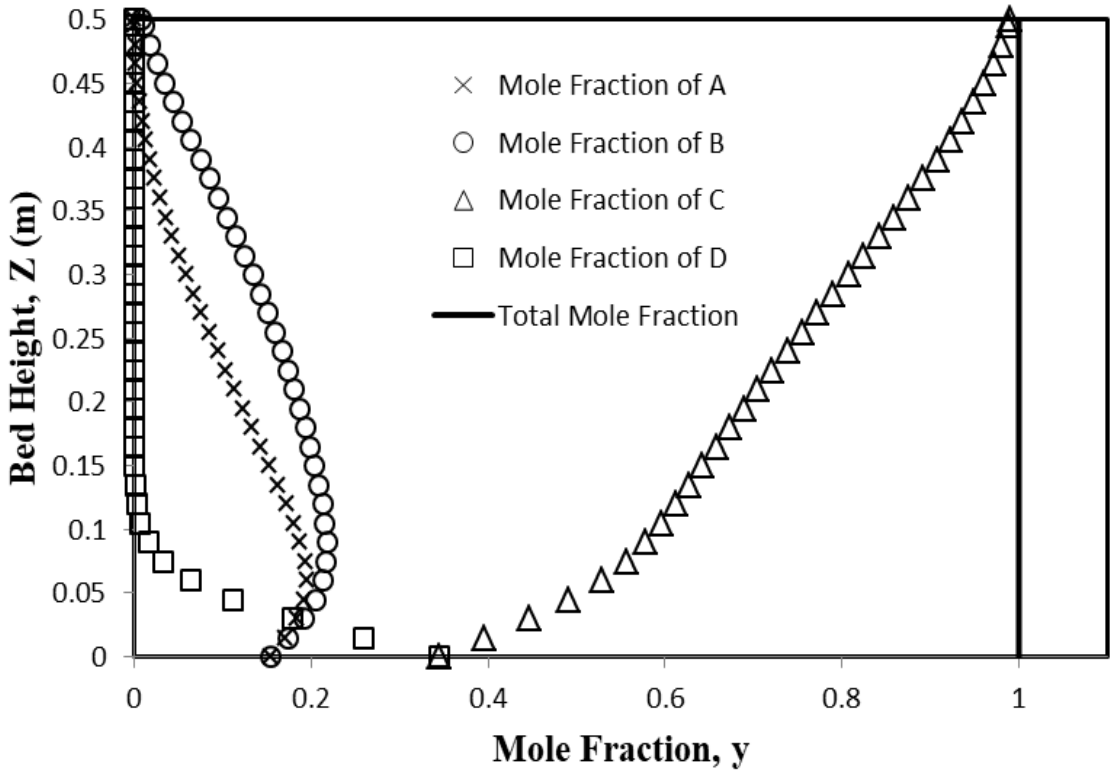
Bed Height, Z (m)
0.5
0.45
0.4
0.35
0.3
0.25
0.2
0.15
0.1
0.05
0
0
0.2
0.4
0.6
0.8
1
Mole Fraction, y
Mole Fraction of A
Mole Fraction of B
Mole Fraction of C
Mole Fraction of D
Total Mole Fraction

(a)

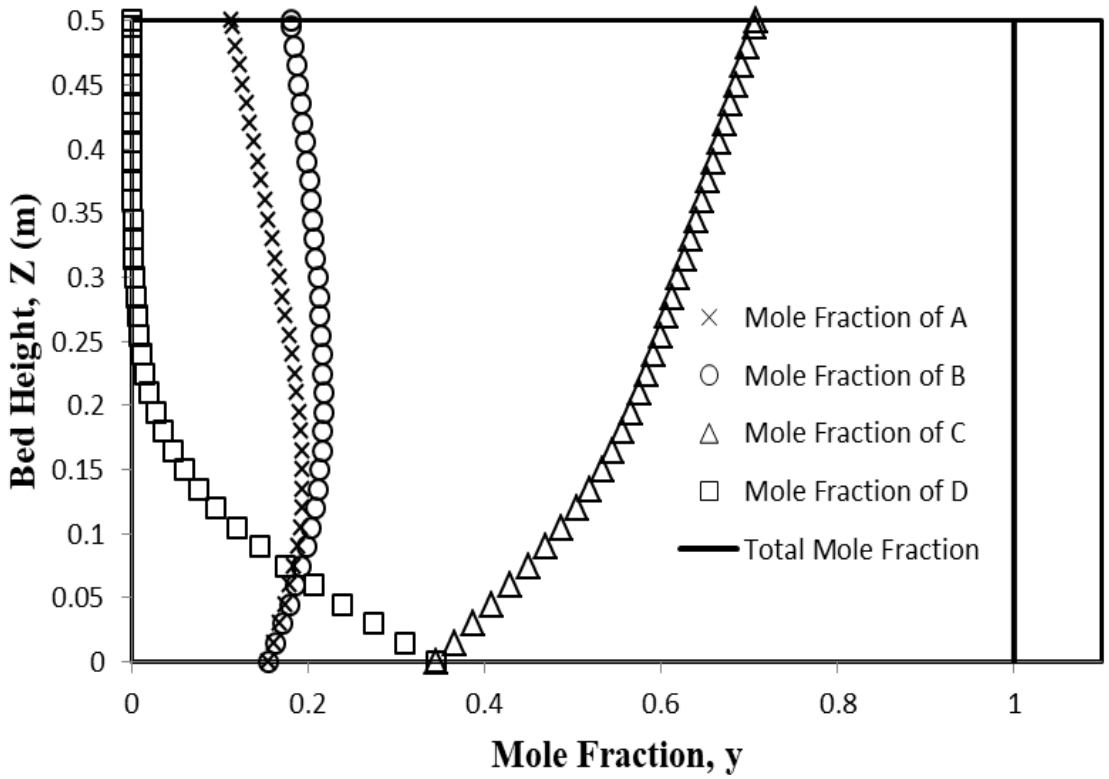
Bed Height, Z (m)
0.5
0.45
0.4
0.35
0.3
0.25
0.2
0.15
0.1
0.05
0
0
0.2
0.4
0.6
0.8
1
Mole Fraction, y
Mole Fraction of A
Mole Fraction of B
Mole Fraction of C
Mole Fraction of D
Total Mole Fraction

(b)

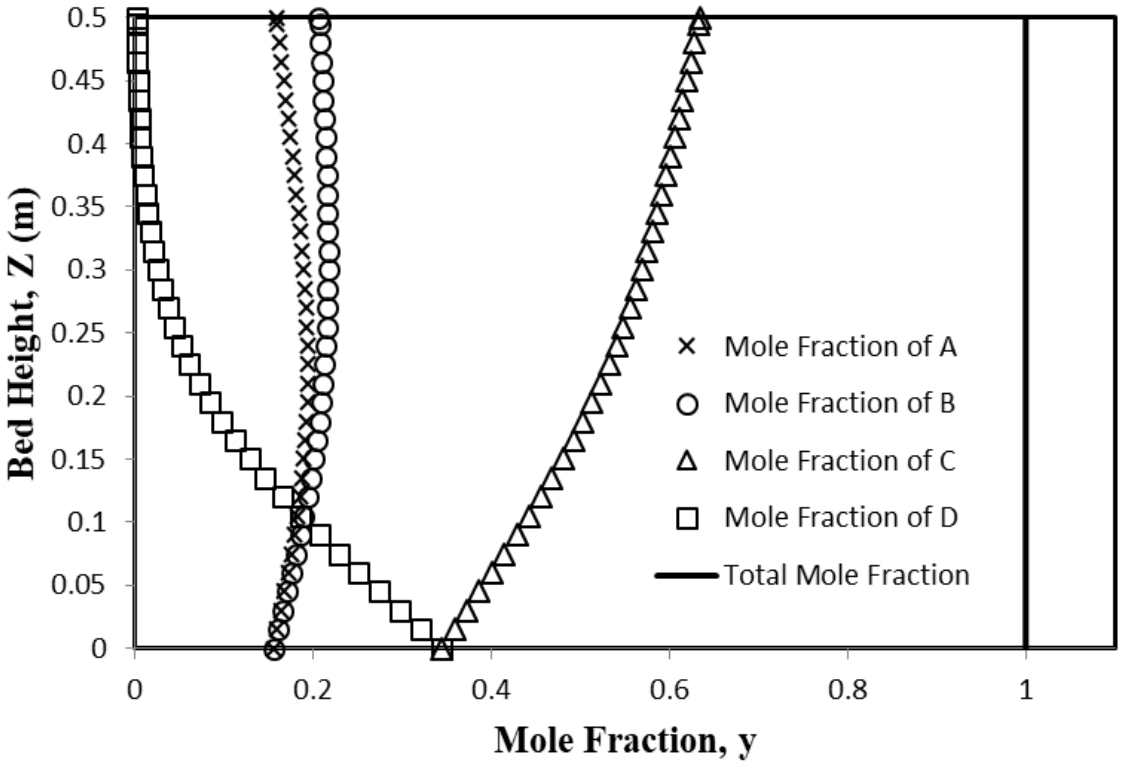

(c)

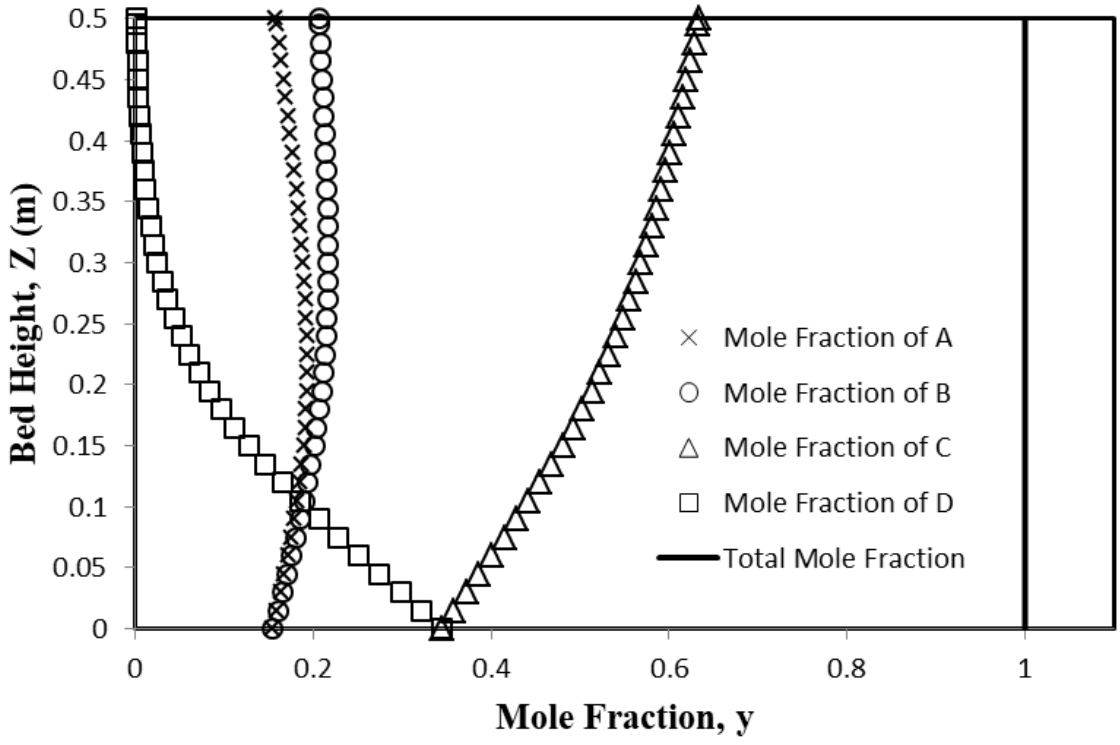

(d)

Fig. 6.19 Mole fraction of components in vapor of packed column with (a) Q = 32 Watt and a_c =90 m^2/m^3 (b) Q = 50 Watt and a_c = 60 m^2/m^3 (c) Q = 100 Watt and a_c = 90 m^2/m^3 (d) Q = 150 Watt and a_c = 120 m^2/m^3.

For small heat input rates and with moderate specific surface area of the packing it is shown possible through simulation that methyl acetate can be obtained in pure form in the distillate. As we increase the heat input rate owing to shorter residence time or contact between the liquid and vapor in the column, it can be inferred that the distillate contains less pure form of methyl acetate owing to the appearance of methanol and acetic acid.

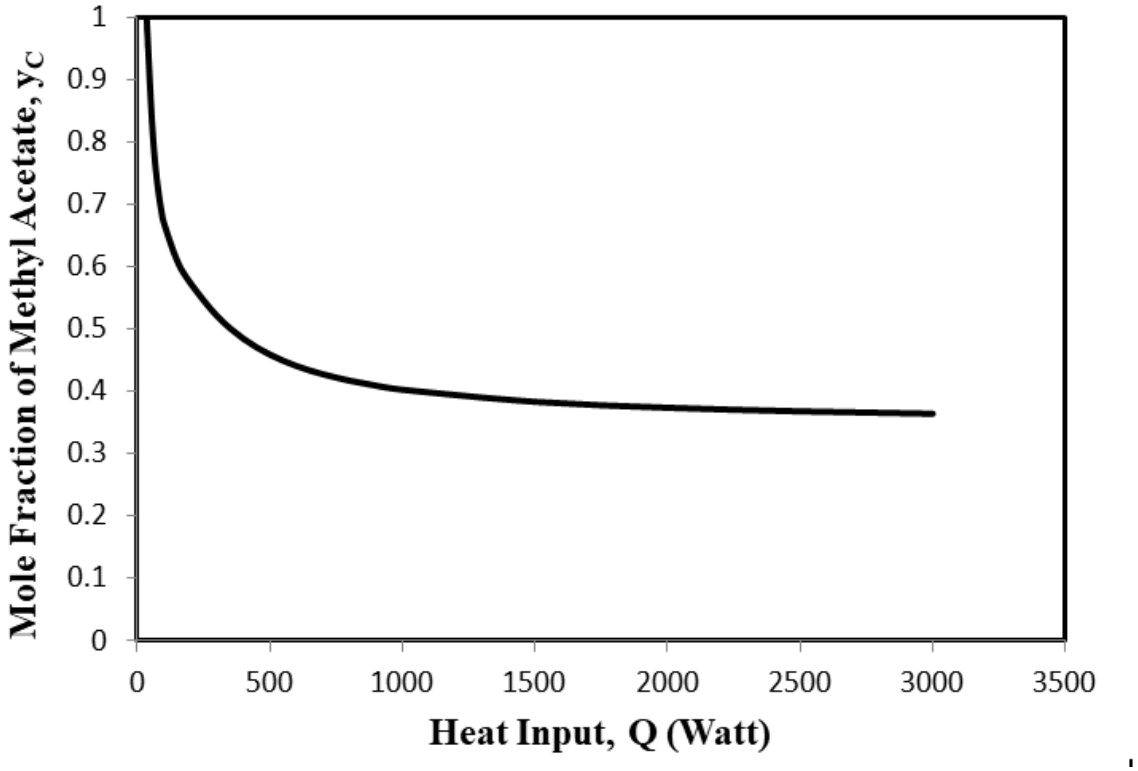

Fig. 6.20 Simulation result of effect of heat input (Q) on distillate composition of Methyl acetate (y_c) with a_c = 100 m^2/m^3.

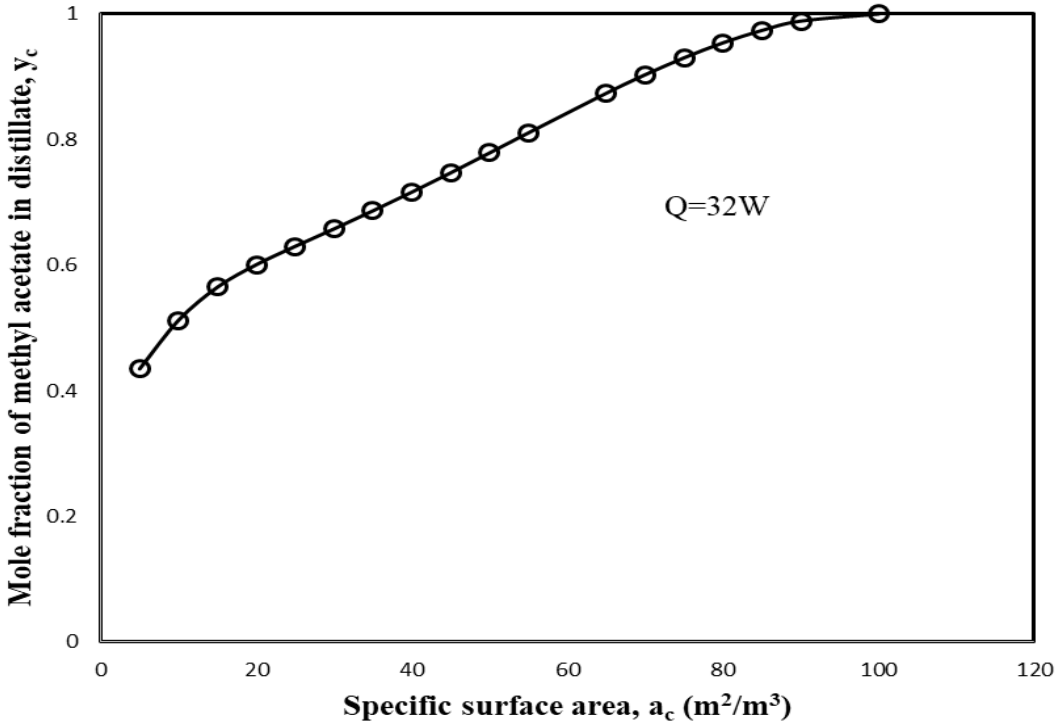

Fig. 6.21 Simualtion result of effect of heat input (Q) on distillate composition of Methyl acetate (y_c) with a_c as variable.

A simulation study for the present model of BRD shows that the distillate composition can be of high methyl acetate for heat input rate less than 100W as can be seen in Fig. 6.20. But lower heat input rate leads to very high start-up time and low throughput. Hence 'ac' the specific surface area of the packed bed in BRD can be increased to certain value like 100 m^2/m^3 which has shown to yield 100 percent pure methyl acetate.

CHAPTER 7
CONCLUSIONS

Conclusions

A particle scale model for heterogeneous reaction has been developed and implemented for carrying out the simulation of the esterification of acetic acid by methanol catalyzed by solids. In this study assumption such as quasi steady state or multi time scale approach using COMSOL Multiphysics as well as well stirred assumption has been relaxed. A more realistic simulation is carried out in which concentration gradients are allowed in the liquid surrounding the catalyst as well. It was observed that pore contribution to overall conversion of acetic acid is higher as compared to bulk of the liquid and is explained with the help of spatial concentration distribution plots. Further kinetic study was carried out at different geometric and intrinsic parameters like particle size, catalyst loading, and temperature. It was found that increase in temperature increases the rate of reaction, increase in particle size for a constant catalyst loading and for a particular temperature decreases slightly. Further with increase in catalyst loading for a particular particle size and at a particular temperature increases the rate of reaction as there is an increase in rate of conversion.

It was shown possible to obtain reaction rate constants from constant heat input rate batch experiments. The availability of advanced multi-parameter optimization tools of software such as MATLAB made it a reality to obtain rate constants from a single experimental data and found to be robust and validated. The gradual variation of reactant is possible with a step heat input rate rather than by a step temperature change and its control. Such gradually changing variables are more suitable for mathematical optimization carried out like in the present work. Hence with advanced data acquisition systems for temperature and online chemical analysis, it can revolutionize the way in which reaction kinetic parameters can be obtained as shown in this work.

Experimental studies were carried out in a lab scale batch packed bed distillation column with various heat input rates to the reboiler for a binary non reacting mixture. For the system of benzene-toluene smaller heat input rates were found to give higher purity of lighter component i.e., benzene in distillate at total reflux. The evaporation rate based model for non-reacting mixture (toluene-benzene system) was developed which was used in predicting the distillate composition accurately. The evaporation mass transfer coefficients were determined experimentally and their fitted curves or expressions were used in the simulations. The mass transfer coefficients for the heavier

component had a good power law fit in the entire range of temperatures starting from reboiler to the condenser. Whereas the mass transfer coefficient of the lighter component had three regimes of linear fit differing in slopes as well as sign of slopes owing to superheated condition of the lighter component in the reboiler and also to some extent in the column. It was found that the simulation of real world distillation processes using rate based model is validated. This has application in modeling reactive distillation such as solid catalyzed esterification reactions in a reboiler connected with a packed distillation column above it.

In another part of this work, variable heat input to the reboiler was used instead of constant temperature control for esterification reaction. The present study showed that the bubble point temperature of the reboiler is constant around 67 ^{0}C at steady state. So if at all the column has to be operated in a continuous reactant input mode then the set point of 60 ^{0}C or so corresponding to methyl acetate boiling point is heuristic. Moreover the heat input rate method is easy for implementation of quality control of distillate purity. Also the column may be provided wall heating corresponding to 60 ^{0}C initially for quick start up dynamics and later brought down back to insulating condition for efficient use of BRD equipment. The handle can also be heat input rate Q to the reboiler to achieve the same. Thus greater insights were obtained in the present work on batch reactive distillation (BRD).

Scope for future work

The activity coefficient models may be incorporated instead of ideal solution assumption based evaporation driving force in the rectification section. The formation of distillate for wall temperature above a threshold value can be studied to aid in startup dynamics of BRD. Process scale up analysis can be carried out both by simulation and experiments. The amount of energy required for unit quantity of methyl acetate can be optimized. A process control system can also be devised to have quick start-up dynamics by adjusting wall heating, reboiler heating and recycle. It can also be applied for continuous RD system.

References

1. Agreda, V. H., & Partin, L. R. (1984). US Patent 4,435,595.
2. Ali, S. H., Tarakmah, A., Merchant, S. Q., & Al-Sahhaf, T. (2007). Synthesis of Esters: Development of the Rate Expression for the Dowex 50 Wx8-400 Catalyzed Esterification of Propionic Acid with 1 Propanol. *Chemical Engineering Science*, 62: 3197–3217.
3. Alopaeus, V., & Aittamaa, J. (2000). Appropriate simplifications in calculation of mass transfer in a multicomponent rate-based distillation tray model. *Ind. Eng. Chem. Res.* 39 (11), 4336-4345.
4. Banchero, M., & Gozzelino, G. (2018). A Simple Pseudo-Homogeneous Reversible Kinetic Model for the Esterification of Different Fatty Acids with Methanol in the Presence of Amberlyst-15. *Energies*, 11(7), 1843.
5. Butcher, H., & Wilhite, B. A. (2016). Enhancing Catalyst Effectiveness by Increasing Catalyst Film Thickness in Coated-Wall Microreactors: Exploiting Heat Effects in Catalytic Methane Steam Micro-reformers. *Chemical Engineering Science*, 143: 47-54.
6. Dhole, V. R., & Linnhoff, B. (1993). Distillation column targets. *Computers & chemical engineering*, *17*(5-6), 549-560.
7. Fogler, H. S. (1999). Elements of Chemical Reaction Engineering. 3rdedition, Upper Saddle River: N. J. Prentice Hall PTR.
8. Gorak, A., & Hoffmann, A. (2001). Catalytic distillation in structured packings: methyl acetate synthesis. *AIChE Journal*, *47*(5), 1067-1076.
9. Higler, A., Krishna, R., & Taylor, R. (1999). Nonequilibrium Cell Model for Packed Distillation Columns The Influence of Maldistribution. *Industrial & engineering chemistry research*, *38*(10), 3988-3999.
10. Himus, G. W., & Hinchley, J. W. (1924). The effect of a current of air on the rate of evaporation of water below the boiling point. *Journal of the Society of Chemical Industry*, *43*(34), 840-845.
11. Huerta-Garrido, M. E., Rico-Ramirez, V., & Hernandez-Castro, S. (2004). Simplified design of batch reactive distillation columns. *Industrial & engineering chemistry research*, *43*(14), 4000-4011.

12. Jagadeesh Babu, P. E., Sandesh, K., & Saidutta, M. B. (2011). Kinetics of Esterification of Acetic Acid with Methanol in the Presence of Ion Exchange Resin Catalysts. *Industrial and Engineering Chemistry Research*, 50: 7155–7160.
13. Jana, A. K., & Maiti, D. (2013). An ideal internally heat integrated batch distillation with a jacketed still with application to a reactive system. *Energy*, *57*, 527-534.
14. Joshi, S. Y., Harold, M. P., & Balakotaiah, V. (2009). On the use of internal mass transfer coefficients in modeling of diffusion and reaction in catalytic monoliths. *Chemical Engineering Science*, 64(23), 4976-4991.
15. Kim, Y. J., Hong, W. H., & Wozny, G. (2002). Effect of recycle and feeding method on batch reactive recovery system of lactic acid. *Korean Journal of Chemical Engineering*, *19*(5), 808-814.
16. Kreul, L.U., Gorak, A., & Barton, P.I. (1999). Dynamic rate-based model for multicomponent batch distillation. *AIChE Journal*. 45(9), 1953-1962.
17. Kumar, R., & Mahajani, S. M. (2007). Esterification of lactic acid with n-butanol by reactive distillation. *Industrial & Engineering Chemistry Research*, *46*(21), 6873-6882.
18. Levenspiel, O. (1972). Chemical Reaction Engineering. 2nd edition, New York: John Wiley & Sons.
19. Luyben, W. L., Pszalgowski, K. M., Schaefer, M. R., & Siddons, C. (2004). Design and control of conventional and reactive distillation processes for the production of butyl acetate. *Industrial & engineering chemistry research*, *43*(25), 8014-8025.
20. Mao, W., Wang, X., Wang, H., Chang, H., Zhang, X., & Han, J. (2008).Thermodynamic and Kinetic Study of Tert-amyl Methyl Ether (TAME) Synthesis. *Chemical Engineering and Processing: Process Intensification*, 47: 761–769.
21. Mekala, M., Thamida, S.K., & Goli, V. R. (2013). Pore Diffusion Model to Predict the Kinetics of Heterogeneous Catalytic Esterification of Acetic Acid and Methanol. *Chemical Engineering Science*, 104: 565-573.
22. Mortaheb, H. R., & Kosuge, H. (2004). Simulation and optimization of heterogeneous azeotropic distillation process with a rate-based model. *Chem. Eng. Process.* 43(3), 317-326.
23. Moscicka-Studzinska, A., & Ciach, T. (2012). Mathematical Modeling of Buccal Iontophoretic Drug Delivery System. *Chemical Engineering Science*, 80: 182-187.

24. Mozaffari, B., Tischer, S., Votsmeier, M., & Deutschmann, O. (2016). A One-Dimensional Modeling Approach for Dual Layer Monolithic Catalyst. *Chemical Engineering Science*, 139: 196-210.
25. Mueller, I., & Kenig, E.Y. (2007). Reactive distillation in a dividing wall column: rate-based modeling and simulation. *Ind. Eng. Chem. Res.* 46(11), 3709-3719.
26. Mueller, I., & Kenig, E. Y. (2007). Reactive distillation in a dividing wall column: rate-based modeling and simulation. *Industrial & engineering chemistry research*, 46(11), 3709-3719.
27. Mutalib, M. A., & Smith, R. (1998). Operation and control of dividing wall distillation columns: Part 1: Degrees of freedom and dynamic simulation. *Chemical Engineering Research and Design*, 76(3), 308-318.
28. Muthia, R., Reijneveld, A. G., van der Ham, A. G., ten Kate, A. J., Bargeman, G., Kersten, S. R., & Kiss, A. A. (2018). Novel method for mapping the applicability of reactive distillation. *Chemical Engineering and Processing-Process Intensification*, *128*, 263-275.
29. Patan, A. K., Mekala, M., & Thamida, S. K. (2018). Dynamic Simulation of Heterogeneous Catalysis at Particle Scale to Estimate the Kinetic Parameters for the Pore Diffusion Model. *Bulletin of Chemical Reaction Engineering & Catalysis*, *13*(3), 420-428.
30. Peng, B., Shuang, S., Sheng, M., & Xiaofeng, L. I. (2010). A dynamic modeling for cyclic total reflux batch distillation. *Chinese Journal of Chemical Engineering*, *18*(4), 554-561.
31. Peng, J., Edgar, T. F., & Eldridge, R. B. (2003). Dynamic rate-based and equilibrium models for a packed reactive distillation column. *Chem. Eng. Sci*. 58 (12), 2671-80.
32. Peng, J., Lextrait, S., Edgar, T. F., & Eldridge, R. B. (2002). A comparison of steady-state equilibrium and rate-based models for packed reactive distillation columns. *Industrial & engineering chemistry research*, 41(11), 2735-2744.
33. Pietrzyk, S. M., Redekop, E. A., Yablonsky, G. S., & Marin, G. B. (2015). Precise Kinetic Measurements and Spatial Uniformity of Catalytic Beds. *Chemical Engineering Science*, 134: 367-373.
34. Pöpken, T., Götze, L., & Gmehling, J. (2000). Reaction kinetics and chemical equilibrium of homogeneously and heterogeneously catalyzed acetic acid esterification with methanol and methyl acetate hydrolysis. *Industrial & Engineering Chemistry Research*, *39*(7), 2601-2611.
35. Qi, W., & Malone, M. F. (2010). Operating parameters and selectivity in batch reactive distillation. *Industrial & Engineering Chemistry Research*, *49*(22), 11547-11556.

36. Ramesh, K., Aziz, N., Abdshukor, S. R., & Ramasamy, M. (2007). Dynamic Rate Based and Equilibrium Model Approaches for Continuous Tray Distillation Column. *Journal of Applied SciencesResearch*, **3**(12), 2030-2041.
37. Rönnback, R., Salmi, T., Vuori, A., Haario, H., Lehtonen, J., Sundqvist, A., & Tirronen, E. (1997). Development of a kinetic model for the esterification of acetic acid with methanol in the presence of a homogeneous acid catalyst. *Chemical Engineering Science*, *52*(19), 3369-3381.
38. Silva, J. M. F., Knoechelmann, A., Meirelles, A. J., Wolf-Maciel, M. R., & Lopes, C. E. (2003). On the dynamics of nonequilibrium simple batch distillation processes. *Chemical Engineering and Processing: Process Intensification*, *42*(6), 475-485.
39. Sørensen, E., & Skogestad, S. (1994). Control strategies for reactive batch distillation. *Journal of Process Control*, *4*(4), 205-217.
40. Taylor, R., & Krishna, R. (2000). Modelling reactive distillation. *Chemical engineering science*, 55(22), 5183-5229.
41. Taylor, R., Krishna, R., Kooijman, H. (2003). Real-world modeling of distillation. *Reactions and Seperations*, www.cepmagazine.org, pp. 28-39.
42. Tesser, R., Di Serio, M., Guida, M., Nastasi, M., & Santacesaria, E. (2005). Kinetics of oleic acid esterification with methanol in the presence of triglycerides. *Industrial & engineering chemistry research*, 44(21), 7978-7982.
43. Titus, M. P., Bausach, M., Tejero, J., Iborra, M., Fite, C., Cunill, F., & Izquierdo, J. F. (2007). Liquid-Phase Synthesis of Isopropyl Tert-Butyl Ether by Addition of 2-Propanol to Isobutene on the over Sulfonate Dion-Exchange Resin Amberlyst-35. *Applied Catalysis A:General*, 323: 38–50.
44. Tsai, Y. T., Lin, H. M., & Lee, M. J. (2011). Kinetic Behavior Esterification of Acetic Acid with Methanol over Amberlyst 36. *Chemical Engineering Journal*, 171: 1367-1372.
45. Valdes-Parada, F. J., Aguilar-Madera, C. G., & Alvarez-Ramirez, J. (2011). On Diffusion, Dispersion and Reaction in Porous Media. *Chemical Engineering Science*, 66: 2177-2190.
46. Venimadhavan, G., Malone, M. F., & Doherty, M. F. (1999). A novel distillate policy for batch reactive distillation with application to the production of butyl acetate. *Industrial & engineering chemistry research*, *38*(3), 714-722.

47. Xu, Z., Afacan, A., & Chuang, K. T. (1999). Removal of acetic acid from water by catalytic distillation. Part 1: Experimental studies. *The Canadian Journal of Chemical Engineering*, *77*(4), 676-681.
48. Yang, J. I., Cho, S. H., Park, J., & Lee, K. Y. (2007). Esterification of acrylic acid with 1, 4-butanediol in a batch distillation column reactor over Amberlyst 15 catalyst. *The Canadian Journal of Chemical Engineering*, *85*(6), 883-888.

Appendix

Appendix 1

Derivation of Initial Reaction Conversion Rate as in Equation 2.3

The assumptions involved in developing the model are as follows: The catalyst particles are assumed to be spherical in shape with internal pores. The swelling of catalyst particles is considered to be negligible. The reactants can react in the bulk solution as well as inside the catalyst particle. Acetic acid and methanol diffuse into the catalyst where the reaction occurs due to catalytic activity. The produced methyl acetate and water diffuse back into the bulk solution. In the bulk solution also, a simultaneous homogeneous reaction occurs. The mass transfer resistance external to the catalyst particle is neglected since there is no stagnant film surrounding a catalyst particle due to high stirring. The diffusivities of the reactants and products inside the catalyst particle are important. Though they depend on temperature and local concentration, they are assumed to be same for all species and an average value is assumed. The volumetric change of solution due to reaction is assumed to be negligible.

The overall rate of reaction could be represented as in Eq. (A1.1).

$$\frac{dN_{Ab}}{dt} = -N_P 4\pi R_P^2 J_A\Big|_{r=R_P} + r_{Ab}V \qquad \text{(A1.1)}$$

Where N_{Ab} is the number of moles of A in the bulk solution at a given time. dN_{Ab}/dt represents the rate of change of number of kmoles of A in the bulk solution where it is measured for concentration changes. N_p is the number of catalyst particles, R_p is the radius of catalyst particles and $4\pi R_p^2$ represents the surface area of each catalyst particle. $J_A\Big|_{r=R_P}$ represents the inward flux of acetic acid into the catalyst at its surface. r_{Ab} is the rate of homogeneous reaction in the bulk solution which occurs simultaneously. It primarily depends on temperature but its rate is slow compared to the rate of catalytic reaction inside the catalyst. V is the volume of reaction mixture.

Generally the rate of homogeneous reaction could be represented by Eq. (A1.2)

$$r_{Ab} = \frac{dC_{Ab}}{dt} = -\left(k_{f1}C_{Ab}C_{Bb} - k_{b1}C_{Cb}C_{Db}\right) \qquad \text{(A1.2)}$$

k_{f1} is the forward reaction rate constant and k_{b1} is the backward reaction rate constant. C_{Ab}, C_{Bb}, C_{Cb} and C_{Db} are the concentrations in kmol/m^3 or gmol/lit in the bulk solution.

Eq. (A1.2) could be simplified as

$$r_{Ab} = -k_{f1} C_{A0}^2 \left[(1 - X_A)^2 - \frac{X_A^2}{K_e} \right] \tag{A1.3}$$

Where $K_e = k_{f1}/k_{b1}$, In experiments it is found that $K_e = 4.95$ from equilibrium data [Mekala et al, 2013], that is $K_e = \frac{X_{Ae}^2}{(1 - X_{Ae})^2}$, where X_{Ae} is equilibrium conversion of acetic acid.

Now, the first term in Eq. (A1.1) due to flux of A into the catalyst particle could be simplified by the following transformation in terms of reaction conditions that is catalyst loading w_c and radius of catalyst particle R_p.

$$N_P 4\pi R_P^2 = \frac{N_P \left(\frac{4}{3} \pi R_P^3 \right) \rho_P}{V_0} \frac{3V_0}{R_P \rho_P} = \frac{m_{cat}}{V_0} \frac{3}{R_P \rho_P} = w_c \frac{3}{R_p \rho_p} \tag{A1.4}$$

Where m_{cat} is total mass of catalyst, R_p is the radius of catalyst particle, ρ_p is the true density of catalyst particle in g/cc and w_c is the catalyst loading in g/cc. The inward flux of acetic acid, $J_A\big|_{r=R_P}$ at catalyst surface is represented as

$$J_A = D_A \frac{\partial C_A}{\partial r}\Big|_{r=R_P} \tag{A1.5}$$

This J_A has to be obtained by solving reaction-diffusion equation inside the catalyst particle as given below.

$$\frac{\partial C_A}{\partial t} + \underline{\nabla}.\underline{n}_A = \varepsilon r_A \tag{A1.6}$$

Where C_A is the concentration of the acetic acid at a location (r, t) inside the catalyst particle. $\underline{n}_A$ is the total flux of A due to convection and diffusion as given below in Eq. (A1.7).

$$\underline{n}_A = \left(\sum \underline{n}_i \right) x_A + \underline{J}_A \tag{A1.7}$$

Where $\left(\sum \underline{n}_i \right)$ is the vector sum of fluxes of all components. x_A is the mole fraction of acetic acid and J_A is the molecular diffusion flux. If we assume that the reaction proceeds according to

stoichiometry then $\left(\sum \underline{n}_i\right)$=0 which implies that equimolar counter diffusion of reactants and products occurs inside the catalyst particle. Hence the flux of A inward into the particle is equal to flux of B and of opposite sign with respect to C and D. Now, the total flux of A in Eq. (A1.7) is given by J_A itself which in turn is as given below in Eq. (A1.8) according to Fick's law of diffusion.

$$\underline{J}_A = -D_A \frac{\partial C_A}{\partial r} \tag{A1.8}$$

The reaction rate inside the catalyst may be assumed as follows

$$r_A = -\left(k_{f2} C_A C_B - k_{b2} C_C C_D\right) \tag{A1.9}$$

Where C_A, C_B, C_C and C_D are local concentrations inside the catalyst particle. k_{f2} and k_{b2} are the forward and backward reaction rate constants which are different from those of homogeneous reaction. Note that C_A is inside the catalyst and C_{Ab} is in the bulk solution.

By substituting Eq. (A1.7), Eq. (A1.8) and Eq. (A1.9) in Eq. (A1.6) it gives the equation

$$\frac{\partial C_A}{\partial t} - D_A \nabla^2 C_A = -\varepsilon\left[k_{f2} C_A C_B - k_{b2} C_C C_D\right] \tag{A1.10}$$

Where ε is the void fraction in the catalyst filled with reactant liquids. Here, a pseudo-homogeneous rate equation is used because the pore volume is utilized instead of the pore surface area. In spherical coordinates Eq. (A1.10) becomes

$$\frac{\partial C_A}{\partial t} = D_A \frac{1}{r^2} \frac{\partial}{\partial r}\left(r^2 \frac{\partial C_A}{\partial r}\right) - \varepsilon\left[k_{f2} C_A C_B - k_{b2} C_C C_D\right] \tag{A1.11}$$

By using non-dimensionalization as $t^*=t/\tau$, $r^*=r/R_P$, $C_A^*=C_A/C_{A0}$ and by assuming the reactants and products to be in stoichiometric ratio that is $C_B=C_A$, $C_C=C_{A0}-C_A$, $C_D=C_{A0}-C_A$, Eq. (A1.11) gives

$$\frac{\partial C_A^*}{\partial t^*} = \frac{1}{r^{*2}} \frac{\partial}{\partial r^*}\left(r^{*2} \frac{\partial C_A}{\partial r^*}\right) - \frac{\varepsilon k_{f2} C_{A0} R_P^2}{D_A}\left[C_A^{*2} - \frac{\left(1 - C^*_A\right)^2}{K_e}\right] \tag{A1.12}$$

Where $\tau=R_p^2/D_A$ and $K_e=k_{f2}/k_{b2}$.

By solving Eq. (A1.12) with boundary conditions as $\frac{\partial C_A^*}{\partial r^*} = 0$ at $r^*=0$ and $C_A^*=C_A/C_{A0}=1-X_A$ at $r^*=1$ inside the catalyst particle, we could determine the flux of A at catalyst surface as

$$J_A = \frac{D_A C_{A0}}{R_P} \frac{\partial C_A *}{\partial r *}\Big|_{r*=1} \tag{A1.13}$$

By substituting Eq. (A1.13), Eq. (A1.4) and Eq. (A1.3) in Eq. (A1.1), it gives the overall reaction rate in terms of conversion of acetic acid as in Eq. (A1.14)

$$\frac{dX_A}{dt} = w_C \left(\frac{3D_A}{R_P^2 \rho_P} \right) \left(\frac{\partial C_A *}{\partial r *} \right)\Big|_{r*=1} + C_{A0} k_{f1} \left[(1 - X_A)^2 - \frac{X_A^2}{K_e} \right] \tag{A1.14}$$

It is assumed that the equilibrium constant K_e is same for both homogeneous reaction as well as for reaction inside the catalyst particle. From Eq. (A1.14) it can be seen that the initial reaction conversion rate at t → 0 and $X_A=0$, is a linear function of catalyst loading w_c and it could be rewritten as below where β is a coefficient.

$$\frac{dX_A}{dt}\Big|_{t \to 0} = \beta w_C + C_{A0} k_{f1} \tag{A1.15}$$

Appendix 2

Algorithm – 1

(Particle scale simulation of reaction by using COMSOL Multiphysics. Ref.: Sec. 5.1)

Step 1: Geometry:
Select 3D Geometry. Create a cube of liquid. Create a sphere of solid. Subtract sphere from cube. Again create sphere of solid as catalyst.

↓

Step 2: Add Physics:
Select convection-diffusion-reaction equation for both catalyst and surrounding liquid. Assign different diffusivities and reaction rates.

Boundary Condition: Assign Neumann condition on edges of cube. At particle-liquid interface, apply concentration and flux continuity/Dirichlet condition.

Initial Condition: Both in liquid and pores of solid phase, the concentration is initially C_{A0}.

↓

Step 3: Create Mesh: Use physics-controlled option.

↓

Step 4: Add Study: Transient solver to be selected. Time range as 0:900:12600 s

↓

Step 5: Post Processing of Results:
$C_{A,Avg}$ is evaluated in liquid phase. Overall conversion is also evaluated at each time step.

Algorithm - 2

(For non-reacting binary mixture in a batch packed bed distillation column. Ref.: Sec. 5.4)

Step 1: Define mole fractions of components of liquid in reboiler

↓

Step 2: The column length is divided into 100 segments or 101 nodes with dz=0.5 cm. The geometry parameters of specific surface area of packing and cross-sectional area of column are specified. First Node is assigned the same composition as the reboiler both in liquid and vapor.

↓

Step 3: A 'for loop' is used to update vapor flow rates at each node for each of the two components using evaporation rate from liquid and the contact area between liquid and vapor between every adjacent nodes. Evaporation rate is evaluated using local mass transfer coefficient based on local temperature and saturation vapor pressures from Antoine equations.

↓

Step 4: Distillate composition is evaluated as the same value as that of vapor composition in top most node in the column.

↓

Step 5: Plot Graphs such as mole fraction of each component along the height of the column in vapor or liquid.

Algorithm - 3

(For batch reactive distillation. Ref.: Sec. 5.5)

Step 1: Define mole fractions of components of liquid in Reboiler using equilibrium constant

↓

Step 2: The column length is divided into 50 segments or 51 nodes with dz=1 cm. The geometry parameters of specific surface area of packing and cross-sectional area of column are specified. First Node is assigned the same composition as the reboiler both in liquid and vapor.

↓

Step 3: A 'for loop' is used to update vapor flow rates at each node for each of the four components using evaporation rate from liquid and the contact area between liquid and vapor between every adjacent nodes. Evaporation rate is evaluated using local mass transfer coefficient based on local temperature and saturation vapor pressures from Antoine equations.

↓

Step 4: Distillate composition is evaluated as the same value as that of vapor composition in top most node in the column.

↓

Step 5: Plot Graphs such as mole fraction of each component along the height of the column in vapor or liquid.

Publications in Present Work

Journals

1. Patan, A. K., Mekala, M., & Thamida, S. K. (2018). Dynamic Simulation of Heterogeneous Catalysis at Particle Scale to Estimate the Kinetic Parameters for the Pore Diffusion Model. *Bulletin of Chemical Reaction Engineering & Catalysis*, 13(3), 420-428.

2. Ameer Khan Patan, Sunil Kumar Thamida. (2019) Novel Method for Determination of Kinetic Constants from Dynamics in a Batch Reactor with Constant Heat Input Rate. *International Journal of Thermodynamics and Chemical Kinetics*, 5(1) 1–5.

3. Ameer Khan Patan, Sunil Kumar Thamida. Modeling and Simulation of distillation of a binary non-reacting mixture using rate based approach in packed column under total reflux. *Iranian Journal of Chemistry and Chemical Engineering.* (Accepted for Publication).

4. Ameer Khan Patan, Sunil Kumar Thamida, Srinath Surananai, Suresh Siliveri, Venkatathri Narayanan. Effect of various heat input modes on the start-up dynamics and product purity in batch reactive distillation. *International Journal of Chemical Reactor Engineering.* (Accepted for Publication).

Conference Presentations

1. Patan, A. K., Mekala, M., & Thamida, S. K. (2016). "Dynamic Simulation Using COMSOL Multiphysics for Heterogeneous Catalysis at Particle Scale", COMSOL Conference 2016, 20-21 October, 2016 at Bangalore.